ISTANBUL TECHNICAL UNIVERSITY ★ GRADUATE SCHOOL OF SCIENCE ENGINEERING AND TECHNOLOGY

FATIGUE CRACK GROWTH UNDER NON-PROPORTIONAL LOADING

M.Sc. THESIS

Nait MUTLU

Department of Mechanical Engineering

Solid Mechanics Programme

Thesis Advisor: Prof. Dr. Ata MUĞAN

DECEMBER 2011

ISTANBUL TECHNICAL UNIVERSITY ★ GRADUATE SCHOOL OF SCIENCE ENGINEERING AND TECHNOLOGY

FATIGUE CRACK GROWTH UNDER NON-PROPORTIONAL LOADING

M.Sc. THESIS

Nait MUTLU
(503091528)

Department of Mechanical Engineering

Solid Mechanics Programme

Thesis Advisor: Prof. Dr. Ata MUĞAN

DECEMBER 2011

İSTANBUL TEKNİK ÜNİVERSİTESİ ★ FEN BİLİMLERİ ENSTİTÜSÜ

ORANTISIZ YÜKLEME DURUMUNDA
YORULMA ÇATLAK BÜYÜMESİ

YÜKSEK LİSANS TEZİ

Nait MUTLU
(503091528)

Makina Mühendisliği Anabilim Dalı

Katı Cisimlerin Mekaniği Programı

Tez Danışmanı: Prof. Dr. Ata MUĞAN

ARALIK 2011

Nait Mutlu, a **M.Sc.** student of ITU **Graduate School of Science, Engineering and Technology -** student ID **503091528**, successfully defended the **thesis** entitled "**FATİGUE CRACK GROWTH UNDER NON-PROPORTIONAL LOADING**", which he prepared after fulfilling the requirements specified in the associated legislations, before the jury whose signatures are below.

Thesis Advisor : **Prof. Dr. Ata MUĞAN** ....
İstanbul Technical University

Jury Members : **Prof. Dr. Alaaddin ARPACI** ....
İstanbul Technical University

Prof. Dr. Zahit MECİTOĞLU ....
İstanbul Technical University

Date of Submission : 30 September 2011
Date of Defense : 07 December 2011

FOREWORD

This thesis is submitted in partial fulfillment of the requirements for obtaining the degree of Master of Since in mechanical engineering. The work was carried out at the Department of Mechanical Engineering, Solid Mechanics, Technical University of Denmark in Copenhagen during the period Agust 2010 to Agust 2011. Supervision was received from Professor Dr. Viggo Tvergaard and associate professor Christian Frithiof Niordson at DTU and Professor Dr. Ata Muğan at ITU as university supervisors and Tore Lucht from MAN Diesel A/S as industrial supervisor.

I am very grateful to all my supervisors for their outstanding guidance during the project and my family.

I have had close collaboration with Chris Valentin Nielsen and I have been pleased with always to get a positive and quick response from him when I have reported errors and suggested improvements.

Finally I wish to thank colleagues and fellow PhD and MScD students at the Department of Mechanical Engineering, Solid Mechanics for creating a friendly and stimulating environment.

August 2011

Nait MUTLU
(Mechanical Engineer)

TABLE OF CONTENTS

Page

FOREWORD .... **vii**
TABLE OF CONTENTS .... **ix**
ABBREVIATIONS .... **xi**
SYMBOLS .... **xiii**
LIST OF TABLES .... **xvii**
LIST OF FIGURES .... **xix**
SUMMARY .... **xxi**
ÖZET .... **xxiii**
1. INTRODUCTION **1**
2. FRACTURE MECHANICS **5**
2.1 Origin of Linear Elastic Fracture Mechanics 5
2.2 Basics Modes of the Fracture Mechanic 7
2.3 Sie of Plastic Zone and Concept of Small Scale Yielding 8
2.4 Path Independent J-integral 9
3. FINITE ELEMENT METHOD **11**
3.1 Governing Equatıons 11
3.2 Element Discretization 12
3.3 Element Stiffness and Global Stifness Matrices 14
3.4 Gauss Integration Method 15
4. EXTENDED FINITE ELEMENT METHOD **17**
4.1 Element Discretization 17
4.1.1 Heaviside enrichment 17
4.1.2 Crack tip enrichment 19
4.1.3 General X-FEM approximation for crack modeling 20
4.2 Element Stiffness and Global Stifness Matrices for xFEM 21
4.3 Integration of Discontinuous Elements 24
5. DEFINATION OF THE CRACK PATH **27**
5.1 Defining Heaviside Function 29
6. STRESS INTENSITY FACTORS FOR A MIXED MODE CRACK **31**
7. PROGRAM VERIFICATION FOR DIFERENT CRACKED PLATES **35**
7.1 Center Cracked Rectangular Plate Under Uniform Displacement 35
7.2 Finite Width Plate with a Center Crack Parallel to the Clamped Edges 38
7.3 Finite Width Plate with a Edge Crack Parallel to the Clamped Edges 39
7.4 An Angled Center Crack in a Finite Plate Under Uniform Tension 40
7.5 An Angled Edge Crack in a Finite Plate Under Uniform Tension 43
7.6 A Skew – Symmetric Bent Crack 45
8. FATIGUE CRACK GROWTH **49**
8.1 Fatigue Crack Growth Rate 51
8.2 Prediction of Mixed Mode Fatigue Crack Growth Direction 51
8.2.1 Maximum tangential stress criteration 52

8.2.2 Minimum strain energy density criteration 53
9. FATIGUE CRACK GROWTH UNDER MIXED MODE NON-PROPORTIONAL LOADING 55
9.1 Experimental Suggestion: Thin Walled Tube Under Tension P and Torsion M 55
9.2 Mixed Mode Fatigue Crack Growth 58
9.3 Numerical Similation of a Fatigue Crack Growth Under Non-proportional Loading Given by Case I 60
10. PROGRAM FLOW CHART 65
11. CONCLUSION 67
REFERENCES 71
APPENDICES 75
APPENDIX A 76
APPENDIX B 78
APPENDIX B.1 78
APPENDIX B.2 79
APPENDIX B.3 80
APPENDIX B.4 82
APPENDIX C 84
APPENDIX D 85
APPENDIX D.1 85
APPENDIX D.2 87
APPENDIX D.3 88
APPENDIX E 92
APPENDIX E.1 92
APPENDIX E.2 94
APPENDIX E.3 96
APPENDIX E.4 98
APPENDIX F 101
CURRICULUM VITAE 105

ABBREVIATIONS

The following abbreviations will appear in the report.

AACCFPUUT	: An angled center crack in a finite plate under uniform tension
AAECFPUUT	: An angeled edge crack in a finite plate under uniform tension
ACCRPUUD	: A center cracked rectangular plate under uniform displacement
ACECHRPUT	: A crack emanating from a circular hole in a rectangular plate under tension
ACERHRPUT	: A crack emanating from a rectangular hole in a rectangular plate under tension
AFWPCCPCE	: A finite a finite width plate with a center crack parallel to the clamped edges
AFWPECPCE	: A finite width plate with an edge crack parallel to the clamped edges
ASSBC	: A skew – symmetric bent crack
DOF	: Degree of freedom
FEA	: Finite element analysis
FEM	: Finite element method
LEFM	: Linear elastic fracture mechanics
MTS	: Maximum Tangential Stress
S	: Minimum Strain Energy Density
SSY	: Small-scale yielding
xFEM	: Extended finite element method

SYMBOLS

List of important symbols which may be used in different combinations including superscripts and subscripts

a	Current crack length or current half crack length
A	Area
A_e	Area of an element
b	Length of a branch
b_i	Heaviside enriched nodal degree of freedom
$[B]$	Strain-displacement matrix
C	Paris law constant
c_i	Branch function enriched nodal degree of freedom
C_{ijkl}	The constitutive law
C_s	A material constant for crack growth law given by Equation (8.4)
$[C]$	Constitutive matrix relating strains to stresses
ct_i	i^{th} crack tip
da	Crack incensement
dN	Number of cycle
e_n	Unit normal vector to crack path
$\boldsymbol{e_s}$	Unit tangential vector to crack path
E	Young’s modulus
E'	Effective Young’s modulus for plane stress or plane strain
f^b	Body forces
f^t	Traction vectors
$\{f\}$	Force vector
F	The work done by external forces
F_l	Branch function or set of branch functions in linear combination
$[F]$	Matrix of branch functions
$[F]'$	Matrix of branch function derivatives with respect to global coordinates
F_I	Mode I shape factor
F_{II}	Mode II shape factor
f_5	The shape factor for the plane stress by Isida [16]
f_h	The function used to define a hole
G	Energy release rate
g	The step wise linear function used to define an arbitrary shaped crack
g_5	The shape factor for the plane strain by Isida [16]
h	The characteristic length of a crack tip element
H	Height of a specimen
$H(f)$	Heaviside funcition
I	The interacting integral
J	J-integral
[J]	Jacobian matrix
$\|J\|$	Jacobian, determinant of Jacobian matrix
$[k]$	Local stiffness matrix

$[K]$ Global stiffness matrix
K_I Mode I stress intensity factor
K_{II} Mode II stress intensity factor
K_{III} Mode III stress intensity factor
ΔK_{th} The change of the threshold value
K_{eff} Effective stress intensity factor
ΔK Range of stress intensity factor
ΔK_{eff} Range of effective stress intensity factor
$[L]$ Matrix transforming displacement derivatives to strains
M Applied moment
$[N]$ Shape funcition matrix
$[N,]$ Matrix of shape function derivatives with respect to natural coordinates
n_s A material constant for crack growth law given by Equation (8.4)
n_g Number of gauss points
n Paris law constant
P Applied force
q Weighting function
r Radius in local crack tip coordinate system
r_d The radius of J-evaluation
r_p Size of plastic zone based on elastoplasticity
r_y Size of plastic zone based on elasticity
R The ratio K_{max}/K_{min}
S_{cr} Critical value of strain energy density factor
S Strain energy density factor
t Thickness of specimen
u_i Classical degree of freedom
U The strain energy stored in the body
W Width of specimen
W_i Weight factor in numerical integration
x_i Global coordinates
$\tilde{x}_i$
α The ratio of crack length to the width of plate
β The ratio of the height of plate to the width of plate
Γ Curve
$[\Gamma]$ Inverse of Jacobian
δ Indication of virtual quantity
δ_{ij} Kronecker's delta
ε_{ij} Strain tensor
η_j Element natural coordinate
θ Angle of crack growth in local crack tip coordinate system
θ_c Critical value of crack growth angle for the maximum tangential stress criterion and The minimum strain energy density factor
κ Kolosov constant, $\kappa = \kappa(\nu)$ defined for plane stress or plane strain
ν Poisson's ratio
ξ_i Element natural coordinate
σ Applied tensile stress
σ_{ij} Stress tensor
σ_y Yield stress

τ Shear stress

σ_c Critical value of Tangential stress

σ_f Griffith's expression for the stress field near the crack tip

Π The potential energy of an elastic body

ϕ Any field variable

Ψ_j The integrand of the interaction integral

Ω The domain

γ_p The plastic work per unit area of surface created

γ_s The elastic work per unit area of surface created

LIST OF TABLES

Page

Table 7.1 : The ratio g_5 taken from Isida [21] and $g_{5-calculated}$ for ACCRPUUD while β is varying from 0.4 to 0.8. 37
Table 7.2 : The ratio g_5 taken from Isida [21] and $g_{5-calculated}$ for ACCRPUUD while β is varying from 1.0 to 1.2. 37
Table 7.3 : The stress intensity factors for AFWPCCPCE, respect to Equation (7.6) by Rice [2] and the MATLAB code. 39
Table 7.4 : The stress intensity factors for AFWPECPCE, respect to Equation (7.8) by Rice [2] and the MATLAB code 40
Table 7.5 : The F_I and F_{II} factors for AACCFPUUT by Kitagawa and Yuuki [22] and Wilson [23], and the MATLAB code 42
Table 7.6 : The F_I and F_{II} factors for AAECFPUUT by Kitagawa and Yuuki [22] and Wilson [23], and the MATLAB code 44
Table 7.7 : The F_I and F_{II} factors for ASSBC WİTH θ=30° and φ_o=90° by Kitagawa and Yuuki [26] and the MATLAB code 46
Table 7.8 : The F_I and F_{II} factors for ASSBC WİTH θ=45° and φ_o=90° by Kitagawa and Yuuki [26] and the MATLAB code 47
Table 7.9 : The F_I and F_{II} factors for ASSBC WİTH θ=60° and φ_o=90° by Kitagawa and Yuuki [26] and the MATLAB code 47
Table 7.10 : The F_I and F_{II} factors for ASSBC WİTH θ=30° and φ_o=0° by Kitagawa and Yuuki [26] and the MATLAB code........ 47
Table 7.11 : The F_I and F_{II} factors for ASSBC WİTH θ=45° and φ_o=0° by Kitagawa and Yuuki [26] and the MATLAB code........ 48
Table 7.12 : The F_I and F_{II} factors for ASSBC WİTH θ=60° and φ_o=0° by Kitagawa and Yuuki [26] and the MATLAB code........ 48
Table 8.1 : The deviation of the crack growth angles for a loading cycle respect to MTS criterion and S criterion 54
Table 9.1 : Deviation of the crack growth angle determinated by each K_{eff} formula separately 64
Table C.1 : Gauss points and weights for rectangular elements 84
Table C.2 : Gauss points and weights for triangular elements........ 84
Table D.1 : The factors F_I for ACECHRPUT with variation of α and β by Stress Intensity Factors Handbook [36] and the MATLAB code 87
Table D.2 : The factors F_I for ACERHRPUT with h/w=1 and a/w=0.05 and variation of c/a by Murakami [37] and the MATLAB code........ 89
Table D.3 : The factors F_I for ACERHRPUT with h/w=1 and a/w=0.10 and variation of c/a by Murakami [37] and the MATLAB code........ 89

LIST OF FIGURES

Page

Figure 2.1 : Elliptical hole in a flat plate 5
Figure 2.2 : Defination of the coordinate systems 7
Figure 2.3 : Basic modes of fracture: Mode I, II and III 8
Figure 2.4 : Plastic zone models: Elastic and Elastoplastic 9
Figure 3.1 : A body in the state of equilibrium with atraction free crack 12
Figure 3.2 : Element illustration 14
Figure 4.1 : Crack tip represented by a classical mesh and a uniform mesh with anenriched node used in the extended finite element formulation 18
Figure 4.2 : Uniform mesh to define an edge crack 20
Figure 4.3 : Discontinuous elements 25
Figure 4.4 : Mapped triangles for the c and b enriched elements 25
Figure 5.1 : Arbitrary crack path approximated by a stepwise linear funcition g 27
Figure 5.2 : An edge crack with an additional branch 28
Figure 5.3 : The normal and tangential vectors for a segment of the crack path and value of Heaviside function on each side of the crack segment 29
Figure 6.1 : The two integration contours near crack tip 33
Figure 6.2 : The selection of the elements take part in the domain integral respect to the radius of J-evaluation 34
Figure 7.1 : Illustration of the selection of the nodes enriched by Heaviside funcition or Branch funcitions 36
Figure 7.2 : A center cracked rectangular plate under uniform displacement 36
Figure 7.3 : A finite width plate with a center crack parallell to the clamped edges 38
Figure 7.4 : A finite width plate with an edge crack parallell to the clamped edges 40
Figure 7.5 : An angled center crack in a finite plate under uniform tension 41
Figure 7.6 : Errors in the F_I and F_{II} factors for several of the crack angle θ and various of the ratio a/W for a center crack 42
Figure 7.7 : An angled edge crack in a finite plate under uniform tension 43
Figure 7.8 : Errors in the F_I and F_{II} factors for several of the crack angle θ and various of the ratio a/W for an edge crack 44
Figure 7.9 : A skew - symetric bent crack 45
Figure 7.10 : Illustration of the step wise linear funcition 46
Figure 8.1 : Typical relation between the fatigue load ΔK and the crack growth rate for metals 49
Figure 9.1 : Thin tume under tension P and torsion M 56
Figure 9.2 : The defination of the thin walled tube problem in the xFEM program 57
Figure 9.3 : Fitting Paris law to measurements o crack growth in SENB test speciment 58

Figure 9.4 : Estimated crack paths for Case I by each K_{eff} formula 61
Figure 9.5 : Stress intensity factors calculated at the first iteration for Case I 61
Figure 9.6 : Variation of the effective stifness on the crack tips for each of K_{eff} formulas at the fifth iteration 62
Figure 9.7 : The change of crack growth rate respect to the employed K_{eff} formula at each crack tip for Case I.. 63
Figure 10.1 : Program flow chart 66
Figure B.1 : An element with four crack tip enriched nodes 81
Figure D.1 : A crack emanating from a circular hole in a rectangular plate under tension 85
Figure D.2 : Illustration of the piecewise function f_h for a circular hole 86
Figure D.3 : A crack emanating from a rectangular hole in a rectangular plate under tension 87
Figure D.4 : Illustration of the piecewise function f_h for a rectangular hole 88
Figure D.5 : A series of crack part for different positions of the rectrangular hole defined by (D.8) 90
Figure D.6 : A series of crack part for different positions of the rectrangular hole defined as a hard inclusion.. 91
Figure E.1 : Estimated crack paths for additional Case I by each K_{eff} formula........ 92
Figure E.2 : Stress intensity factors calculated at the first iteration for additional Case I 93
Figure E.3 : The change of crack growth rate respect to the employed K_{eff} formula at each crack tip for additional Case I.. 93
Figure E.4 : Estimated crack paths for Case II by each K_{eff} formula 94
Figure E.5 : Stress intensity factors calculated at the first iteration for Case II 95
Figure E.6 : The change of crack growth rate respect to the employed K_{eff} formula at each crack tip for Case II 95
Figure E.7 : Estimated crack paths for Case III by each K_{eff} formula 96
Figure E.8 : Stress intensity factors calculated at the first iteration for Case III 97
Figure E.9 : The change of crack growth rate respect to the employed K_{eff} formula at each crack tip for Case III 98
Figure E.10 : Estimated crack paths for Case IV by each K_{eff} formula 98
Figure E.11 : Stress intensity factors calculated at the first iteration for Case IV 99
Figure E.12 : The change of crack growth rate respect to the employed K_{eff} formula at each crack tip for Case IV 99

FATIGUE CRACK GROWTH UNDER NON-PROPORTIONAL LOADING

SUMMARY

In the literature, there are several methods to demonstrate the all modes of fracture where any domain with an arbitrary shaped crack is discretized into elements and the discretization is necessary to be upload for each crack extension so that the elements defines the shape of the arbitrary growing crack correctly. Thus, to simulate the fatigue crack growth under non-proportional loading, Extended Finite Element Method (xFEM) is selected.

The extended finite element method is a powerful tool to simulate the crack growth by means of that it is capable of defining discontinuities, such as cracks, holes and inclusions, within elements easily. Any discontinuities within elements are modeled by introducing extra degrees of freedom with enrichment functions into the nodes. That is why xFEM removes the need for matching element boundaries with a crack, a hole boundary and/or an inclusions.

This enables usage of a single mesh even if the crack propagates in many times. Thus, there is no need for remeshing in each step of crack propagation except the mesh refinement may be necessary in any stage.

Numerical modeling of a fatigue crack growth under non-proportional loading has been done by implementing the extended finite element method (X-FEM) into a MATLAB code, which is capable of handling crack propagation. Heaviside function has been used to model crack faces inside elements and four branch functions has been applied to model crack tips inside elements.

To handle the stress intensity factors, the path independent J-integral has been implemented into the program by the way of interacting integral. The program is tested for several cracked plate to determine the mixed mode stress intensity factors. After that a model based on effective stress intensity factor is succeeded to determine both crack growth rate and crack growth angle to illustrate the propagation of fatigue crack under non-proportional loading with high cycle.

Furthermore, the crack analyses carried out in this paper are based on linear elastic fracture mechanic by neglecting the plastic zone that is sufficiently small near the crack tips. That is why the problems cowered are considered linear elastic all the way to brittle fracture. The crack is subject to the mixed mode loadings that force the evaluation of the both of KI and KII stress intensity factors. The stress intensity factors for each mode are evaluated by means of the interaction integral based on the path-independent J-integral. The interaction integral has been converted into a domain integral, which simplifies implementation of the interaction integral into numerical integration, by applying the divergence theorem and making tensor calculus. As the J-integral is path-independent, the domain form of the interaction integral is domain independent as long as it surrounds the crack tip.

On the other hand, to verify results obtained by the developed xFEM program, many problems are solved to ensure that the program is works properly. The results have good agreement with reference ones. Thus, it can be said that the xFEM program can be used to simulate the mixed mode fatigue crack growth with a sufficient accuracy.

To sustain the non-proportional loading, the four cases are covered. For each case, several loadings are tested and in this paper each case has been presented with an illustrative example

At the end of this paper, the fatigue crack growth under mixed mode non-proportional loading is analyzed for four cases that used to describe the non-proportional loading. To compare the crack growth rate and the crack angle given by several K_{eff} formulas, a test case will be also derived.

ORANTISIZ YÜKLEME DURUMUNDA YORULMA ÇATLAK BÜYÜMESİ

ÖZET

Yüksek lisans tezi olarak oldukça yeni ve çalışılmamış bir alan olması hasebiyle orantısız yükleme durumunda yorulma çatlak büyümesi ele alınmıştır. Öncelikli olarak orantısız yükleme durumunda yorulma çatlak büyümesi konulu yüksek lisan tezin de kırılma mekaniği kısmında yapılan temel varsayımlar ve kabuller irdelenmiştir. Yapılan bukabuller liner elastik kırılma mekaniği ve küçük ölçekli akmadır. Bu iki kabu yüksek tekrarlı yorulma içiçin geçerlidir. Yorulma durumunda malzeme ler akla dayanımından düşük değerlerde bile hasara uğrayabilmette ve yorulma çatlağı ilerlemeye başlamaktadır. Liner elastisite kabulü yapılmasının temelnedeni yapılan çalışmada kulanılan malemeler için hesaplanan plastic zonun oldukça küçük çıkması ve dolayısıyla ihmaledilmesinden kaynaklanmaktadır. Ayrıca butez boyunca sadece 2 boyutlu plane problemler elealınmış ve dolayısıyla kırılma mekaniğinin Mode I (açılma - oppening) ve Mode II (kayma - sliding) durumları gözlenmektedir.

Çatlak büyümesinin modellenmesi için sonlu elemanlar yöntemi ve genişletilmiş sonlu elemanlar yöntemi en çok kullanılan iki methot tur. Klasik sonlu elemanlar yönteminde çatlak, boşluk ve yapısal düzensiliklerin tanımlanması oldukça karmaşık ve zorlayıcır. Bu düzensiliklerin tanımlanmasında klasıl sonlu elemanlar haklaşımında düzansizlikler eleman sınırlarında yer almalıdır. Deformasyon veya çatlak büyümesi gerçekleştiğinde meshin yenilenmesi gerekir. Yapılan bu mesh ortagonalikten uzak olmaklabir likle birden fala eleman çeşidinin kullanılmasına ihtiyaç vardır. Genişleilmiş sonlu elemanlar yönteminde ise her adımda meshin yenilenmesine ihtiyaç yoktur. Çünkü çatlak, boşluk ve yapısal bozukluklar zenginleştirme fonksiyonları yardımıyla kolayca tanımlanabilir. Çatlak modellemesinde iki tip zenginleştirme fonksiyonu kullanılmıştır. Bunlar Heaviside ve çatlak ucu zenginleştirmesi dir. Heaviside zenginleştirilmesi çatlak gövdesinin tanımlanması ve modellemesinde, çatlak ucu zenginleştirmesi ise çatlak ucunun bir eleman içinde tanımlanması ve modellenmesi için kullanıldı. Bu sayede her iterasyon adımın da tekrardan başa dönüp mesh yapma ihtiyacı ortadan kalkmış oldu.

Genişletilmiş sonlu elemanlar yönteminin for mülas yonunu oluşturmak ve genel teorisini açıklamak maksadı ile öncelikli olarak klasik sonlu elemanlar yönte mi tanımlandı ve formülasyonu verildi. Bunun içinde denge konumun dabulunan bir body ele alınarak virtüel iş denklemi yazılmış ve genel sonlu elemanlar yöntemi korunum denklemleri vasırasıyla elde edildi. Genişletilmş sonlu elemanlar yön teminin formülasyonuda aynı yaklaşımla elde edildi. Heaviside ve çatlak ucu zenginleştirme fonksiyonlarıda çatlağın tanımlan ması ve modellenmesinde kullanıldı. Sürekliliği çatlak tarafın dan bozulan elemanlar ve çatlak ucunu içeren elemanlar düzensizliğin oryantasyonuna bağlı olarak 4+4 veya 5+3 üçhene bölünerek stiffness matrisleri hesaplandı. Stiffness matrisleri yesaplamada “Gauss integrasyon methodu” kullanıldı. Eğer kare eleman crack gövdesini içeriyorsa 7 gauss

integrasyon noktalı üçgen elemanlar, eğer kare eleman çatlak ucu içeriyo ise 3 gauss integrasyon noktalı üçgen elemanlar kullanıldı. Bu sayede sayısal integras yon kolayca gerçekleştirilmiş oldu. Çatlağı tanımlamak için parçalı liner fonk siyon kullanıldı. Bu sayede her çatlak büyümesi kolayca programa eklene bilmektedir.

Mode I ve Mode II gerilme şiddet faktörlerini J-integral teorisi yardımıyla hesaplaya bilmek için interaction integral formülas yonları çıkartıldı. J-integrallin en önemli özelliği yoldan bağımsız olması ve kolayca hesaplana bilmesidir. J-integralini hesaplamak için J-yarıçapı denen ve hangi elemanların integrali hesaplamada kullanılacağını belirlememizi sağlar. J-integral yarıçapı genelde eleman boyunun 4-8 katı arasında seçilmesi önerilmektedir. Mode I gerilme şiddet fakörünü hesaplamak için 2. Durum pure mode I olarak seçildi ve gerilme, yerdeğiştirme ve geriinim denklemleri appendis A'da verildi. Mode II gerilme şiddet fakörünü hesaplamak için 2. Durum pure mode II olarak seçildi ve gerilme, yerdeğiştirme ve geriinim denklemleri appendis A'da verildi. Bu sayede gerilme şiddet fak törleri kolay ca hesaplana bilmektedir.

Mode I ve Mode II gerilme şiddet faktörlerini hesaplamak amacıyla genişletilmiş sonlu elemanlar yöntemi formülasyonu ve J-integral teorisi yardımıyla MATLAP'ta bir xFEM xprogramı yazıldı. Program tarafından elde edilen sonuçların doğrulunu irdelemek amacıyla 6 farklı problem irdelendi. Bu problemler

- metkez çatlağı içeren dörtgen bir plaka yer değişrirme sınır koşulu altında

- sabit mesnetli kenarlara paralel olarak uzanan merkez çatlağı içeren sonlu genişlikli bir plaka

- sabit mesnetli kenarlara paralel olarak uzanan köşe çatlağı içeren sonlu genişlikli bir plaka

- döndürülmüş metkez çatlağı içeren dörtgen bir plaka düzgün dağılımlı çekme gerilmesi altında

- döndürülmüş köşe çatlağı içeren dörtgen bir plaka düzgün dağılımlı çekme gerilmesi altında

- çarpık simetrik dönmüş çatlak

şeklinde listelene bilir. Hapılan karşılaşmakar da hesapalamlarda görülen en büyük hata %6'dan az olduğu görülmüştür. Bu da MATLAP'ta yazılan xFEM peogramı ile Mode I ve Mode II gerilme şiddet faktörlerinin istene doğruluk ile hesaplana bildiğini göstermekte dir.

Yorulma çatlak büyümesi tekrarlı yükleme altında çatlağıl ilerlemesi şeklinde tanımlanabilir. Yorulma çatlak büyümesini anlamak için iki temel büyüklüğün bilinmesi gerekir. Bunlar çatlak ilerleme oranı ve çatlak ilerleme doğrultusu dur. Çatlak ilerleme oranı ve stiffnesstaki değişme arasınsa ilişkiyi gösteren eğri üç farklı bölümden oluşmaktadır. Birinci bölüm de çatlak ilerleme oranı oldukça düşüktür ve stiffnesstaki değişme $K_{eşik}$ değerine ulaşmadan çatlak ilerlemeye başlamaz. Üçüncü bölümde ise çatlak ilerleme oranı oldukça büyüktür ve plastik zone dikate alınmalıdır. Ayrıca bu bölümde nonliner malzeme özelikleri de işin içine girmekte ve elastikplastik kırılma mekaniğinin kullanılmasını zorunlu kılmaktadır. İkinci bölgede ise çatlak ilerleme oranı 10^{-9} – 10^{-6} m/cycle aralığında kalır ve liner elastik kırılma mekaniği ve küçük ölçekli akmanın (britle kırılma) geçerli olduğu bölgedir. Diğer taraftan yorulma çatlak ilerleme doğrultusunu göstermek için litaratürde pek çok kriter mevcuttur. Fakat bunlardan ençok kullanılan ikisi maksimum teğetsel gerilme kriteri ve minimum gerilme enerji yoğunluğu faktörü kriteri dir. Maksimum teğetsel gerilme kriteri çatlağın teğetsel gerilmenin maksimum olduğu doğrultuda geçekleşeceğini söyler. Buda kayma gerilmesinin sıfır omasını gerektirir. Minimum gerilme enerji yoğunluğu faktörü kriteri çatlağın gerilme enerji yoğunluğu faktörünün minimum olduğu doğrultuda geçekleşeceğini söyler. Yapılan karşılaştırmada minimum gerilme enerji yoğunluğu faktörü kriteri için gereken çözüm zamanının çok fazla olduğundan, çatlak ilerleme doğrultusunu belirlemede maksimum teğetsel gerilme kriteri kullanıldı.

Bu tezin temel konusu orantısız yükleme durumunda yorulma çatlak büyümesi dir. Bunun içinde eğilme ve çekme gerilmeleri altında ve merkez çatlağı içeren ince cidarlı bir boru dan dan oluşan bir deney düeneği düşünüldü. Hem eğilme gerilmesi hem de çekme gerilmesi sabit ve cyclic kısımlardan oluşmaktadır. Bu sayede orantısız mixed mode yükleme durumu sağlanmıştır. Önerilen deney düzeneyi ise kayma ve çekme gerilmeleri altında merkez çatlağı içeren bir dikdörtgen plaka ile tanımlanmıştır. Orantısız mixed mode yükleme durumu sağlanmak için, hem kayma gerilmesi hem de çekme gerilmesi sabit ve cyclic kısımlardan oluşmaktadır. Orantısız mixed mode yükleme durumu sağlanmak için 4 farklı birleşim
- Durum 1: orantılı cyclic mix mode yükleme + sabit mode I ve/veya II
- Durum 2: cyclic mode I or II yükleme + orantılı sabit mix mode yükleme
- Durum 3: cyclic mode II + sabit mode I yükleme
- Durum 4: cyclic mode I + sabit mode II yükleme

düşünülebilir. Orantısız yükleme durumunda yorulma çatlak ilerlemesini belirlemek için hem çatlak ilerleme oranın hem de çatlak ilerleme doğrultusunun belirlenmesi gerekir. Çatlak ilerleme oranı hesaplamak üzere Paris Law'ın efektif gerilme şidet foktörü ile modifiye edilmiş hali kullanıldı. Efektif gerilme şidet foktörü Mode I ve Mode II gerilme şidet faktörlerinin fonksiyonu olup, literatürde sıklıkla mix mode yorulma çatlak ilerleme oranın belirlemede kullanılır. Literatürde ençok kullanılan 4 farklı efektif gerilme şidet foktörü formülü vardır. Bu formüller arasındaki fark sadece Mode I and Mode II gerilme şidet faktörlerinin efektif gerilme şidet foktörü içindeki ağırlıklarıdır. Çatlak ilerleme doğrultusu daha öncede belirtildiği üzere maksimum teğetsel gerilme kriteri uyarınca hesaplanmaktadır. Bir yükleme çevrimi boyunca çatlak ilerleme doğrultusu ortalama şeklinde K_{eff} ile ağırlıklandırılarak hesaplandı. Hesaplama sırasında K_{eff} değerlerinin yalnızca artan kısımları dikate alındı. Diğer taraftan, yorulma çatlağı belirli sayıdaki yükleme çevrimi için çatlağın aynı çatlak ilerleme oranı ve çatlak ilerleme doğrultusu ile ilerler.
Daha öncede belirtildiği üzere orantısız yükleme durumunda yorulma çatlak ilerlemesini simule etmek için 4 farklı durum ele alındı. Dört farklı durum birer örnrk ile sunulmuştur. Her örnekte 4 farklı K_{eff} formülü için orantısız yükleme durumunda yorulma çatlak ilerlemesi simule edilmiştir. Yapılan bu hesaplamalar neticesinde elde edilen sonuçlar yazılan bu tezde detaylı olarak sunulmutur. Elde edilen sonuçlar uyarınca daha önceden yapılan liner elastik kırılma mekaniği ve küçük ölçekli akma kabulerinin geçerli olduğu görülmüştür. Çatlak ilerlemesi tüm K_{eff} formüleri için aynı olarak tahmin edilmiştir. Çatlak ilerleme oranı 10^{-9} – 10^{-6} m/cycle aralığında kalmakla birlikte yorulma çatlağı için tanımlanan ikinci bölgede kalmaktadır. Bu bölge liner elastik kırılma mekaniği ve küçük ölçekli akma kabulerinin geçerli olduğu bölgedir.

Bu tezin diğer önemli bir amacı ise 4 farklı K_{eff} formülü için bir karşılaştırma criteri bulmaktır. Bu doğrultuda pek çok denemeden sonra bi test durumu bulundu. Bu durum için yapılan simulasyon sonucunda elde edilen sonuşlar da göstermektedirki orantısız yükleme durumunda yorulma çatlak ilerlemeleri her formül için farklılık göstermektedir. Buyüzden bulunan test durumu hangi K_{eff} formülü orantısız yükleme durumunda yorulma çatlak ilerlemesinin belirlenmesinde en iyi neticeyi verdiğini tespit etmekte kullanılabilir.

1. INTRODUCTION

The most of advanced mechanical application includes both static load and cycle load like engine components. The crack growth for such components is consisting of both growth due to static loading and growth due to cyclic loading. The combination of two loadings creates non-proportional loading where the crack growth behavior is slightly different from proportional loading. To examine the fatigue crack growth, many parameters and several methods are suggested for obtaining enough correlations between numerical and experimental anabasis under all loading conditions. The experiments done by Qian and Fatemi [1] on fatigue crack growth imply that the crack growth associates with material properties, load magnitude and its modes, initial crack tip conditions, and mean stress. That is why multiple comparisons between numerical and experimental results are needed to evaluate the fatigue crack growth correctly.

In the literature, there are several methods to demonstrate the all modes of fracture where any domain with an arbitrary shaped crack is discretized into elements and the discretization is necessary to be upload for each crack extension so that the elements defines the shape of the arbitrary growing crack correctly. Thus, to simulate the fatigue crack growth under non-proportional loading, Extended Finite Element Method (xFEM) is selected. The extended finite element method is a powerful tool to simulate the crack growth by means of that it is capable of defining discontinuities, such as cracks, holes and inclusions, within elements easily. Any discontinuities within elements are modeled by introducing extra degrees of freedom with enrichment functions into the nodes. That is why xFEM removes the need for matching element boundaries with a crack, a hole boundary and/or an inclusions. This enables usage of a single mesh even if the crack propagates in many times. Thus, there is no need for remeshing in each step of crack propagation except the mesh refinement may be necessary in any stage.

The analyzed problems in this paper are limited with Linear Elastic Fracture Mechanics and Small Scale Yielding where it is valid for high cycle fatigue. The low cycle fatigue is ignored in this paper where large deformation occurs and the effects of plasticity cannot be vanished. The modes of fracture are represented at each crack tip by stress intensity factors, generally based on the path independent J integral by Rice [2]. The first expression between the stress intensity factor and the crack growth rate was derived by Paris and Erdogan [3]. It is known as Paris law and demonstrates the region II on the plot of the crack growth rate respect to the stress intensity factors in logarithmic scale. Latterly, another expression was derived by Erdogan and Ratwani [4] which takes the ratio $R = K_{max}/K_{min}$ into account. The expression describes all three regions between the threshold stress intensity factor and the critical stress intensity factor. Although Paris law was derived for cracks only exposed to mode I loading, it have been suggested by several researchers for mixed mode loading by introducing an effective stress intensity factor into Paris law. Furthermore, beside the fatigue crack growth rate it is important to determine the crack growth angle for the fatigue crack growth. Maximum tangential stress criterion and Minimum strain energy density criterion are the most used criterions to determine the crack growth direction. The two criteria will be discussed in more detail in the later sections.

To simulate fatigue crack growth under mixed mode non-proportional loading, linear elastic fracture mechanic and small scale yielding (concept of brittle fracture) are assumed by employing the modified Paris law and maximum tangential stress criterion where the mixed mode non-proportional loading is sustain with four different cases. The non-proportional loading can be sustained by four cases, depending on definition of the torsion and the tension,

Case 1: a cyclic proportional mixed mode loading + a static mode I and/or II

Case 2: a cyclic mode I or II + a static proportional mixed mode loading.

Case 3: a cyclic mode II + a static mode I loading

Case 4: a cyclic mode I + a static mode II loading

The modified Paris law is used to evaluate fatigue crack growth rate while the fatigue crack growth angle is calculated as an average where it is weighted by K_{eff} for increasing part of K_{eff}. Furthermore, four examples are performed for determination of the fatigue crack growth under mixed mode non-proportional loading.

At the end of this paper, the fatigue crack growth under mixed mode non-proportional loading is analyzed for four cases that used to describe the non-proportional loading. To compare the crack growth rate and the crack angle given by several K_{eff} formulas, a test case will be also derived.

2. FRACTURE MECHANICS

An overview of the Linear Elasric Fracture Mechanic concept will be mentioned in this section related to xFEM.

2.1 Origin of Linear Elastic Fracture Mechanics

One of the most useful tools for simulating crack in fracture mechanic is extended finite element method, used in this paper to simulate mix-mode fatigue crack growth under non proportional loading. The mix-mode fatigue crack growth or propagation is simulated based on linear elastic fracture mechanic. So that, in this section of the paper the basic concept of linear elastic fracture mechanic is presented.

In recent years in fracture mechanic much study has been done. It is not an exaggeration if anyone says that one of the earliest work done by Inglis [5] who analyzed elliptical holes in flat plates under tension as illustrated in Figure 2.1.

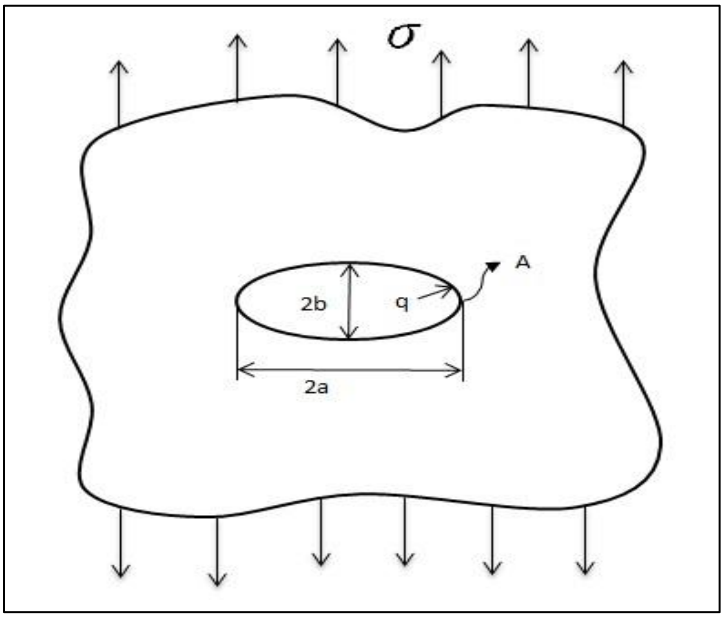

Figure 2.1 : Elliptical hole in a flat plate - if 2b goes to near zero, the elliptical hole is converted to a sharp crack where point A becomes the crack tip.

If the length of any ellipse is kept constant while the width is closing to zero, the elliptical hole will turn into a sharp crack. Inglis' works showed that at the crack tip of the crack shaped elliptical hole, the stress went to infinity while the radius of curvature ρ approaches to zero. But in reality no material can be kept infinite stress at crack tip before fracture occurs. To solve the paradox, Griffith [6] successes a n energy based fracture theorem such as the crack initiate or propagate only if such a process results in the total energy to decrease or no change. Based on the energy balance theory, Griffith derived an expression for the stress at crack tip of an infinite plate. The expression for an ideally brittle solid, like glass, becomes as:

$$\sigma_f = \left(\frac{2\,E\,\gamma_s}{\pi\,a}\right)^{1/2} \qquad (\mathbf{2.1})$$

where E is Young's modulus, a is half crack length and $\gamma_s$is the elastic work per unit area of surface created. The Griffith's expression of the remote stress is lack of capturing the plastic flow. It is enlarged to materials, capable to plastic flow – like metals, by both Irwin [7] and Orowan [8] independently. The modified Griffith's expression is

$$\sigma_f = \left(\frac{2\,E\,(\gamma_s+\gamma_p)}{\pi\,a}\right)^{1/2} \qquad (\mathbf{2.2})$$

where γ_p is the plastic work per unit area of surface created and mostly larger than γ_s. In 1956, Irwin [9] derived a fracture theory, fundamentally equivalent to Griffith's model, based on energy. Irwin defined an energy release rate G, which is a measure of the energy available for an increscent of crack extension:

$$G = -\frac{d\Pi}{dA} \text{ and } \Pi = U - F \qquad (\mathbf{2.3})$$

where Π is the potential energy of an elastic body, U is the strain energy stored in the body and F is the work done by external forces. All of the works that briefly mentioned above made an essential contribution to Linear Elastic Fracture Mechanic.

Linear elastic fracture predicts that the stress reaches infinity in the crack tip, but in practice it is just assumed as creating a plastic zone at the crack tip. If the size of the plastic zone is sufficiently small, the LEFM or Brittle Fracture is still valid. Thus elastic analysis for many different mechanical problems, like mix-mode fatigue crack growth under non-proportional loading, is still valid if plastic zone is too small.

2.2 Basics Modes of the Fracture Mechanic

Examination of many different types of catastrophic fractured strictures shows that the fracture is originate from stress concentration and geometrical discontinues, a sharp change of geometry like an opening, a hole, a notch, a crack, etc. For isotopic linear elastic materials the stress field in a cracked body under any loading condition can be easily derived as a closed form expression. Westergaard [10], Irwin [9] and Williams [11] published many salutations for the stress fields. For such configurations as illustrated in Figure 2.2, the stress field σ_{ij} near the crack tribe is given by

$$\sigma_{ij} = \left(\frac{k}{\sqrt{r}}\right) f_{ij}(\theta) + \sum_{m=0}^{\infty} A_m r^{\frac{m}{2}} g_{ij}^{(m)}(\theta) \qquad \mathbf{(2.4)}$$

where r and θ are local polar coordinates at crack tip, k is a constant, f_{ij} is a function of θ and Higher order terms, A_m is aplitute and $g_{ij}^{(m)}$ is a dimensionless function of θ depends, on the configuration.

The solution for any configuration the stress field has a singularity of $1/\sqrt{r}$ near crack tip while the displacement field has a $\sqrt{r}$ singularity because of the term $1/\sqrt{r}$ approaching to infinity while r goes to zero and first part of stress equation also approaching to infinity although the higher order terms remains finite. The full expressions for the pure mode I and mode II stresses and displacements are given in Appendix A, reproduced from Jensen [12], for both Cartesian and Polar coordinate

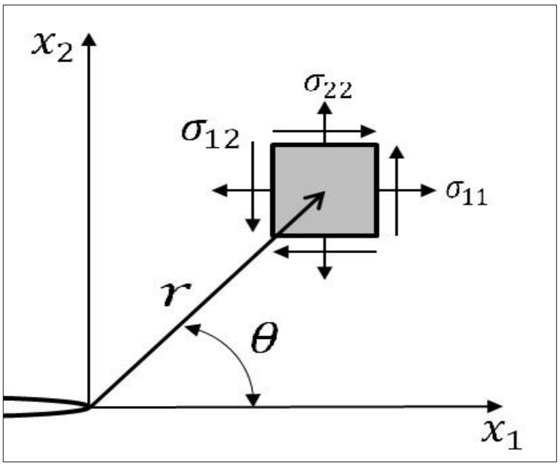

Figure 2.2 : Definition of the coordinate systems, the Polar coordinates- $\mathbf{r}, \boldsymbol{\theta}$ and, the Cartesian coordinates - $\mathbf{x_1}, \mathbf{x_2}$.

systems. Figure 2.3 illustrates the tree independent crack opening modes. In the opening mode *I*, crack surfaces are pulled apart in the normal direction x_2 but remain symmetric about the x_1x_3 and x_1x_2 planes. The shearing mode II represents the sliding mode of movement of crack surfaces in the x_1 direction, while remaining symmetric about the x_1x_2 plane and skew symmetric about the x_1x_3 plane. Finally, in the tearing mode III, the crack surfaces slide over each other in the x_3 direction, while remaining skew symmetric about the x_1x_2 and x_1x_3 planes.

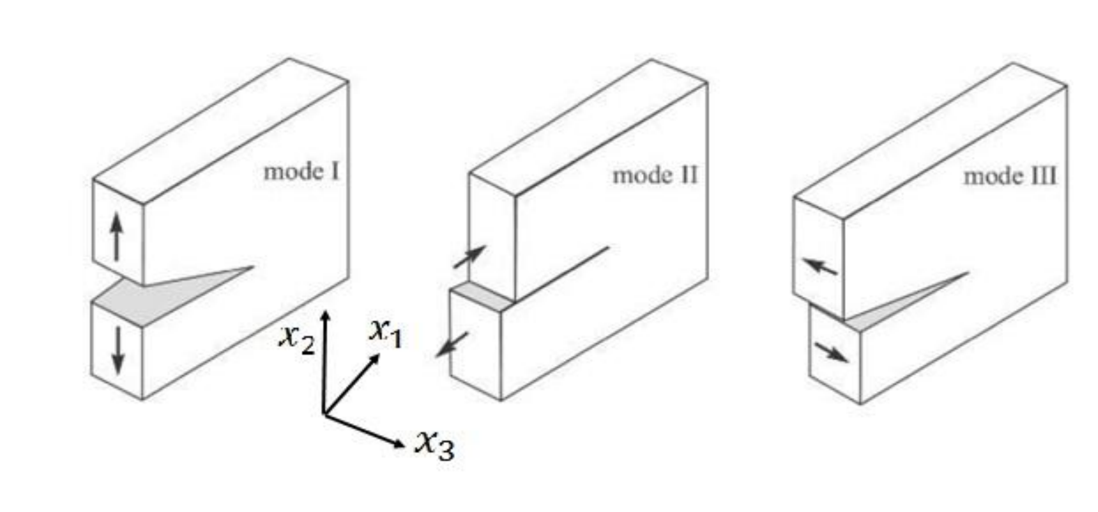

Figure 2.3 : Basic modes of fracture: Mode I, II and III.

In this paper, only 2D plane problems are going to cower to simulate mix-mode fatigue crack growth under non proportional loading. Thus, mod III is not considered any more in this paper.

2.3 Size of Plastic Zone and Concept of Small Scale Yielding

Linear elastic fracture mechanic is valid for a sufficiently small plastic zone. Linear elastic fracture mechanic can be applied to plastically deforming materials provided the region of plastic deformation is small. To estimate the size plastic zone, two approaches, elastic and elastoplastic models, can be considered. As seen from the Figure 2.4 (a), the elastic model simply ignores all the stresses that exceed the yield stress near crack tip, where r_y is the radius of plastic zone. The elastic model is lack of satisfying the equilibrium anymore. Thus, more complicated model is needed. The elastoplastic model was developed by Irwin by means of redistribution of the stress near the crack tip to satisfy the equilibrium in Figure 2.4 (b). the elastoplastic model estimates the radius of plastic zone r_p as twice of r_y.

The size of plastic zone can be estimated as

$$r_p = 2r_y = \begin{cases} \frac{1}{\pi}\left(\frac{K}{\sigma_y}\right)^2 \; for\ plane\ stress \\ \frac{1}{3\pi}\left(\frac{K}{\sigma_y}\right)^2 \; for\ plane\ strain \end{cases} \tag{2.5}$$

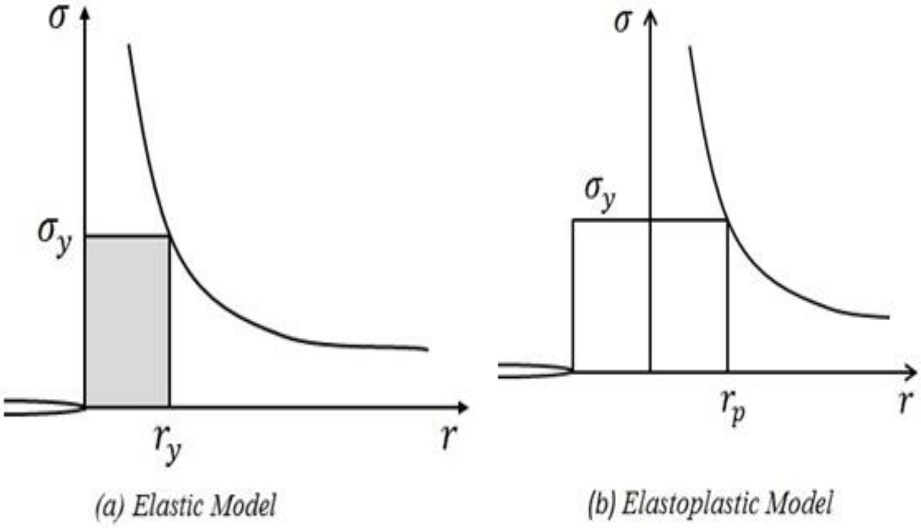

Figure 2.4 : Plastic zone models: Elastic and Elastoplastic.

where K is the stress intensity factor it gives exact solution just for pure mode III and it becomes a circle.

The stress reaches theoretically infinity at the crack tips under the assumptions of linear elastic fracture mechanics. But, in fact, any material cannot resist infinite stress, and a small plastic zone will be formed around the crack tip. But, during this report the effect of the plastic zone is ignored due to fact that brittle crack propagation will be modeled based on linear elastic fracture mechanics (LEFM) where small scale yielding still valid.

2.4 Path Independent J-integral

The path independent J-integral was firstly defined by Eshelby [13] and then it was applied to the fracture mechanic by Rice [14]. The J-integral is given by

$$J = \int_{\Gamma} \left(W\delta_{1j} - \sigma_{ij}u_{i,1}\right)n_j d\Gamma \tag{2.6}$$

where $W = \frac{1}{2}\sigma_{ij}\varepsilon_{ij}$ is the strain energy dencity for linear elasticmaterial and n_j is the outward normal of the path Γ. The integral is independent for any choice of the path Γ. LEFM with small-scale yielding leads the J-integral to be written as a function of the stress intensity factors,

$$J = \frac{K_I^2}{E'} + \frac{K_{II}^2}{E'} \quad \mathbf{(2.7)}$$

where plane stress and plane strain conditions can be written as

$$E' = \begin{cases} E & for\ plane\ stress \\ \dfrac{E}{1-\nu^2} & for\ plane\ strain \end{cases} \quad \mathbf{(2.8)}$$

E and ν are Young modulus and passion's ratio, respectively.

The J-integral will be used through this report for the problems which involves the small strains (SSY), no body force (the stress are negligible due to gravity or magnetic field) and linear elastic material behavior.

3. FINITE ELEMENT METHOD

Classical FEM is mentioned in this section to establish some matrix necessary for xFEM. The classical FEM is applied to solve mechanical problems, like crack growth, by discretizing a domain into a finite number of elements. For increase the accuracy of the solution, it is necessary to decrease the element length. But, decreasing the element length too much is unnecessary due to fact that the approximated solution does not converge any more. Thus, it is necessary to use a proper element length to save both solution time and storage capacity.

3.1 Governing Equations

Consider a body in the state of equilibrium with the boundary conditions, the traction and the displacement conditions, as shown in Figure 3.1. In domain **Ω**, the equilibrium equation of elasticity can be written as:

$$\sigma_{ij,j} + f_i^b = 0 \qquad \mathbf{(3.1)}$$

with the associated boundary conditions according to the domain **Ω**:

$$\left.\begin{array}{lll} \sigma_{ij} \cdot n_i = f_i^t & \text{on} & \Gamma_t \\ u = \bar{u} & \text{on} & \Gamma_u \\ \sigma_{ij} \cdot n_i = 0 & \text{on} & \Gamma_c \end{array}\right\} \qquad \mathbf{(3.2)}$$

where Γ_t , Γ_u and Γ_c are traction, displacement and crack boundaries, σ is stress tensor and, f^b and f^t are body forces and tractıon vectors. The weak form of the principle of virtual work can be defined as:

$$\left.\begin{array}{c} W^{internal} = W^{external} \\ or \\ \displaystyle\int_{\Omega} \sigma \;\delta\varepsilon \, d\Omega = \int_{\Omega} f^b \,\delta u \, d\Omega + \int_{\Gamma^t} f^t \;\delta u \, d\Gamma \end{array}\right\} \qquad \mathbf{(3.3)}$$

where constitutive law is given by $\sigma_{ij} = C_{ijkl}\,\varepsilon_{kl}$ and the strain - displacement relations for small scale yielding is given by $\varepsilon_{kl} = \frac{1}{2}\left(u_{k,l} + u_{l,k}\right)$. Without any body

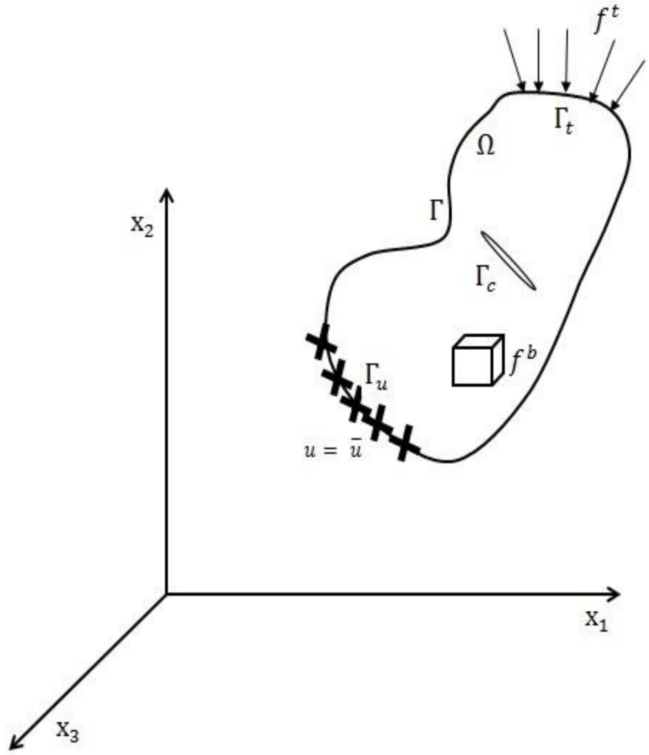

Figure 3.1 : A body in the state of equilibrium with a traction free crack.

forces and an initial strain and, by substituting constitutive law (the strain - displacement relations) in to principle of virtual work, one can easily find that:

$$\int_{\Omega} \{\delta\varepsilon\}^T \, [C] \, \{\varepsilon\} d\Omega \; = \; \int_{\Gamma^t} \{\delta u^h\}^T \{f^t\} d\Gamma \qquad (\mathbf{3.4})$$

over T means transpose of varıable matrices it is added to take care for matrices dimensions.

The principle of virtual work states that the stored strain energy due to an applied admissible virtual displacement field is balanced by the applied outer work. The principle of virtual work can be applied to the full domain as well as to a subdomain corresponding to the boundary conditions. That is why the principle of virtual work can be applied to each element by composing the necessary element matrices.

3.2 Element Discretization

The body is discretized in many elements that consist of a set of nodes, each having a number of degrees of freedom. Those unknowns are generally displacements and/or rotations for mechanical problems. In the present project only 2D plane problems are going to be covered by using 2D quadrilateral elements with four nodes. As seen from Figure 3.2 (a), each node has two unknown displacements, means two degrees of freedom. The approximation of the standard FEM is of the form

$$u^h(x) = \sum_{i \in I} N_i(x) u_i \qquad (\mathbf{3.5})$$

where I is the set of nodes, $N_i(x)$ are values of classical finite element shape functions at each nodes. For 2D quadrilateral elements with four nodes, the shape functions are

$$\left.\begin{aligned} N_1 &= \frac{1}{4}(1-\xi)(1-\eta), \quad N_2 = \frac{1}{4}(1+\xi)(1-\eta) \\ N_3 &= \frac{1}{4}(1+\xi)(1+\eta), \quad N_4 = \frac{1}{4}(1-\xi)(1+\eta) \end{aligned}\right\} \qquad (\mathbf{3.6})$$

which takes value of one at the current node and value of zero at all other nodes. In matrix notation the approximation of the standard FEM is of the form

$$\{u^h\} = [N]\{u\}, [N] = \begin{bmatrix} N_1 & 0 & N_2 & 0 & N_3 & 0 & N_4 & 0 \\ 0 & N_1 & 0 & N_2 & 0 & N_3 & 0 & N_4 \end{bmatrix} \qquad (\mathbf{3.7})$$

By using the strain-displacement matrix [B], the strain field can be write as

$$\{\varepsilon\} = [B]\{u\} \qquad (\mathbf{3.8})$$

where the strain-displacement matrix includes derivatives of the shape functions according to the global coordinate system. But, the shape functions cannot be directly differentiated respect to the global coordinate system in the isoperimetric formulation that enables to use non-rectangular elements. By following the mythology in Cook *et al.* [15], the link between derivatives of shape functions respect to global coordinate system (x_1 – x_2) and derivatives of shape functions respect to mapped coordinate system (ξ - η) can be easily set up for any field variable ϕ by applying chain rule as:

$$\begin{Bmatrix} \phi_{,\xi} \\ \phi_{,\eta} \end{Bmatrix} = \begin{Bmatrix} \phi_{,1}\, x_{1,\xi} + \phi_{,2}\, x_{2,\xi} \\ \phi_{,1}\, x_{1,\eta} + \phi_{,2}\, x_{2,\eta} \end{Bmatrix} = \begin{bmatrix} x_{1,\xi} & x_{2,\xi} \\ x_{1,\eta} & x_{2,\eta} \end{bmatrix} \begin{Bmatrix} \phi_{,1} \\ \phi_{,2} \end{Bmatrix} = [J] \begin{Bmatrix} \phi_{,1} \\ \phi_{,2} \end{Bmatrix} \qquad (\mathbf{3.9})$$

where $[J]$ is the Jacobean matrix. Referring to Appendix B.1 the strain-displacement matrix [B] can be written as

$$[B] = [L][\Gamma][N,] \tag{3.10}$$

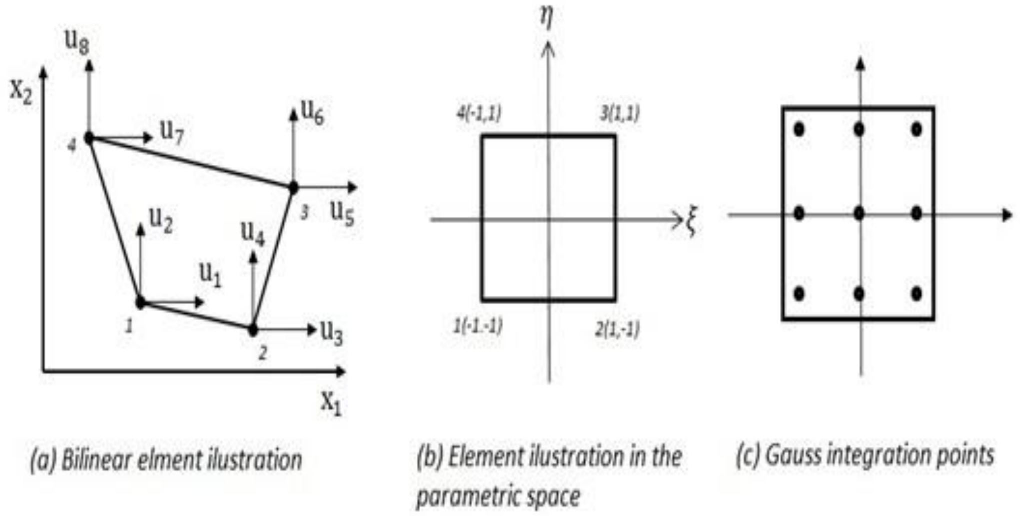

Figure 3.2 : Element illustration in global and mapped coordinates systems and, gauss integration point illustration for number of order of 3.

where [N,] is derivatives of shape functions respect to the mapped coordinate system, $[\Gamma] = [J]^{-1}$ is the inverse of the Jacobean matrix and [L] is link matrix.

3.3 Element Stiffness and Global Stiffness Matrices

From $\{u^h\} = [N]\{u\}$ virtual displacements and $\{\varepsilon\} = [B]\{u\}$ virtual strains can be written as $\{\delta u^h\}^T = \{\delta u\}^T[N]^T$, $\{\delta\varepsilon\}^T = \{\delta u\}^T[B]^T$. By means of δu and δε formulations, the principle of virtual work can be written as:

$$\int_{\Omega} \{\delta u\}^T\, [B]^T[C][B]\,\{u\}\, d\Omega \;= \int_{\Gamma_T} \{\delta u\}^T\, [N]^T\{T\}\, d\Gamma \tag{3.11}$$

Due to the virtual displacements $\{\delta u\}^T$ and its independency of the coordinates of nodes, the principle of virtual work can be rearranged as:

$$\{\delta u\}^T \left(\int_{\Omega} [B]^T[C][B]\,\{u\}\, d\Omega - \int_{\Gamma_T} [N]^T\{T\}\, d\Gamma \right) = 0 \tag{3.12}$$

where the volume integral takes place over current element and the surface integral on the current element surfaces, which contains applied loads, like tension or shear.

Equation (3.11) can be written for an element as:

$$[k]\{u\} = [f] \qquad (\mathbf{3.13})$$

where $[k]$ the element stiffness matrix and $[f]$ the load vector for the current element are expressed by

$$[k] = \int_{\Omega} [B]^T[C][B]\,\{u\}\,d\Omega\ , \qquad [f] = \int_{\Gamma_T} [N]^T\{T\}\,d\Gamma \qquad (\mathbf{3.14})$$

To assemble the global equation system, $[K]\{U\} = [F]$, for the whole body, it is necessary to set up the link between K_{kl} and k_{ij}. During the assemble presses, the K_{kl} become summation of the k_{ij} for any elemant and ij mapes the k_{ij} for the current element to kl, indicate the location of the K_{kl} in the global equation system. The force vector is also assembled the similar way, except it just a vector.

To solve the global equation system it is necessary to apply the sufficient boundary conditions to avoid singularity. Boundary condition is generally to fix the displacements in x_1 and/or x_2 in any node. To fix the displacement for the current node, n, nth row and coulomb are skipped from the global equation system and then it is solved by any solver.

3.4 Gauss Integration Method

Due to usage of the shape functions in the isoperimetric formulation to interpolate many field variables in the equation system, especially in the stiffness matrix, it is necessary to assemble a numerical integration procedure. One of the most popular and the best suited procedures is the Gauss quadrature method, cf. Cook *et al.* [15], enables to write the integral as a summation of the integrand over a set of Gauss points indicated in Figure 3.2 (c). Let $\phi(\xi_i, \eta_j)$ as the integrands in the stiffness matrix, in Equation (3.13). The stiffness matrix for the current element, by using the Gauss integration method, can be evaluated as

$$[k] = \sum_{i=1}^{n_g}\sum_{j=1}^{n_g} W_i W_j \phi(\xi_i, \eta_j)\ t\,|J|\,d\xi d\eta \qquad (\mathbf{3.15})$$

where $|J|$ is the determinant of the Jacobian matrix defined in Equation (B.3) and t is the thickness of the current element.

Depending on number of Gauss order, the values of ξ_i, η_j and W_i are presented in Appendix C.

4. EXTENDED FINITE ELEMENT METHOD

In this section formulations and methodology of xFEM is described by extended the FEM described in the previous section. Extension is mainly based on enrichment functions. Any arbitrarily oriented discontinuities, for example a crack, an inclusion and a hole etc., can be modeled independent of the finite element mesh by enriching all elements cut by a discontinuity using enrichment functions, which satisfy the discontinuous behavior and result in additional nodal degrees of freedom. Thus, xFEM is one of the most useful tools to simulate the crack problems.

4.1 Element Discretization

The discretization of the body is made by the enrichment functions in xFEM, remove the necessity of that the discontinuities must take place in the element boundary in standard FEM. Although different types of Enrichment function exists in the literature, only the Heaviside enrichment for defining the crack body and the crack tip enrichment for defining the crack tip will be covered in this paper.

4.1.1 Heaviside enrichment

To illustrate the heavy side enrichment and the discretization by means of xFEM formulations, consider an edge crack modeled by four elements illustrated in Figure 4.1(a) According to standard FEM formulation (3.5), any displacement for the mesh in Figure 4.1(a) is given by

$$\{u^h\} = \sum_{i=1}^{10} N_i \, u_i \qquad \mathbf{(4.1)}$$

To formulate Equation (4.1) according to xFEM formulation with a Heaviside enriched node, the mesh is used as illustrated in Figure 4.1(b). The edge crack problem has the uniform mesh shown in Figure 4.1(b) and a strong discontinuity, the crack. Both the mesh in Figure 4.1(a) and the mesh in Figure 4.1(b) represent the same edge crack problem. For reformulation of Equation (4.1) in the xFEM, the way, followed, is represented by Moës *et al.* [16].

Although the uniform mesh in Figure 4.1(b) is lack of defining the crack geometrically as the mesh defines in Figure 4.1(a), by introducing the function $f(x)$, it is possible to define the crack. The function $f(x)$ is defined according to the local coordinate system at the crack tip and changes its sign by passing the discontinuity, the crack. Heaviside function, in terms of $f(x)$, can be defined as

$$H\big(f(x)\big) = \begin{cases} -1, & f(x) < 0 \\ \ \ 1, & f(x) > 0 \end{cases} \tag{4.2}$$

The evaluation of the Heaviside function, in terms of $f(x)$, will be cover in the next section in more detail.

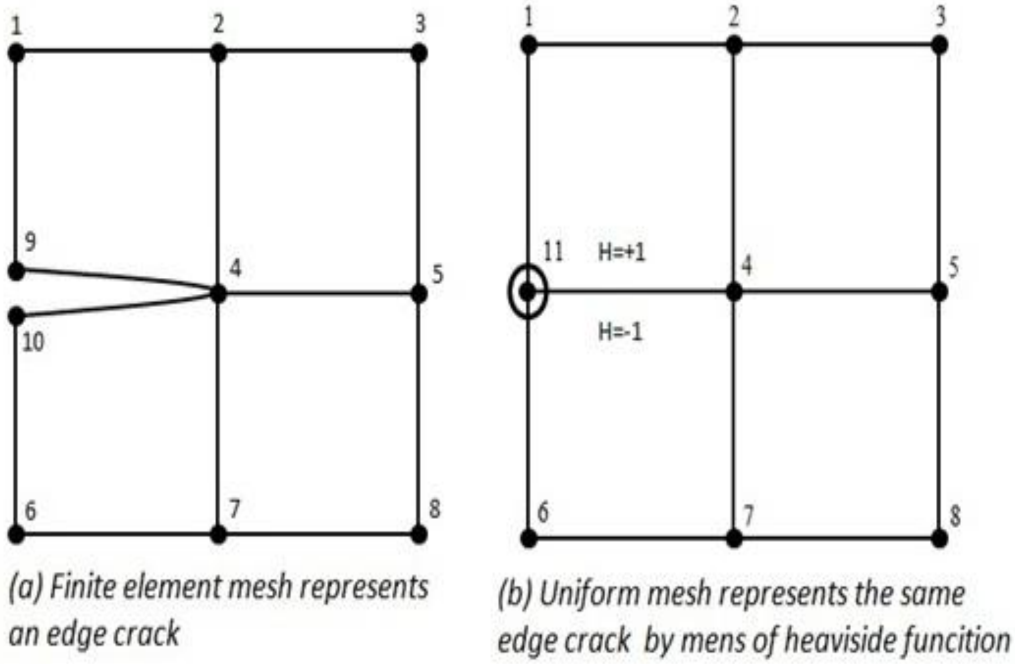

Figure 4.1 : Crack tip represented by a classical mesh and by a uniform mesh with an enriched node used in the extended finite element formulation.

By defining a and b as

$$a = \frac{u_9 + u_{10}}{2}, \qquad b = \frac{u_9 - u_{10}}{2} \tag{4.3}$$

and the displacement u_9 *and* u_{10} can be written in terms of a and b as

$$u_9 = a + b, \qquad u_{10} = a - b \tag{4.4}$$

By substituting (4.4) into (4.1), it gives

$$\{u^h\} = \sum_{i=1}^{10} N_i\, u_i = \sum_{i=1}^{8} N_i\, u_i + N_9(a+b) + N_{10}(a+b)$$

$$= \sum_{i=1}^{8} N_i\, u_i + (N_9 + N_{10})\, a + (N_9 - N_{10})\, b \qquad \mathbf{(4.5)}$$

Heaviside function takes the values of minus one at the node 9, where $f(x) > 0$ and one at the node 10, where $f(x) < 0$, it yields that

$$(N_9 - N_{10}) = H\big(f(x)\big)(N_9 + N_{10}) \qquad \mathbf{(4.6)}$$

As seen from the mesh in Figure 4.1(b), $N_9 + N_{10}$ can be replaced by N_{11} and, a by u_{11}. The FEM approximation in Equation (4.5) transform into

$$\{u^h\} = \underbrace{\sum_{i=1}^{8} N_i\, u_i + N_{11}u_{11}}_{sclassical\ FEM\ formulation} + H\big(f(x)\big)N_{11}b \qquad \mathbf{(4.7)}$$

As seen from Equations (4.7) and (4.1), the FEM discretization transform into the xFEM discretization. The discretization according to the standard finite element method formulation is equivalent of the extended finite element method formulation.

4.1.2 Crack tip enrichment

Crack tip enrichment is done by the way of the branch functions, which enable to define the crack tip ended inside of an element as illustrated in Figure 4.2. To define the branch functions, the local crack tip coordinate system is used. The branch functions are given by the formula

$$F_l = \left\{\sqrt{r}\sin\frac{\theta}{2},\ \ \sqrt{r}\cos\frac{\theta}{2},\ \ \sqrt{r}\sin\theta\sin\frac{\theta}{2},\ \ \sqrt{r}\sin\theta\cos\frac{\theta}{2}\right\} \qquad \mathbf{(4.8)}$$

where $r\ and\ \theta$ are the local crack tip coordinate system for each of the crack. By using a linear combination of four branch functions in Equation (4.8), eight additional degree of freedoms must be added to each crack tip enriched node.

The branch functionF_1, only, is discontinues at the crack faces due to $\theta = \pm\pi$ while the tree remaining branch functions $F_{2,3,4}$ are continuous. Although, the branch function F_1 is enough to simulate the discontinuity, the crack tip - ends inside of an element, all of the branch functions will be used through this report to increase the accuracy of the solution, obtained by xFEM.

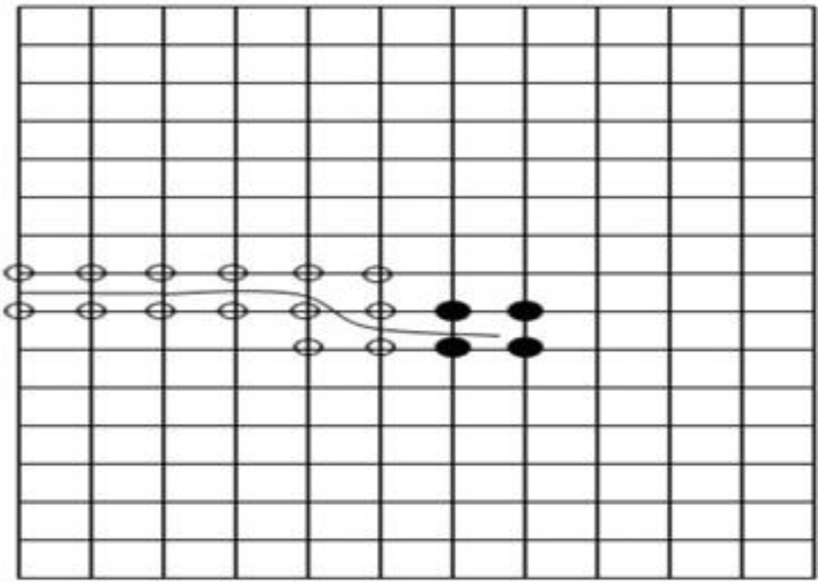

Figure 4.2 : Uniform mesh to define an edge crack, where nodes marked by open circles are enriched by the Heaviside function to define the crack body, and nodes marked by filled circles are enriched by branch functions to define the crack tip.

4.1.3 General X-FEM approximation for crack modeling

Moës *et al.* [16] proposed that in order to model crack surfaces and tips the extended finite element method can be generalized as below

$$u^h = \sum_{i=1}^{n} N_i(x)\ u_i + \sum_{j=1}^{m} H\big(f(x)\big)N_j(x)\ b_j\ + \sum_{k=1}^{mct_1} N_k(x)\left(\sum_{l=1}^{4} F_l^{ct_1}(x)\ c_k^{l1}\right)$$
$$+ \sum_{k=1}^{mct_2} N_k(x)\left(\sum_{l=1}^{4} F_l^{ct_2}(x)\ c_k^{l2}\right) \qquad (\mathbf{4.9})$$

n is the set of nodes that follows the classical finite element approximation due to not containing any discontinuity where u_i are the nodal displacements (standard DOFs). m is the set of nodes that includes the discontinuity such that starts and ends on the element faces, not inside of the element. Those set of nodes are the nodes, are used to describe the crack faces. mct_1 and mct_2 are the set of nodes associated with crack tip 1 and 2 due to fact that they describe the discontinuity ends inside of the two elements, include each of crack tips separately. b_j, c_k^{l1} and c_k^{l2} are the vectors of additional degrees of nodal freedom for modeling crack faces by means of Heaviside enrichment and the two crack tips by means of Crack tip enrichment, respectively, and $F_l^{ct_1}(x)$ and $F_l^{ct_2}(x)$ represent the crack tip enrichment functions at each of the crack tips.

4.2 Element Stiffness and Global Stiffness Matrices for the xFEM

The xFEM approximation presented in Equation (4.9) on the element level can be written with matrix notation as

$$\{u^h\}_{2x1} = [N]_{2x8}\,\{u\}_{8x1} + H[N^b]_{2x2j}\,\{b\}_{2jx1} + [N^c]_{2x2k}[F]_{2kx16k}\,\{c\}_{16kx1} \quad (\mathbf{4.10})$$

The matrix formulation of discretization above allows the crack tips to be implicit and the evaluation of Heaviside function or the branch functions based on the nodal values of the shape functions at the current point (in practice at the current gauss integration point). The superscripts b and c present the shape functions related to b – DOFs and c – DOFs, respectively. j and k in the equation (4.10) represent the number of the nodes associated with b – enrichment (Heaviside enrichment) and c – enrichment (the crack tip enrichment), respectively. The structures of the last two terms of Equation (4.10) are given by Appendix B.2 and B.3, separately.

As the procedure followed in the previous section, it is necessary to recall the principle of virtual work to evaluate the necessary matrices for the xFEM approximation. The principle of virtual work from Equation (3.4) is

$$\int_{\Omega} \{\delta\varepsilon\}^T\,[C]\,\{\varepsilon\}d\Omega \;=\; \int_{\Gamma^t} \{\delta u\}^T\{f^t\}d\Gamma \qquad (\mathbf{4.11})$$

Strain-displacement matrices are needed to obtain the strains from $\{u\}, \{b\}$ and $\{c\}$. The Strain-displacement matrices related with the classical degree of freedom is already given in Equations (3.8). The strain-displacement matrix relates the b – DOFs is similar the matrix obtained for the classical degree of freedom previously due to fact that the derivation just incudes shape function. The Heaviside function takes the values of -1 and +1 when passing the crack where its derivative is zero and it appears as a coefficient in front of the strain-displacement matrix. The evaluation of Strain-displacement matrix $[B^b]$ for b – DOFs is presended in Appendix B.2. $[B^b]$ is given by

$$[B^b] = [L][\Gamma][N_{,}^{b}] \tag{4.12}$$

For the c – DOFs the situation is not similar because both derivatives of the shape functions and the branch functions. The derivatives can be obtained easily by employing the chain rule. The evaluation of strain-displacement matrix $[B^c]$ for c – DOFs is presented in Appendix B.3. $[B^c]$ is given by

$$[B^c] = [L]\,\big([\Gamma]\,[N_{,}^{c}]\,[F] + [N^c]\,[F']\big) \tag{4.13}$$

By means of the evaluation of the $[B^b]\ and\ [B^c]$ matrices, the strain can be writen as

$$\{\varepsilon\} = [B]\{u\} + H[B^b]\{b\} + [B^c]\{c\} \tag{4.14}$$

Equations (4.10) and (4.14) can be rewritten for the virtual displacements and stains as

$$\{\delta u^h\}^T = \{\delta u\}^T[N]^T + H\{\delta b\}^T[N^b]^T + \{\delta c\}^T[F]^T[N^c]^T \tag{4.15}$$

$$\{\delta\varepsilon\}^T = \{\delta u\}^T[B]^T + H\{\delta b\}^T[B^b]^T + \{\delta c\}^T[B^c]^T \tag{4.16}$$

Implementing the virtual fields (4.15) and (4.16) into the principle of virtual work yields to

$$\int_{\Omega} (\{\delta u\}^T[B]^T + H\{\delta b\}^T[B^b]^T + \{\delta c\}^T[B^c]^T)\,[C]\,([B]\{u\} + H[B^b]\{b\} + [B^c]\{c\})d\Omega$$

$$= \int_{\Gamma^t} (\{\delta u\}^T[N]^T + H\{\delta b\}^T[N^b]^T + \{\delta c\}^T[F]^T[N^c]^T)\{f^t\}d\Gamma \tag{4.17}$$

Equation (4.17) is kinematical admissible for any choice of $\{\delta u\}^T, \{\delta b\}^T$ and $\{\delta c\}^T$ where $\{u^h\}$ becomes, also, admissible. Thus, Equation (4.17) can be separate into three Equations for any choice of $\{\delta u\}^T, \{\delta b\}^T$ and $\{\delta c\}^T$as:

Related to $\{\delta u\}^T$ field:

$$\underbrace{\int_{\Omega}[B]^T\,[C]\,[B]d\Omega\,\{u\}}_{\equiv[k_{uu}]}+\underbrace{\int_{\Omega}H[B]^T\,[C]\,[B^b]d\Omega\,\{b\}}_{\equiv[k_{ub}]}+\underbrace{\int_{\Omega}[B]^T\,[C]\,[B^c]d\Omega\,\{c\}}_{\equiv[k_{uc}]}$$

$$=\underbrace{\int_{\Gamma^t}[N]^T\{f^t\}d\Gamma}_{\equiv\{f^u\}} \qquad \mathbf{(4.18)}$$

Related to $\{\delta b\}^T$ field:

$$\underbrace{\int_{\Omega}H[B^b]^T\,[C]\,[B]d\Omega\,\{u\}}_{\equiv[k_{bu}]}+\underbrace{\int_{\Omega}[B^b]^T\,[C]\,[B^b]d\Omega\,\{b\}}_{\equiv[k_{bb}]}+\underbrace{\int_{\Omega}H[B^b]^T\,[C]\,[B^c]d\Omega\,\{\delta c\}}_{\equiv[k_{bc}]}$$

$$=\underbrace{\int_{\Gamma^t}[N^b]^T\{f^t\}d\Gamma}_{\equiv\{f^b\}} \qquad \mathbf{(4.19)}$$

Related to $\{\delta c\}^T$ field:

$$\underbrace{\int_{\Omega}[B^c]^T\,[C]\,[B]d\Omega\,\{u\}}_{\equiv[k_{cu}]}+\underbrace{\int_{\Omega}H\,[B^c]^T\,[C]\,[B^b]d\Omega\,\{b\}}_{\equiv[k_{cb}]}+\underbrace{\int_{\Omega}[B^c]^T\,[C]\,[B^c]d\Omega\,\{\delta c\}}_{\equiv[k_{cc}]}$$

$$=\underbrace{\int_{\Gamma^t}[N^c]^T\{f^t\}d\Gamma}_{\equiv\{f^c\}} \qquad \mathbf{(4.20)}$$

Some necessary equations to simplify the stiffness matrices are given below as

$$\left.\begin{array}{c}[C]=[C]^T\\ [k_{bu}]=[B^b]^T\,[C]\,[B]=\left[[B]^T\,[C]\,[B^b]\right]^T=[k_{ub}]^T\\ [k_{cu}]=[B^c]^T\,[C]\,[B]=\left[[B]^T\,[C]\,[B^c]\right]^T=[k_{uc}]^T\\ [k_{cb}]=[B^c]^T\,[C]\,[B^b]=\left[[B^b]^T\,[C]\,[B^c]\right]^T=[k_{bc}]^T\end{array}\right\} \qquad \mathbf{(4.21)}$$

By using Equations from (4.18) to (4.21), the element formulation of xFEM is given by

$$\begin{bmatrix} [k_{uu}] & [k_{ub}] & [k_{uc}] \\ [k_{ub}]^T & [k_{bb}] & [k_{bc}] \\ [k_{uc}]^T & [k_{bc}]^T & [k_{cc}] \end{bmatrix} \begin{Bmatrix} \{u\} \\ \{b\} \\ \{c\} \end{Bmatrix} = \begin{Bmatrix} \{f^u\} \\ \{f^b\} \\ \{f^c\} \end{Bmatrix} \quad (\mathbf{4.22})$$

The dimension of the element equation varies from 8x8 to 40x40 according to the element to be enriched or not. The minimum size 8x8 occurs for the elements that only have u – degree of freedom. For the elements that have the four nodes enriched by Heaviside function, the size of the element equation is 16x16. If the four nodes are enriched by only Branch functions, the size increases to its maximum as 40x40.

The global stiffness matrix can be written as

$$\begin{bmatrix} [K_{uu}] & [K_{ub}] & [K_{uc}] \\ [K_{ub}]^T & [K_{bb}] & [K_{bc}] \\ [K_{uc}]^T & [K_{bc}]^T & [K_{cc}] \end{bmatrix} \quad (\mathbf{4.23})$$

respect to the sizes of the local stiffness matrices that are $\underset{8nx8n}{[K_{uu}]}, \underset{8nx2j}{[K_{ub}]}, \underset{2jx2j}{[K_{bb}]}, \underset{8nx16k}{[K_{uc}]}, \underset{2jx16k}{[K_{uu}]}\ and\ \underset{16kx16k}{[K_{uu}]}$ where n, j and k are u – DOFs (the number of the un-enriched nodes), b – DOFs (the number of the Heaviside enriched nodes) and c – DOFs (the number of the Crack tip enriched nodes) , respectively.

During the assemble process of the global stiffness matrix, the additional DOFs (b – enrichment and c – enrichment, respectively) are placed after the classical DOFs.

4.3 Integration of Discontinuous Elements

To evaluate the global stiffness matrix, it is necessary not only the integration of the continuous elements, as done in the classical finite element method, but also the integration of the discontinuous elements, b or c enriched elements. The elements divided by the crack or the elements that the crack ends inside of them could not be integrated as the elements, involve no discontinuity and the standard Gauss integration method could not be applied adequately to integrate the discontinuity, the crack. To integrate the discontinuity, the elements include any discontinuity (lies

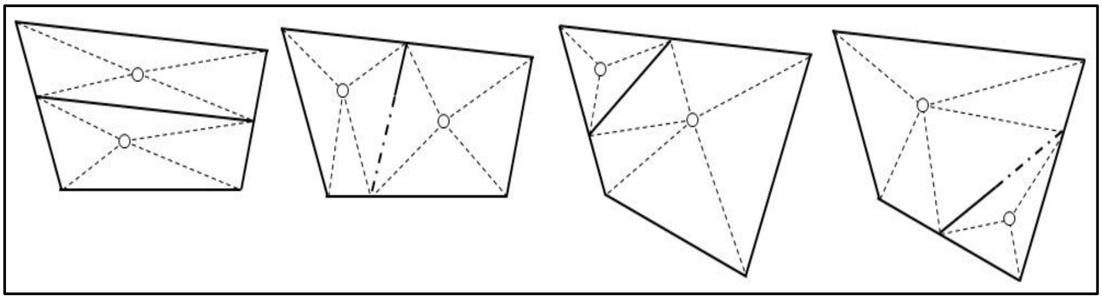

Figure 4.3 : Discontinuous elements divided into two subpolygons which are further divided into three, four or five subtriangles depending on the orientation of the discontinuity. The 3th and 4th elements include a crack tip, and the subpolygons are formed by means of the imaginarily extension of the crack.

through an element or ends inside of an element) can be integrated by dividing the elements into two subpolygons depending on the orientation of the discontinuity in Figure 4.3 by following Moës *et al.* [16].

The sub polygons are divided into 3, 4 or 5 triangles that enable the integration of the discontinuity numerically as illustrated by Cook *et al.* [15]. No additional degree of freedom is necessary for integration of the discontinuity. The integration takes part into the sub triangles that mapped on the reference coordinate system, $\tilde{\xi} - \tilde{\eta}$. The triangulation of the sub polygons and the gauss integration points are illustrated in the Figure 4.3-4, respectively. Then, the gauss integration method can be applied to the elements include any discontinuity with the 3 gauss points for the elements involve the crack body and the 7 gauss points for the elements involve the crack tip.

Depending on number of Gauss point, the values of $\tilde{\xi}_i, \tilde{\eta}_j$ and $\widetilde{W}_i$ are presented in Appendix C.2.

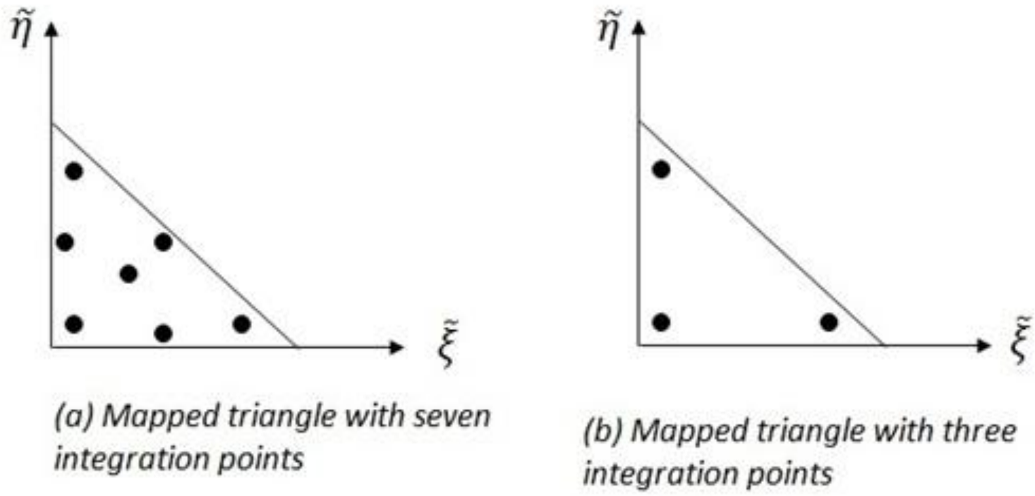

Figure 4.4 : Mapped triangles for the c and b - enriched elements.

5. DEFINATION OF THE CRACK PATH

The crack must be well defined to simulate the crack correctly by selecting the nodes that are enriched by Heaviside function or the four branch functions. For this reason, to define the crack properly with minimal meshing a mapping procedure, defined by Belytschko and Black [17], is applied. The mapping procedure can be done by defining any curved crack as a stepwise linear function. The crack, the stepwise linear function g, can be expressed as

$$g = g(x_i(j)), \qquad i = \{1,2\}\ and\ j = \{1,2,3,4 \ldots . n_j\} \tag{5.1}$$

where g is linear between the points $(x_1(j), x_2(j))$ and n_j is the number of point, defining the crack in Figure 5.1. This is similar with the procedure is followed to calculate analytically an integral over a line. The accuracy of the approximated integral can be improved by an increase in the number of point used in approximation. A similar approximation can be applied to the crack by increasing the

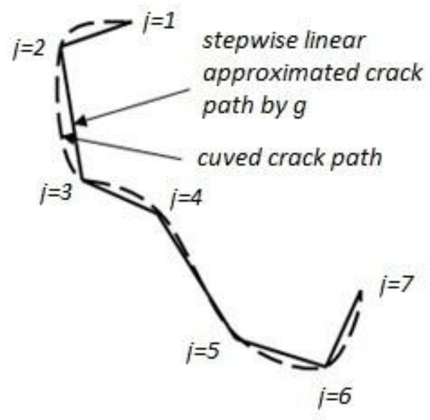

(a) Curved crack path approximated by a stepwise linear path g between points s={1,2,3,4,5,6,7}.

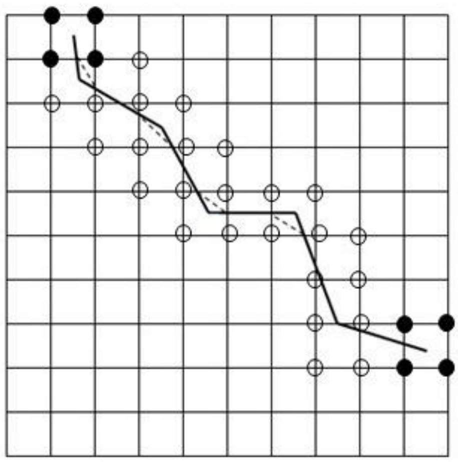

(b) Stepwise linear path g within elments, where g is approximated linearly (dashed line) if it changes its direction inside of the current element

Figure 5.1 : Arbitrary crack path approximSated by a stepwise linear function g.

n_j and mesh density, simultaneously. The mesh density is important for accuracy of the solution of any FEM approximation. The improvement in the accuracy of the crack defined as the stepwise linear function g by increasing the mesh density is presented in Figure 5.2. As seen from the Figure 5.2, increasing the mesh too much is unnecessary because of its to be in need of more solution time and memory. That is why selecting the proper mesh density is an important part of the solution according to the accuracy is needed by the problem.

After the crack, initially defined as $x_i(1)$ first crack tip and $x_i(n_j)$ second crack tip, starts to propagate step by step in both crack tips, the stepwise linear function must be redefined.

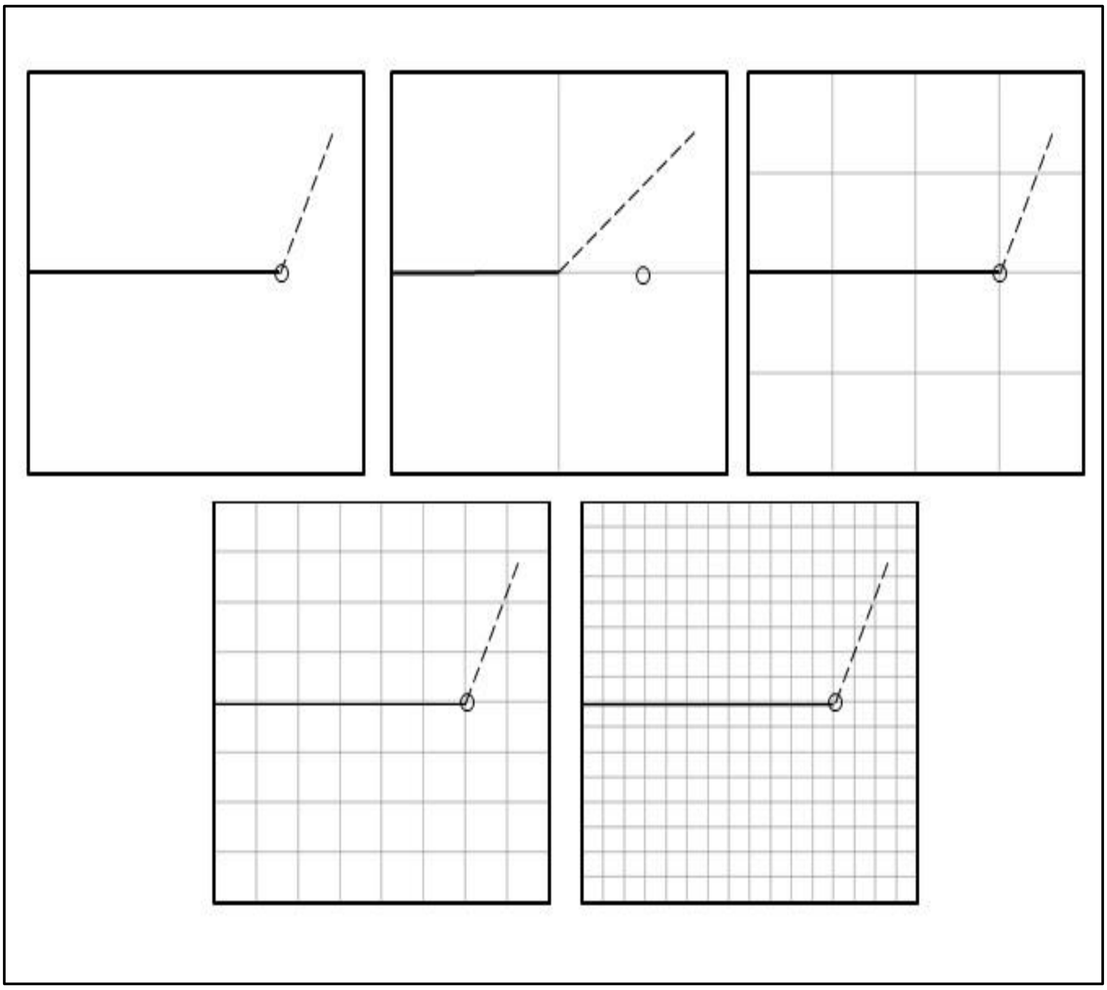

Figure 5.2 : An edge crack with an additional branch (dashed line) while mesh refinement is applied step by step. The last two sketch show that it makes no change in the crack definition although the mesh density is increased. May, the forth sketch can be selected to increase the accuracy, but not the fifth one. Since it just increases the solution time and need of more memory but cause no big change in the accuracy.

5.1 Defining Heaviside Function

To defining the crack body by mans of Heaviside function it is necessary to obtain the value of Heaviside function previously described according to the function *f*. at the current node. $\boldsymbol{e_n}$ and $\boldsymbol{e_s}$ are the normal and the tangential vectors on each segment of g lies from $j = m$ to $j = m + 1$ as illustrated in Figure 5.3. The value of Heaviside function for a given point **x** is defined by the sign of the scalar product $\boldsymbol{e_n} \cdot \left(\boldsymbol{x} - \boldsymbol{x}(j = m)\right)$**.** The Heaviside function is given by

$$H(x) = \begin{cases} -1, & \boldsymbol{e_n} \cdot \left(\boldsymbol{x} - \boldsymbol{x}(j = m)\right) < 0 \\ 1, & \boldsymbol{e_n} \cdot \left(\boldsymbol{x} - \boldsymbol{x}(j = m)\right) > 0 \end{cases} \qquad (\mathbf{5.2})$$

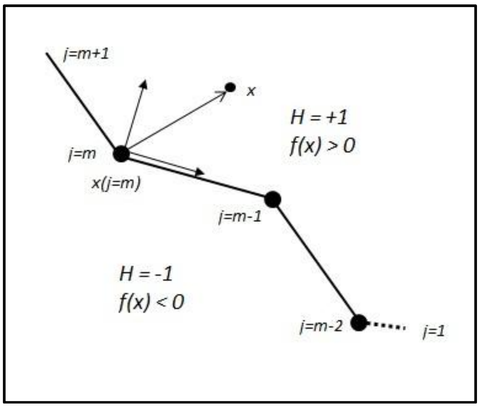

Figure 5.3 : The normal and the tangential vectors for a segment of the crack path and value of Heaviside function on each side of the crack segment.

6. STRESS INTENSITY FACTORS FOR A MIXED MODE CRACK

The evaluation of the stress intensity factors for the mixed mode crack (K_I *and* K_{II}) will covered in this section. Let's starts by recalling the J integral formula, which is given by

$$J = \frac{K_I^2}{E'} + \frac{K_{II}^2}{E'} \tag{6.1}$$

The interaction integral is employed to calculate the stress intensity factors individually by e.g. Moës *et al.* [16], Belytschko and Black [17], Yau *et al.* [18], Moran and Shih [19], Shih and Asaro [20], and, many others. Two stage of a cracked body is considered to obtain the interacting integral from J integral where the first stage is the presented stage and the auxiliary stage is the second. The J integral for the superposition of two stages is given by

$$J^{(1+2)} = \frac{\left(K_I^{(1)} + K_I^{(2)}\right)^2}{E'} + \frac{\left(K_{II}^{(1)} + K_{II}^{(2)}\right)^2}{E'}$$

$$= \underbrace{\frac{1}{E'}\left(K_I^{(1)} + K_{II}^{(1)}\right)}_{\equiv J^{(1)}} + \underbrace{\frac{1}{E'}\left(K_I^{(2)} + K_{II}^{(2)}\right)}_{\equiv J^{(2)}} + \underbrace{\frac{2}{E'}\left(K_I^{(1)}K_I^{(2)} + K_{II}^{(1)}K_{II}^{(2)}\right)}_{\equiv I^{(1,2)}} \tag{6.2}$$

where superscripts (1) and (2) denote stage 1 and 2, respectively, and $I^{(1,2)}$ is the interacting intedral for the stage 1 and 2. Using Equation (2.6) derived by Rice [14] fort the given stages, the interacting integral can be written as

$$I^{(1,2)} = J^{(1+2)} - J^{(1)} - J^{(2)}$$

$$= \int_\Gamma \left[W^{(1+2)}\delta_{1j} - \left(\sigma_{ij}^{(1)} + \sigma_{ij}^{(2)}\right)\left(u_{i,1}^{(1)} + u_{i,1}^{(2)}\right)\right] n_j d\Gamma$$

$$- \int_\Gamma \left(W^{(1)}\delta_{1j} - \sigma_{ij}^{(1)} u_{i,1}^{(1)}\right) n_j d\Gamma - \int_\Gamma \left(W^{(2)}\delta_{1j} - \sigma_{ij}^{(2)} u_{i,1}^{(2)}\right) n_j d\Gamma$$

$$= \int_{\Gamma} \left[\underbrace{\left(W^{(1+2)} - W^{(1)} - W^{(2)}\right)}_{\equiv W^{(1,2)}} \delta_{1j} - \sigma_{ij}^{(1)} u_{i,1}^{(2)} - \sigma_{ij}^{(2)} u_{i,1}^{(1)} \right] n_j d\Gamma \qquad \mathbf{(6.3)}$$

where $W^{(1,2)}$ is the interaction strain energy for a linear elastic material between the two states and can be evaluated as

$$W^{(1,2)} = \frac{1}{2}\left(\sigma_{ij}^{(1)}\varepsilon_{ij}^{(2)} + \sigma_{ij}^{(2)}\varepsilon_{ij}^{(1)}\right) = \sigma_{ij}^{(1)}\varepsilon_{ij}^{(2)} = \sigma_{ij}^{(2)}\varepsilon_{ij}^{(1)} \qquad \mathbf{(6.4)}$$

by means of $C_{ijkl} = C_{klij}$, a 4rht order symetric tensor.

Equation (6.3) is not well suited for finite element calculations so that it must be reformulated. To simplify the calculations, Ψ is assigned as the integrand of the interaction integral as

$$I^{(1,2)} = \int_{\Gamma} \Psi_j n_j d\Gamma, \quad \Psi_j = W^{(1,2)}\delta_{1j} - \sigma_{ij}^{(1)} u_{i,1}^{(2)} - \sigma_{ij}^{(2)} u_{i,1}^{(1)} \qquad \mathbf{(6.5)}$$

Equation (6.5) is rearranged, by defining the integration paths and the weighting function q in Figure 6.1, as

$$I^{(1,2)} = -\int_{\Gamma_0} \Psi_j n_j q d\Gamma - \int_{\Gamma_- \cup \Gamma_+} \Psi_j n_j q d\Gamma + \int_{\Gamma_- \cup \Gamma_+} \Psi_j n_j q d\Gamma - \int_{\Gamma} \Psi_j n_j q d\Gamma \qquad \mathbf{(6.6)}$$

where q=0 on Γ_0 and $n_j = -m_j$. Thus, Equation (6.6) is still equivalent of Equation (6.5). The third term in Equation (6.6) is zero due to ($\sigma_{ij}^{(1)}\varepsilon_{ij}^{(2)} = \sigma_{ij}^{(2)}\varepsilon_{ij}^{(1)} = 0$) and $\delta_{ij}m_j = 0$ and, the interacting integral yields to a closed curve integral as

$$I^{(1,2)} = -\oint_{\Gamma_0 \cup \Gamma_+ \cup \Gamma \cup \Gamma_-} \Psi_j n_j q d\Gamma \qquad \mathbf{(6.7)}$$

$$I^{(1,2)} = -\int_{A} \left(\Psi_j q\right)_{,j} dA \qquad \mathbf{(6.8)}$$

where A is the area that is enclosed by the curve $\Gamma_0 \cup \Gamma_+ \cup \Gamma \cup \Gamma_-$. The term $\left(\Psi_j q\right)_{,j} = \Psi_{j,j}\, q + \Psi_j\, q_{,j}$ reduces to $\left(\Psi_j q\right)_{,j} = \Psi_j\, q_{,j}$ because of $\Psi_{j,j} = 0$, which can be found easily by tensor calculus. At the end, the interacting integral between stages

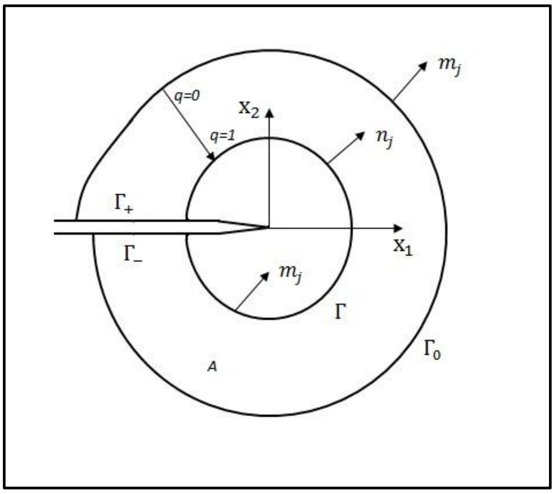

Figure 6.1 : The two integration contours near crack tip which are Γ and $\Gamma_0 \cup \Gamma_+ \cup \Gamma \cup \Gamma_-$, respectively. Unit normal is m_j on Γ_0, Γ_+ and Γ_- and, $n_j = -m_j$ on Γ. A is the area enclosed by the curve $\Gamma_0 \cup \Gamma_+ \cup \Gamma \cup \Gamma_-$. Weight function is defined as a value of unity on Γ and zero on Γ_0.

By applying the divergence theorem to the integral in Equation (6.7) result in a domain integral as

(1) and (2) takes the best form suited for finite element calculations as

$$I^{(1,2)} = -\int_A \Psi_j \, q_{,j} \, dA = \int_A \left[\sigma_{ij}^{(1)} u_{i,1}^{(2)} + \sigma_{ij}^{(2)} u_{i,1}^{(1)} - W^{(1,2)} \delta_{1j}\right] q_{,j} dA \qquad \mathbf{(6.9)}$$

By recall the last term of Equation (6.2), the stress intensity factors (K_I *and* K_{II}) can be evaluate as a funcition of the interacting integral,

$$I^{(1,2)} = \frac{2}{E'}\left(K_I^{(1)} K_I^{(2)} + K_{II}^{(1)} K_{II}^{(2)}\right) \qquad \mathbf{(6.10)}$$

The stage (2) is selected as pure mode I, where $K_I^{(2)} = 1$ *and* $K_{II}^{(2)} = 0$. Equation (6.10) yields to

$$K_I^{(1)} = \frac{E'}{2} I^{(1, mode\ I)} \qquad \mathbf{(6.11)}$$

Similarly, the stage (2) is selected as pure mode II, where $K_I^{(2)} = 0$ *and* $K_{II}^{(2)} = 1$. Equation (6.10) yields to

$$K_{II}^{(1)} = \frac{E'}{2} I^{(1, mode\ II)} \qquad \mathbf{(6.12)}$$

At the present stage the stress intensity factors (K_I and K_{II}) can be calculated easily with (6.9), (6.11) and (6.12). The interacting integral can be calculated numerically over the domain A described in Figure 6.2. The radius of the dashed dot circle, used here to describe the domain A (the enclosed area by the curve $\Gamma_0 \cup \Gamma_+ \cup \Gamma \cup \Gamma_-$), is known as the radius of J-evaluation. The radius r_d can be selected as

$$r_d = n\,h, \quad n = \{1, 2, 3, \dots \dots\} \qquad (\mathbf{6.13})$$

where h is described as the characteristic length of a crack tip element by Moës *et al.* [16]. To increase the accuracy of the J-evaluation, n higher value of n can be selected. It can be calculated as $h = \sqrt{A_e}$ for plane problems. For the presented project the characteristic length of a crack tip element is the element length due to the usage of the square elements. Figure 6.2 describes the selection of the element that takes part in the domain integral.

The thin and thick dashed lines have the values of weight function that vary 0 and 1 respect to $q_{,j}$. The elements in the area A are used to evaluate the interacting integral numerically and then the stress intensity factors, given by Equations (6.11) and (6.12), can be calculated easily for mixed mode crack.

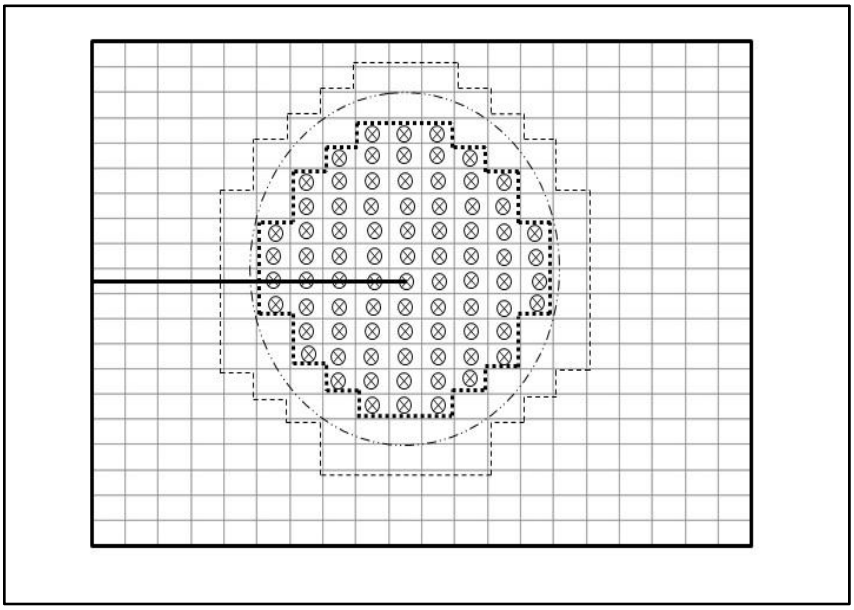

Figure 6.2 : The selection of the elements take part in the domain integral respect to the radius of J-evaluation (dashed dot circle). All element inside of the area limited by thick dashed line (Γ in Figure 6.1) have q=1, so that the gradient $q_{,j}$ is zero. Also, the elements outside of the thin dashed line (Γ_0 in Figure 6.1) The elements, inside of the area A is limited by the thick and thin lines, are the elements take part in the domain integral.

7. PROGRAM VERIFICATION FOR DIFFERENT CRACKED PLATES

The program, firstly, is tested for three cases that given by

I. $\varepsilon_{11} = 0.001\ and\ \varepsilon_{12} = \varepsilon_{22} = 0$

II. $\varepsilon_{22} = 0.001\ and\ \varepsilon_{11} = \varepsilon_{12} = 0$

III. $\varepsilon_{12} = 0.001\ and\ \varepsilon_{11} = \varepsilon_{22} = 0$

For the given three cases a rectangular plate with uniform mesh is simulated to ensure that the program could be able to calculate the strains and stresses correctly. To simulate the three cases with the program, the strains are described as uniform displacement boundary conditions that the displacements are known for the given strains in the three cases.

The program could be able to calculate the three cases easily and follows the finite element method formulation because of the problem includes no crack – no discontinuity. That is why the strains (ε_{11}, ε_{22}, or ε_{12}) and the stresses (σ_{11}, σ_{22}, or σ_{12}) are uniformly distributed through the plate, respectively.

After that the selection of the Heaviside nodes and the Crack tip nodes are verified for many cases by describing the crack as a stepwise linear function as illustrated in Figure 7.1. And then the program extended to the xFEM formulation given in previous sections. The developed program must be also verified to ensure that it works properly. In this sections many cracked body used to verify the programs will be presented.

7.1 Center Cracked Rectangular Plate Under Uniform Displacement

The first example is a center cracked rectangular plate under uniform displacement (ACCRPUUD) in Figure 7.2. To simulate the presented example, the element length used in the uniform mesh is 1/50. During the analysis of the center cracked rectangular plate under uniform displacement, the weight W kept constant while

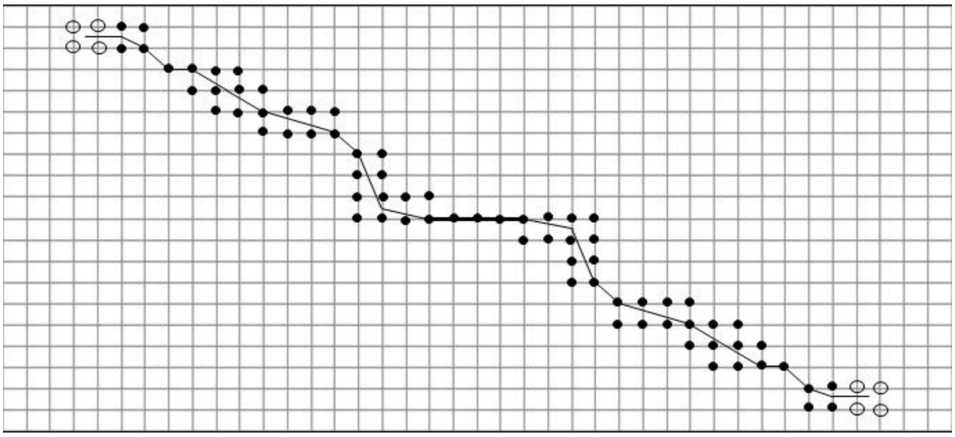

Figure 7.1 : Illustration of the selection of the nodes enriched by Heaviside function or Branch functions for a crack defined with a step wise linear function. Nodes marked by open circles are enriched by branch functions, and nodes marked by filled circles are enriched by the Heaviside function.

half-length of height H is varying with β and the crack length 2a is varying with α. The ratios β and α are given by

$$\beta = \frac{2H}{W} \tag{7.1}$$

$$\alpha = \frac{2a}{W} \tag{7.2}$$

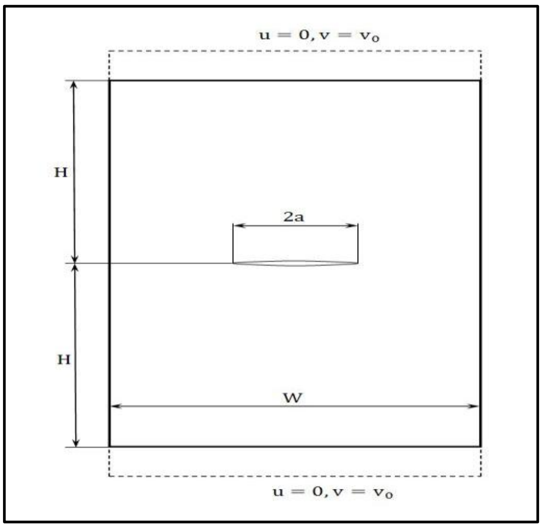

Figure 7.2 : A center cracked rectangular plate under uniform displacement.

The ratio of the stress intensity factors for the plane stress condition is given by

$$f_5(\alpha, \beta) = \frac{K_I}{K_{I_{calculated}}} \tag{7.3}$$

and it can be taken as $f_5 \approx g_5$where g_5 is the ratio for plane strain condition given by Isida [21]. The ratio f_5 and g_5 are also known as shape factors for plane stress and plane strain. The stress intensity factor K_I in Equation (7.3) is given by

$$K_I = \frac{v_0\, E}{\sqrt{H(1+\nu)^2(1-2\nu)}}\; g_5(\alpha, \beta) \tag{7.4}$$

where v_0 is the given uniform displacement and, ν *and* E are poison's ratio and young modulus, respectively. The ratio g_5 is calculated with MATLAB code for a center cracked rectangular plate under uniform displacement. The results are presented in Table 7.1 and Table 7.2 for several α and β values and, compared with the values taken from Isida [21]. The results have a good agreement with the

Table 7.1 : The ratio g_5 taken from Isida [21] and $g_{5\_calculated}$ for ACCRPUUD while β is varying from 0.4 to 0.8.

β	0,4			0,6			0,8		
	Isida [21]	With My MATLAB Code		Isida [21]	With My MATLAB Code		Isida [21]	With My MATLAB Code	
α	CT I and CT II	CT I	CT II	CT I and CT II	CT I	CT II	CT I and CT II	CT I	CT II
0,1	0,8460	0,8688	0,8688	0,7200	0,7260	0,7260	0,6300	0,6274	0,6274
0,2	0,9890	1,0035	1,0034	0,9160	0,9189	0,9189	0,8350	0,8299	0,8299
0,3	1,0040	1,0055	1,0055	0,9830	0,9758	0,9758	0,9340	0,9214	0,9214
0,4	0,9980	0,9913	0,9913	0,9970	0,9798	0,9798	0,9750	0,9537	0,9537
0,5	0,9940	0,9807	0,9807	0,9940	0,9690	0,9690	0,9860	0,9576	0,9576

Table 7.2 : The ratio g_5 taken from Isida [21] and $g_{5\_calculated}$ for ACCRPUUD while β is 1.0 and 1.2.

β	1,0			1,2		
	Isida [21]	With My MATLAB Code		Isida [21]	With My MATLAB Code	
α	CT I and CT II	CT I	CT II	CT I and CT II	CT I	CT II
0,1	0,5640	0,5554	0,5554	0,5120	0,5000	0,5000
0,2	0,7640	0,7522	0,7522	0,7030	0,6869	0,6869
0,3	0,8780	0,8602	0,8602	0,8230	0,8014	0,8014
0,4	0,9400	0,9148	0,9148	0,8980	0,8707	0,8707
0,5	0,9700	0,9376	0,9376	0,9440	0,9103	0,9103

reference ones even if they are not exact for plain strain conditions. During the calculation the max error is less than 4% and it is considered acceptable for the presented problem. The ratio is independent of material properties that are why the material properties used during the analysis is not presented here.

7.2 Finite Width Plate with a Center Crack Parallel to the Clamped Edges

The next example for verifying the program is a finite width plate with a center crack parallel to the clamped edges (AFWPCCPCE) in Figure 7.3. For the presented problem, it is recommended that select the ratio α as larger than or equal to 0,5 in Rice [2] where the ratio is given by

$$\alpha = \frac{2a}{W} \tag{7.5}$$

The stress intensity factor is given in Rice [2] for plane strain by

$$K_I = \frac{1}{1+\nu}\left(\frac{2}{1-2\nu}\right)^{1/2} \frac{E\,\mathrm{v}}{W^{1/2}} \tag{7.6}$$

where the accuracy of the formula is better than 1%. During the simulation of the crack, the ratio α and the width of plate – in the reference it is infinite- are kept constant where α=0,5 and the width=10 and, the half crack length 2a is also

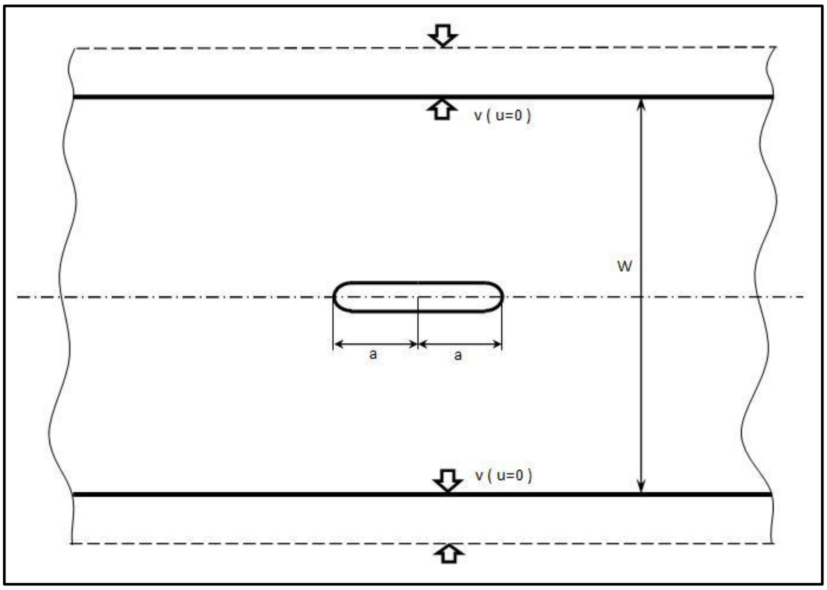

Figure 7.3 : A finite width plate with a center crack parallel to the clamped edges.

increased while the width of plate is increasing to keep the ratio α constant. The calculated stress intensity factors according to both the formula (7.6) and the developed xFEM program are presented in Table 7.3. Although the infinite length plate approximates as a finite plate, the maximum error have been made during the simulation is less than 4%. As seen from results the error decreases while the height W and 2a increase.

Table 7.3 : The stress intensity factors for AFWPCCPCE, respect to Equation (7.6) by Rice [2] and the MATLAB code.

		K_I by Rice [2]	K_I Calculated With MATLAB Code		
Length	Width	CT I and CT II	CT I	CT II	% Error
10	2	6081,30	6275,40	6275,40	-3,19
10	3	4965,40	5029,00	5029,00	-1,28
10	4	4300,10	4315,00	4315,00	-0,35
10	5	3846,20	3787,10	3787,10	1,54
10	6	3511,00	3422,00	3422,00	2,53

After some increase in 2a the error starts to increase because of the finite plate approximation. The error can be easily improved by decreasing the element size or more easily by increasing the length of the plate which seems infinite respect to 2a.

7.3 Finite Width Plate with an Edge Crack Parallel to the Clamped Edges

The next problem is a finite width plate with an edge crack parallel to the clamped edges (AFWPECPCE) in Figure 7.4. Although this example seems similar with previous one, It will be used to show how the accuracy increases with higher value of α. The ration α for the current problem is given in Rice [2] by

$$\alpha = \frac{a}{L} \qquad \mathbf{(7.7)}$$

where a is the length of the edge crack and L is the width of the plate. The srress intensity factor for plane strain condition is given Rice [2] by

$$K_I = \frac{1}{1+\nu}\left(\frac{2}{1-2\nu}\right)^{1/2} \frac{E\,\mathrm{v}}{L^{1/2}} \qquad \mathbf{(7.8)}$$

The simulation takes part into the different plates (only the length of plate kept constant) and increasing α values for the current plate. The results are illustrated in Table 7.4. In the previous problem the largest error occurred for the largest value of the crack length 2a because of the lack of the simulation of the plate with infinite

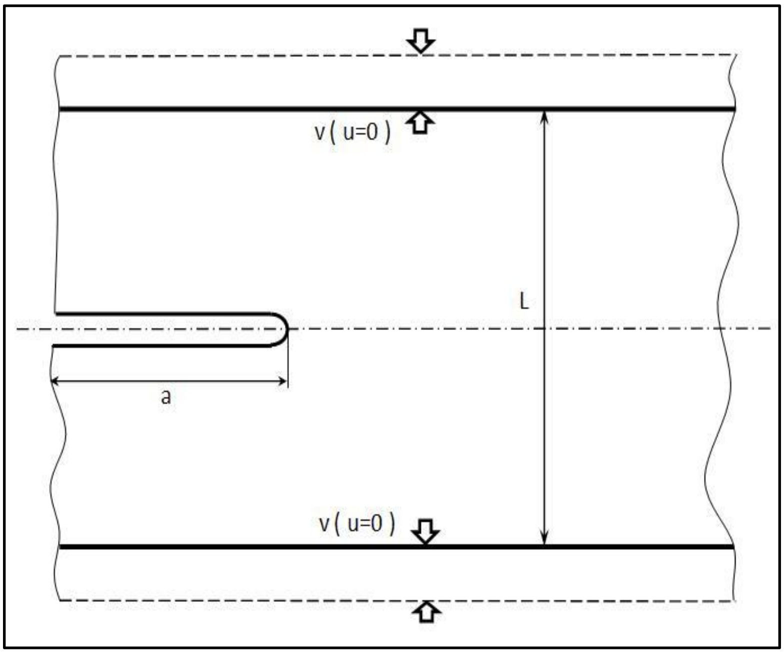

Figure 7.4 : A finite width plate with an edge crack parallel to the clamped edges.

length (the fifth plate). Although the infinite length plate approximation employed again, the error, in the fifth plate, have been made during the simulation decreases up to 0.4% for higher α.

As it is recommended that select the ratio α as larger than or equal to 0.5 in previous example to increase the accuracy, the results larger in the ratio α are better in the accuracy.

Table 7.4 : The stress intensity factors for AFWPECPCE respect to Equation (7.8) by Rice [2] and the MATLAB code.

α=	a/W=	K_I by Rice [2]	K_I Calculated With MATLAB Code			
Width	Height	exact	0,4	0,5	0,6	0,8
10	2	6081,30	5870,00	5978,40	6030,10	6066,80
10	3	4965,40	4791,40	4879,00	4920,20	4952,40
10	4	4300,10	4147,30	4218,90	4251,60	4288,70
10	5	3846,20	3706,10	3763,60	3787,70	3834,80
10	6	3511,00	3379,20	3424,10	3440,30	3497,80

7.4 An Angled Center Crack in a Finite Plate Under Uniform Tension

After verifying the program for several of mode I problems, it is necessary to show that the program properly works for mixed mode problems. To illustrate that, an angled center crack in a finite plate under uniform tension (AACCFPUUT) in Figure 7.5 will be presented here. The crack angle θ is defined respect to the horizontal axis.

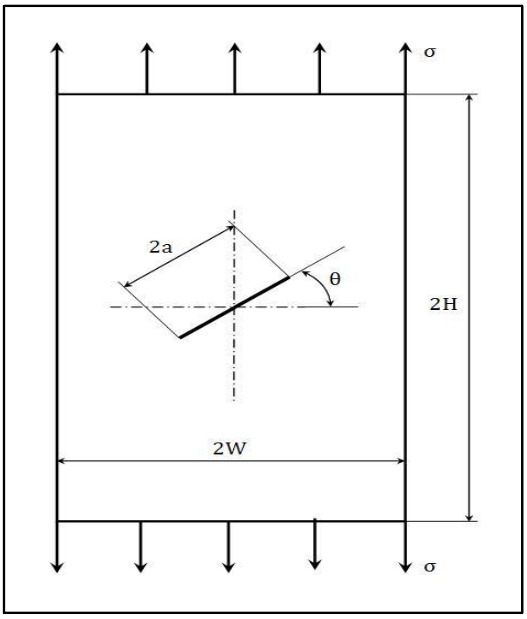

Figure 7.5 : An angled center crack in a finite plate under uniform tension.

In illustrated problem, it is preferred to calculate the two factors related to mode I and II, respectively. The factors for mode I and II are given in Kitagawa and Yuuki [22] and Wilson [23] by

$$F_I = \frac{K_I}{\sigma\sqrt{\pi\,a}} \tag{7.9}$$

$$F_{II} = \frac{K_{II}}{\sigma\sqrt{\pi\,a}} \tag{7.10}$$

where K_I and K_{II} are the calculated stress intensity factors for mode I and mode II respectively, σ is the tensional stress and a is the half of the crack length.

The results for F_I and F_{II} are shown in Table 7.5 for the various values of θ, angle of crack, and a/W ratio. The calculations take place in a plate has the ratio of $H/W = 2$ due to the results, Kitagawa and Yuuki [22] and Wilson [23], prepared for that ratio too. The results that obtained by means of the program have better agreement with the reference ones as the examples done before in this report. The errors occurred during the calculations plotted in Figure 7.6. As seen from the figure the max error, which less than 3%, occurs at θ=30˚ and $a/W = 0{,}8$ for FII.

Various angles and different ratios enable how the program will act in various crack propagation although the presented problem is simple beside the mixed mode crack

Table 7.5 : The F_I and F_{II} factors for AACCFPUUT by Kitagawa and Yuuki [22] and Wilson [23], and the MATLAB code.

		θ = 30°			θ = 45°			θ = 60°		
		By [22] and [23]	With My MATLAB Code		By [22] and [23]	With My MATLAB Code		By [22] and [23]	With My MATLAB Code	
	a/W	CT I and CT II	CT I	CT II	CT I and CT II	CT I	CT II	CT I and CT II	CT I	CT II
	0,1	0,7557	0,7453	0,7453	0,5046	0,4994	0,4994	0,2527	0,2480	0,2480
	0,2	0,7730	0,7696	0,7696	0,5181	0,5135	0,5135	0,2605	0,2584	0,2584
	0,4	0,8456	0,8376	0,8376	0,5719	0,5685	0,5685	0,2896	0,2857	0,2857
	0,6	0,9840	0,9658	0,9658	0,6611	0,6543	0,6543	0,3332	0,3259	0,3259
F_I	0,8	1,2450	1,2342	1,2342	0,7950	0,7808	0,7808	0,3880	0,3842	0,3842
	0,1	0,4339	0,4454	0,4454	0,5018	0,5146	0,5146	0,4352	0,4453	0,4453
	0,2	0,4267	0,4273	0,4273	0,5072	0,5181	0,5181	0,4417	0,4516	0,4516
	0,4	0,4497	0,4578	0,4578	0,5290	0,5393	0,5393	0,4660	0,4734	0,4734
	0,6	0,4800	0,4885	0,4885	0,5674	0,5772	0,5772	0,5022	0,5075	0,5075
F_{II}	0,8	0,5500	0,5658	0,5658	0,6300	0,6390	0,6390	0,5490	0,5580	0,5580

propagation. The program could be easily finds the nodes enriched by Heaviside funcition or branch functions although the crack has various angle.

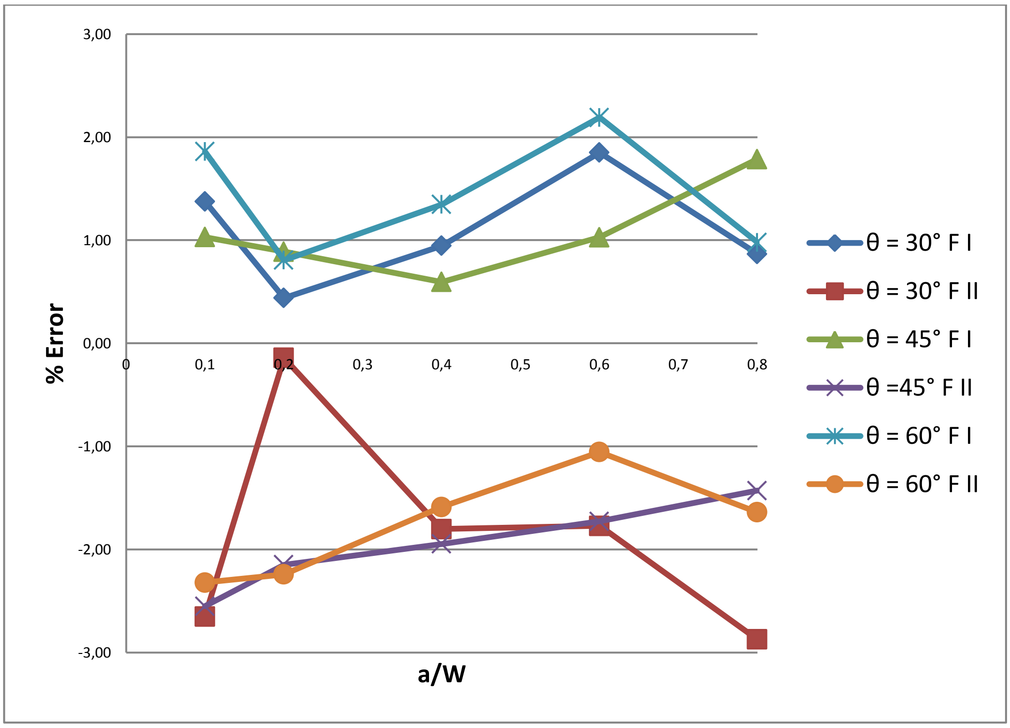

Figure 7.6 : Errors in the F_I and F_{II} factors for several of the crack angle θ and various of the ratio a/W for a center crack.

7.5 An Angled Edge Crack in a Finite Plate Under Uniform Tension

The similar with pervious example, the other example is an angled edge crack in a finite plate under uniform tension (AAECFPUUT) as illustrated in Figure 7.7. During the calculations, the ratio a/W and crack angle vary to illustrate the factors FI and FII. The factors for mode I and II are given in Freese [24] and Wilson [25] by

$$F_I = \frac{K_I}{\sigma\sqrt{\pi a}} \quad (7.11)$$

$$F_{II} = \frac{K_{II}}{\sigma\sqrt{\pi a}} \quad (7.12)$$

where KI and KII are the calculated stress intensity factors for mode I and mode II respectively, σ is the tensional stress and a is the crack length.

The calculations take place in a plate has the ratios of $H_1/W = H_2/W = 1$ wkere H_1 and H_2 are illustrated in Figure 7.7. The results of FI and FII are shown in Table 7.6 for the various values of θ, angle of crack according to horizontal axis, and a/W ratio. The results have better agreement with the reference ones as the angled center crack. The errors occurred during the calculations plotted in Figure 7.8. As seen from the figure the max error, which less than 3%, occurs at θ=60˚ and $a/W = 0{,}4$ for FII.

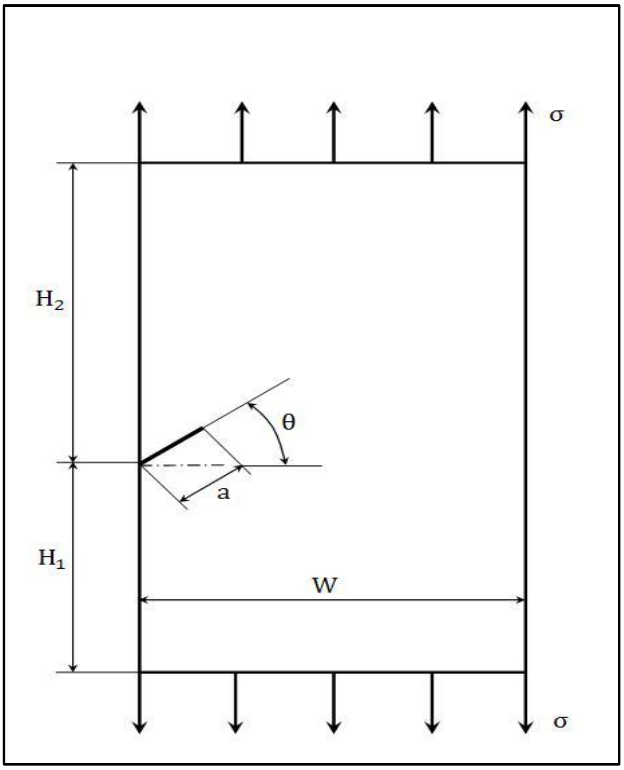

Figure 7.7 : An angled edge crack in a finite plate under uniform tension.

Table 7.6 : The F_I and F_{II} factors for AAECFPUUT by Freese [24] and the the MATLAB code.

		θ = 30°		θ = 45°		θ = 60°	
		By Freese [24]	With My MATLAB Code	By Freese [24]	With My MATLAB Code	By Freese [24]	With My MATLAB Code
	a/W	CT	CT	CT	CT	CT	CT
F I	0,1	0,9697	0,9599	0,7030	0,7073	0,4606	0,4676
	0,2	1,0909	1,0737	0,7879	0,7858	0,4998	0,491
	0,3	1,2485	1,2579	0,8788	0,8859	0,5212	0,5285
	0,4	1,5455	1,5313	1,0182	1,0331	0,5939	0,5868
	0,5	1,9273	1,933	1,2364	1,2486	0,6788	0,6805
F II	0,1	0,3293	0,3298	0,3780	0,3869	0,3415	0,342
	0,2	0,3537	0,3615	0,4122	0,4143	0,3537	0,3557
	0,3	0,4123	0,4122	0,4463	0,4568	0,3780	0,3879
	0,4	0,4695	0,4799	0,5078	0,512	0,4146	0,4192
	0,5	0,5780	0,571	0,5780	0,5784	0,4513	0,4579

Both of angled edge crack and angled crack illustrates that the developed program could evaluate the stress intensity factors K_I and K_{II} correctly for a mixed mode crack problems. Although both example lack of showing how the crack propagates, it can be said that the program could be able to calculate the stress intensity factors correctly for any crack extension.

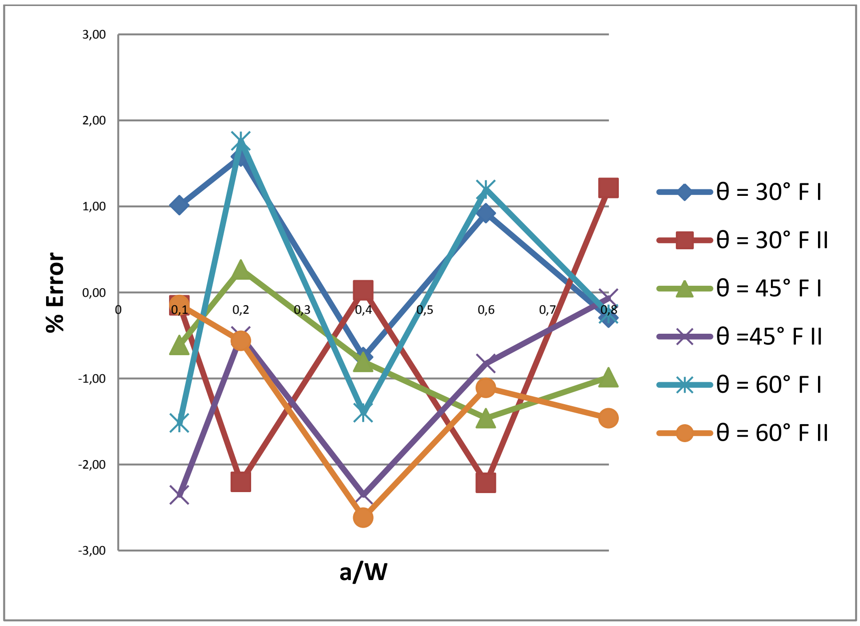

Figure 7.8 : Errors in the F_I and F_{II} factors for several of the crack angle θ and several of the ratio a/W for an edge crack.

7.6 A Skew – Symmetric Bent Crack

In the Definition of the crack path section, the crack is defined by a stepwise linear function. This example is the first time of the usage of the stepwise linear function. The skew – symmetric bent crack (ASSBC) in Figure 7.9 is defined by four points illustrated in Figure 7.10. The first and fourth points are the first and second crack tips. This problem can be thought as a problem that initially the crack lays from 2nd point (initially 1st point of the crack) to 3rd point (initially last point of the crack) and then it propagates in both end where it turns into the bent crack problem.

After the initially center crack propagates with a crack growth angle $\theta_i$and da_i (it is b in bent crack problem), the locations of the new crack tips can be found easily by

$$\left.\begin{aligned} x_{1\ of\ ct_i-new} = x_{1\ of\ ct_1-old} + da_i\ \cos\theta_i \\ x_{2\ of\ ct_i-new} = x_{2\ of\ ct_1-old} + da_i\ \sin\theta_i \end{aligned}\right\} \qquad (\mathbf{7.13})$$

where the stepwise linear function is redefined for each crack propagation in the program. Let's turn back to the crack with a bended branch on both ends which has an angel of θ according to horizontal. The factors for mode I and mode II are defined by Kitagawa and Yuuki [26] as

$$F_I = \frac{K_I}{\sigma\sqrt{\pi\ c}} \qquad (\mathbf{7.14})$$

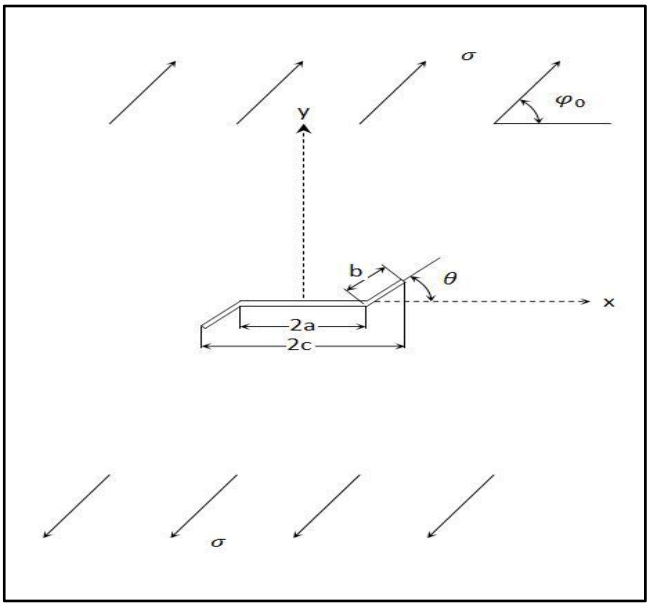

Figure 7.9 : A skew – symmetric bent crack: the bent crack illustrates the situation after a center crack propagated with the angle of θ and b symmetrically in both crack tips.

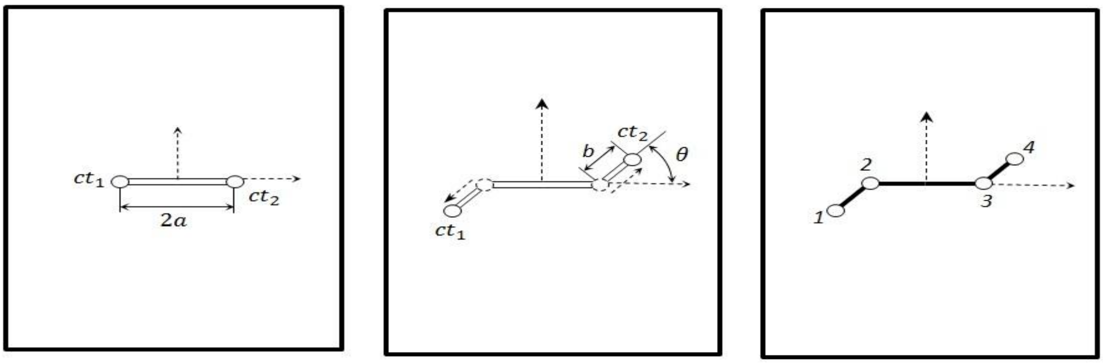

(a) Initial center crack

(b) The crack propagates with θ and b where the crack tips moves as illustrated

(c) The skew symmetric bent crack illustrated by four point where the stepwise linear function lies from 1st point to last point

Figure 7.10 : Illustration of the step wise linear function, used to describe the bended crack.

$$F_{II} = \frac{K_{II}}{\sigma\sqrt{\pi c}} \qquad \mathbf{(7.15)}$$

where $c = a + b\cos\theta$, K_I and K_{II} are the calculated stress intensity factors for mode I and mode II, b is the length of branch and , a is the half length of smooth part of the bent crack.

The results for φ_o = 90˚ (uniaxial tension) are presented in Table 7.7, 7.8 and 7.9 while θ varies as 30˚, 45˚ and 60˚, respectively.

The results for φ_o = 0˚ (shear stress for top and bottom surface of the plate) are presented in Table 7.10, 7.11 and 7.12 while θ varies as 30˚, 45˚ and 60˚, respectively.

Table 7.7 : The F_I and F_{II} factors for ASSBC with θ=30˚ and φ_o =90˚ by Kitagawa and Yuuki [26] and the MATLAB code.

	θ = 30˚ and φ_o = 90˚					
	By Kitagawa and Yuuki [26]		With My MATLAB Code			
b/a	FI	FII	FI		FII	
	CT1 and CT2	CT1 and CT2	CT1	CT2	CT1	CT2
0,4	0,8242	0,4021	0,8236	0,8236	0,4199	0,4199
0,6	0,8187	0,4176	0,8241	0,8241	0,4350	0,4350
0,8	0,8156	0,4271	0,8152	0,8152	0,4417	0,4417
1,0	0,8135	0,4335	0,8181	0,8181	0,4482	0,4482

Table 7.8 : The F_I and F_{II} factors for ASSBC with θ=45˚ and φ_o=90˚ by Kitagawa and Yuuki [26] and the MATLAB code.

b/a	θ = 45˚ and φ_o = 90˚					
	By Kitagawa and Yuuki [26]		With My MATLAB Code			
	FI	FII	FI		FII	
	CT1 and CT2	CT1 and CT2	CT1	CT2	CT1	CT2
0,4	0,6280	0,5284	0,6183	0,6167	0,5417	0,5376
0,6	0,6161	0,5491	0,6199	0,6197	0,5697	0,5696
0,8	0,6095	0,5617	0,6107	0,6107	0,5785	0,5784
1,0	0,6054	0,5698	0,6101	0,6102	0,5892	0,5892

Table 7.9 : The F_I and F_{II} factors for ASSBC with θ=60˚ and φ_o =90˚ by Kitagawa and Yuuki [26] and the MATLAB code.

b/a	θ = 60˚ and φ_o = 90˚					
	By Kitagawa and Yuuki [26]		With My MATLAB Code			
	FI	FII	FI		FII	
	CT1 and CT2	CT1 and CT2	CT1	CT2	CT1	CT2
0,4	0,3934	0,5794	0,3932	0,3932	0,5962	0,5962
0,6	0,3734	0,6031	0,3739	0,3739	0,6228	0,6228
0,8	0,3629	0,6170	0,3622	0,3622	0,6309	0,6309
1,0	0,3576	0,6253	0,3577	0,3577	0,6423	0,6423

As seen from the results the error decreases for higher b. For each case, the maximum error done during the calculations is less than %6 and in acceptable range. The maximum error is a little bit high compared to previous examples due to fact that the dimensions of plate must be sufficiently larger than a and b to simulate the plate as an infinite plate. In Matlab, simulation is done for a 40x40 plate with a crack

Table 7.10 : The F_I and F_{II} factors for ASSBC with θ=30˚ and φ_o=0˚ by Kitagawa and Yuuki [26] and the MATLAB code.

b/a	θ = 30˚ and φ_o = 0˚					
	By Kitagawa and Yuuki [26]		With My MATLAB Code			
	FI	FII	FI		FII	
	CT1 and CT2	CT1 and CT2	CT1	CT2	CT1	CT2
0,4	0,1291	-0,2214	0,1275	0,1275	-0,2336	-0,2336
0,6	0,1506	-0,2572	0,1501	0,1501	-0,2692	-0,2692
0,8	0,1661	-0,2832	0,1638	0,1638	-0,2911	-0,2911
1,0	0,1780	-0,3031	0,1770	0,1770	-0,3121	-0,3121

Table 7.11 : The F_I and F_{II} factors for ASSBC with θ=45˚ and φ_o=0˚ by Kitagawa and Yuuki [26] and the MATLAB code.

b/a	θ = 45˚ and φ_o = 0˚					
	By Kitagawa and Yuuki [26]		With My MATLAB Code			
	FI	FII	FI		FII	
	CT1 and CT2	CT1 and CT2	CT1	CT2	CT1	CT2
0,4	0,2670	-0,2691	0,2605	0,2605	-0,2768	-0,2768
0,6	0,3140	-0,3150	0,3139	0,3139	-0,3291	-0,3291
0,8	0,3485	-0,3487	0,3453	0,3453	-0,3578	-0,3578
1,0	0,3753	-0,3749	0,3792	0,3792	-0,3896	-0,3896

Table 7.12 : The F_I and F_{II} factors for ASSBC with θ=60˚ and φ_o=0˚ by Kitagawa and Yuuki [26] and the MATLAB code.

b/a	θ = 60˚ and φ_o = 0˚					
	By Kitagawa and Yuuki [26]		With my x_FEM			
	FI	FII	FI		FII	
	CT1 and CT2	CT1 and CT2	CT1	CT2	CT1	CT2
0,4	0,4206	-0,2562	0,4151	0,4151	-0,2676	-0,2676
0,6	0,5003	-0,3030	0,5011	0,5011	-0,3155	-0,3155
0,8	0,5608	-0,3384	0,5523	0,5523	-0,3425	-0,3425
1,0	0,6086	-0,3636	0,6056	0,6056	-0,3732	-0,3732

length 2a=2 and 400x400 element mesh. But, neither an increase in the dimensions of the plate nor an increase in mesh density is not possible due to lack of memory to simulate the problem where presented simulation is done with highest mesh density of 400x400. So that to handle more accurate results that correlate with the standards either dimensions height and width of plate or mesh density must be increased by adding more memory.

The mixed mode fatigue crack growth will be simulated in a finite plate that maximum size of mesh is enough to obtain more accurate results. That is why the more memory is unnecessary.

In this section different types of examples are covered to illustrate the program is working properly and the evaluated results have good agreement with the references.

8. FATIGUE CRACK GROWTH

Fatigue crack growth can be describes the propagation of the crack under cycling loading. The needed force magnitude for fatigue crack growth is highly less than one necessary fort the crack growth under monotonic loading. That is why many structures under cycling loading failure earlier than expected due to fatigue. The linear elastic fracture mechanic is valid for high cycle fatigue crack growth.

Over the years, many fatigue crack growth law was developed and can be expressed in the form of

$$\frac{da}{dN} = f(\Delta K) \qquad \mathbf{(8.1)}$$

where a is the length of the crack, N is the number of cycles and ΔK is the range of the stress intensity factor as $\Delta K = K_{max} - K_{min}$. Although that fatigue crack growth law says that the fatigue crack growth rate- da/dN - just varies as a fonction of ΔK for one load cycle, it gives a good approximation for quick estimations.

Many experiments shows that the link between da/dN and ΔK in logarithmic scale takes the form in Figure 8.1.

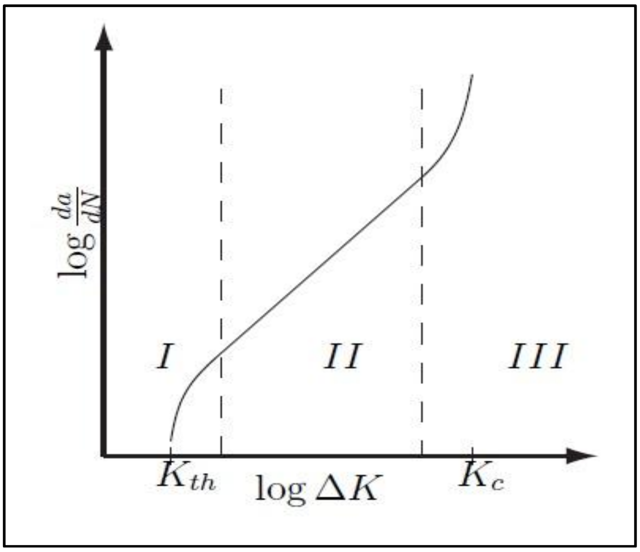

Figure 8.1 : Typical relation between the fatigue load ΔK and the crack growth rate for metals.

The fatigue crack propagation behavior divided into three regions as shown in the Figure 8.1. Region I is the fatigue threshold region where the ΔK is too low to propagate a crack, less than the order 10^{-9} m/cycle. This region is extremely sensitive and is largely influenced by the microstructure features of the material such as grain size, the mean stress of the applied load, the operating temperature and the environment present. The most important feature of this region is the existence of a stress intensity factor range below which fatigue cracks should not propagate. This value is defined as the fatigue crack growth threshold and is represented by the symbol ΔK_{th}.

Region II encompasses data where the rate of crack growth changes roughly linearly with a change in stress intensity fluctuation. Region II represents the intermediate crack propagation zone where the length of the plastic zone ahead of the crack tip is long compared with the mean grain size, but much smaller than the crack length. The use of linear elastic fracture mechanics (LEFM) concepts is acceptable and the data follows a linear relationship between log da/dN and log ΔK. The crack growth rate is typically on the order of 10^{-9} to 10^{-6} m/cycle, which corresponds to the majority of the test data results. This region corresponds to stable crack growth and the influence of microstructure, mean stress, ductility, environment and thickness are small.

In region III, small increases in the stress intensity amplitude, produce relatively large increases in crack growth rate since the material is nearing the point of unstable fracture. Region III represents the fatigue crack growth at very high rates, $da/dN > 10^{-3}$ m/cycle due to rapid and unstable crack growth just prior to final failure. The da/dN versus ΔK curve becomes steep and asymptotically approaches the fracture toughness K_c for the material. The corresponding stress level is very high and causes a large plastic zone near the crack tip as compared with the specimen geometry. Because large scale yielding occurs, the influence of the nonlinear properties of the material cannot be ignored. Therefore, the use of LEFM is not entirely correct and nonlinear fracture mechanics should be applied to this stage. The mean stress, materials microstructure and thickness have a large influence in this region and the environment has little influence. Fatigue crack propagation analysis is very complex in this region but often ignored because it has little importance in most fatigue situations. The reason that the fatigue crack growth rates are very high and little fatigue life is involved.

8.1 Fatigue Crack Growth Rate

Many fatigue crack growth law was developed in recent years, but the best known is formulated by Paris and Erdogan [3], and it can be expressed as

$$\frac{da}{dN} = C\ (\Delta K)^n \qquad (\mathbf{8.2})$$

where C and n are material constants such that they are generally determinated by curve fitting to the experiment results. Although it gives relatively good approximation for the fatigue crack growth rate in the region II, this law does not take into account the effect of the R ratio. The R ratio is described as $R = K_{max}/K_{min}$ where K_{min} is generaly negative, and it tends to shift to left the fatigue crack growth rate curve for increasing values. That is why a modification is need for Paris law to take into account the effect of R. An extension of the Paris law was proposed by Erdogan and Ratvani [15] and it can be expressed by

$$\frac{da}{dN} = \frac{C\ (\Delta K - \Delta K_{th})^n}{(1-R)K_c - \Delta K} \qquad (\mathbf{8.3})$$

where C and n are material constants, ΔK_{th} is the change of the threshold value and K_c is the fracture toughness of the material.

Another fatigue crack growth law, which is a Paris type equation, has been used by Sih and Barthelemy [27], and Badaliance [28]. They use strain energy density factor to correlate fatigue crack growth rate which can be expressed by

$$\frac{da}{dN} = C_s\ (\Delta S)^{n_s} \qquad (\mathbf{8.4})$$

where C_s and n_s are material constants, and ΔS is the strain energy density factor range.

8.2 Prediction of Mixed Mode Fatigue Crack Growth Direction

A crack subject to mixed mode loadings changes its crack growth direction in non-self-similar manner. Therefore, either the fatigue crack growth rate or the fatigue crack growth direction is of importance during the crack propagation under mixed mode loading conditions. Several mix-mode fatigue crack growth criteria have developed regarding to the crack growth direction under mixed mode loadings. Some of them are reviewed in this section.

8.2.1 Maximum tangential stress criterion (MTS criterion)

The maximum tangential stress criterion is one of the mostly used theories for mix-mode fatigue crack growth, derived by Erdogan and Sih [29]. It is states for starting the crack growth that:

(i) Crack propagation starts at the radial direction, $\theta = \theta_c$, on which $\sigma_{\theta\theta}$ becomes maximum, where it can be mathematically sumurized as :

$$\frac{\partial \sigma_{\theta\theta}}{\partial \theta} = 0 \ and \ \frac{\partial^2 \sigma_{\theta\theta}}{\partial \theta^2} < 0 \qquad (\mathbf{8.5})$$

(ii) And fracture starts when the maximum tangential stress reaches a critical value as

$$\sigma_{\theta\theta} = \sigma_c \qquad (\mathbf{8.6})$$

The stress field near the crack tip according to polar coordinates is given by

$$\sigma_{\theta\theta} = \frac{1}{\sqrt{2\pi r}} \cos\frac{\theta}{2}\left[K_I cos^2\frac{\theta}{2} - \frac{3}{2}K_{II}\sin\theta\right] \qquad (\mathbf{8.7})$$

$$\sigma_{r\theta} = \frac{1}{\sqrt{2\pi r}} \cos\frac{\theta}{2}\left[K_I \sin\theta + K_{II}(3\cos\theta - 1)\right] \qquad (\mathbf{8.8})$$

where $\sigma_{\theta\theta}$ is the stress normal to the direction given by θ and $\sigma_{r\theta}$ is the shear stress. The tangential stress becomes maximum at the maximum principle directions which is defined by zero shear stress and results in

$$\sigma_{r\theta} = \frac{1}{\sqrt{2\pi r}} \cos\frac{\theta}{2}\left[K_I \sin\theta + K_{II}(3\cos\theta - 1)\right] = 0 \qquad (\mathbf{8.9})$$

$$K_I \sin\theta + K_{II}(3\cos\theta - 1) = 0 \qquad (\mathbf{8.10})$$

By using the equation above, the crack growth angle can be expressed as

$$\theta = 2\tan^{-1}\left(\frac{K_I}{4K_{II}} \pm \frac{1}{4}\sqrt{\left(\frac{K_I}{4K_{II}}\right)^2 + 8}\right) \quad (8.11)$$

8.2.2 Minimum strain energy density criterion (S criterion)

The minimum strain energy density factor has been used to predict the mixed mode fatigue crack growth direction by Sih [30]; Sih and Barthelemy [27] and Badaliance [28]. The S criterion is based on the local energy density near the crack tip. The S criterion assumes that the crack will extend in the direction that the strain energy density factor becomes minimum. The strain energy density factor can be determined for any crack propagation by

$$S(\theta) = a_{11}K_I^2 + 2a_{12}K_IK_{II} + a_{22}K_{II}^2 + a_{33}K_{III}^2 \quad (\mathbf{8.12})$$

where

$$a_{11} = \frac{1}{16\pi\mu}(3 - 4\upsilon - \cos\theta)(1 + \cos\theta) \quad (\mathbf{8.13})$$

$$a_{12} = \frac{1}{8\pi\mu}\sin\theta\,(\cos\theta - 1 + 2\upsilon) \quad (\mathbf{8.14})$$

$$a_{22} = \frac{1}{16\pi\mu}[4(1 - \upsilon)(1 - \cos\theta) + (3\cos\theta - 1)(1 + \cos\theta)] \quad (\mathbf{8.15})$$

$$a_{33} = \frac{1}{4\pi\mu} \quad (\mathbf{8.16})$$

$$\mu = \frac{E}{2(1 + \upsilon)} \quad (\mathbf{8.17})$$

It is states the initial crack growth takes place in the direction along which S criterion results in a minimum value,

$$\frac{\partial S}{\partial\theta} = 0 \;\; and \;\; \frac{\partial^2 S}{\partial\theta^2} > 0 \; for \; \theta = \theta_c \quad (\mathbf{8.18})$$

and crack propagation occurs when it reaches a critical value

$$S = S_{cr} \quad for \; \theta = \theta_c \quad (\mathbf{8.19})$$

For mixed mode I and II loading, the minimum strain energy density criterion result in the equation for the determination of the crack growth angle as

$$\sin 2\theta - 0.92\ \sin\theta + 4R\ (\cos 2\theta - \cos\theta) + R^2(0.92\ \sin\theta - 3\sin\theta) = 0 \quad (\mathbf{8.20})$$

where $= K_{II}/K_I$.

The maximum tangential stress formula and minimum strain energy density factor formula are compared for an load cycle and the results are given in Table 8.1. To calculate the crack

Table 8.1 : The deviation of the crack growth angles for a loading cycle respect to MTS criterion and S criterion.

Load step		1	5	10	15	20	25	30	36
CT I	MTS criterion	43,22	44,44	23,58	13,15	52,39	60,03	30,50	40,24
	S criterion	43,28	44,48	23,64	13,27	52,63	60,08	30,57	40,29
CTII	MTS criterion	223,25	224,47	203,61	193,17	232,41	240,04	210,52	220,26
	S criterion	223,35	224,37	203,55	193,29	232,44	240,06	210,42	220,28

growth angle according to the strain energy density factor, it is necessary to solve Equation (8.20) by an iterative method. The iterative solution is performed by Newton-Rapson method where the maximum tangential creation is used to initialize the point where the iterative solution is performed. As seen from Table 8.1 the result obtained for both case is nearly the same. Thus, MTS criterion is decided to demonstrate the crack growth angle for each loading stem to increase the efficiency of the program.

9. FATIGUE CRACK GROWTH UNDER MIXED MODE NON-PROPORTIONAL LOADING

In this section, fatigue crack growth under mixed mode non-proportional loading will be cowered. To cover non-proportional loading, it is necessary to describe the problem as being equivalent of the experiment will be done to compare the obtained results. That is why it is needed to describe a fatigue crack growth under mixed mode non-proportional loading that reflects the experimental suggestion correctly.

9.1 Experimental Suggestion: Thin Walled Tube Under Tension P and Torsion M

The one of the objectives of this paper is to derive a test condition to compare different models that will be discussed in the next sub sections. To cover non-proportional loading, it is necessary to describe the problem as being equivalent of the experiment will be done to compare the obtained results. That is why it is needed to describe a fatigue crack growth under mixed mode non-proportional loading that reflects the experimental suggestion correctly. That is why in this sub section the experiment specimen and how it will be described in the developed program will be presented.

The Figure 9.1 illustrates the specimen that will be used in the experiment. The thin walled tube in Figure 9.1 is under tension P and torsion M. Both tension and torsion consist of static and cycle parts to establish non-proportional loading case for mixed mode fatigue crack growth. The non-proportional loading can be sustained by four cases, depending on definition of the torsion and the tension,

Case 1: a cyclic proportional mixed mode loading + a static mode I and/or II

Case 2: a cyclic mode I or II + a static proportional mixed mode loading.

Case 3: a cyclic mode II + a static mode I loading

Case 4: a cyclic mode I + a static mode II loading

To include all those four cases, the stress intensity factors can be written as

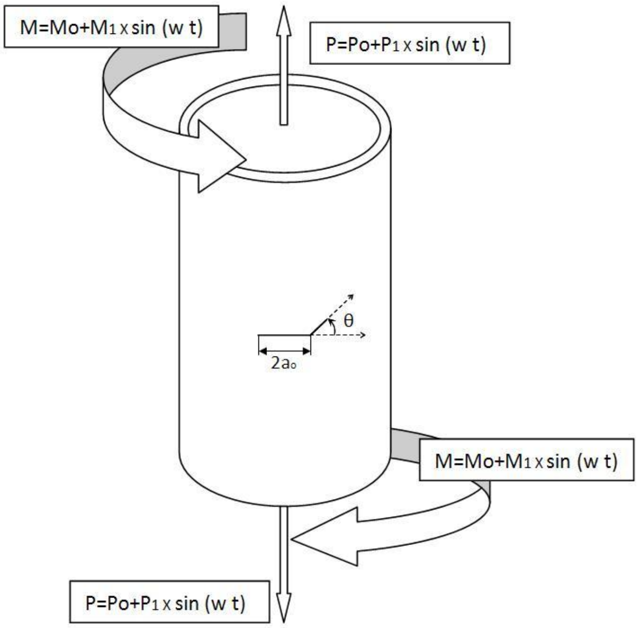

Figure 9.1 : Thin tube under tension P and torsion M.

$$K_I = K_{I,stat} + K_{I,cycl} \quad (\mathbf{9.1})$$

$$K_{II} = K_{II,stat} + K_{II,cycl} \quad (\mathbf{9.2})$$

where

$K_{I,stat}$: static part of KI origates from Po (the static part of tension)

$K_{I,cycl}$: cyclic part of KI origates from P1 * sin (wt) (the cyclic part of tension)

$K_{II,stat}$: static part of KII origates from Mo (the static part of torsion)

$K_{I,cycl}$: cyclic part of KI origates from M1 * sin (wt) (the cyclic part of torsion)

The term sin (wt) in cycle part of loads can be replaced by any trigonometric function and it is just used to illustrate the cycle part of both tension P and torsion M. The experimental suggestion, thin walled tube under tension P and torsion M, is approximated in the developed xFEM program as illustrated in Figure 9.2. Since the problem illustrated in Figure 9.2 with applied loads σ and τ is equivalent of the test illustrated in Figure 9.1, The non-proportional loading can be easily perform on the current program. The loads illustrated in the Figure 9.2 can be described as

$$\sigma = \frac{P}{2\,\pi r h} = \sigma_0 + \sigma_1 \sin(a\,wt) \quad (\mathbf{9.3})$$

$$\tau = \frac{M}{2\,\pi r^2 h} = \tau_0 + \tau_1 \sin(b\,wt) \tag{9.4}$$

where

σ_0 : static part of our normal stress

$\sigma_1\ \sin(a\,wt)$: cycle part of our normal stress

τ_0 : static part of our shear stress

$\tau_1\ \sin(b\,wt)$: cycle part of our shear stress and, a and b are arbitrary chosen constants to establish cycle part of loadings change in different manner. And the calculated stress intensity factors are given depending on the loading case by Equations (9.1) and (9.2) where they vary during a load cycle due to the cycle part of the load.

To avoid the singularity of the solution, the bottom left edge of the plate is fixed in both direction and the bottom right edge off the plate is also fixed in x_2 direction. The experimental suggestion can be approximated by the problem illustrated in Figure 9.2 with the boundary conditions on the bottom left and right edges of the problem.

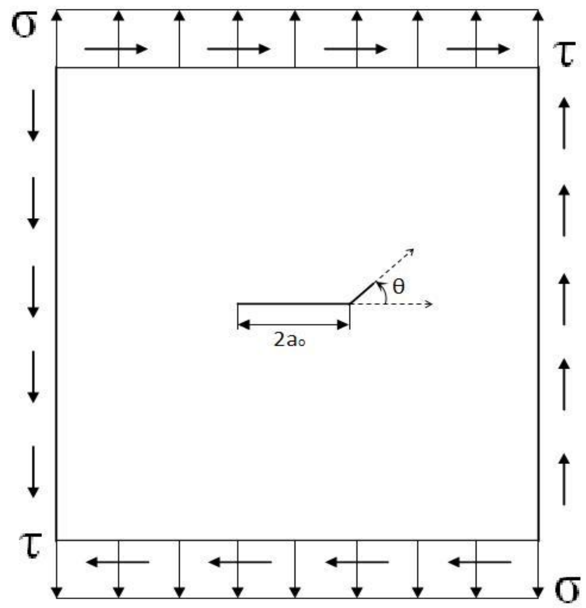

Figure 9.2 : The definition of the thin walled tube problem in the xFEM program.

Due to fact that the loads σ and τ vary during the load cycle, it is necessary divide a load cycle into sub cycles.

9.2 Mixed Mode Fatigue Crack Growth

To analyze the mixed mode fatigue crack, the Paris law, given by Equation (8.1), must be redefined where in this form it is generally initial with Mode I. Paris law is selected to simplify the calculations.

Analyses of mixed-mode fatigue crack growth based on Paris law are possible by the definition of an effective stress intensity factor which takes all two modes of fracture into account for the plate problem in Figure 9.2. Redefined Paris law by means of the effective stress intensity factor is given by

$$\frac{da}{dN} = C\left(\Delta K_{eff}\right)^{n} \qquad (\mathbf{9.5})$$

where C and n are material constants that are generally determinate by curve fitting to the experiment results illustrated in Figure 9.3 taken from Lucht [31] by curve

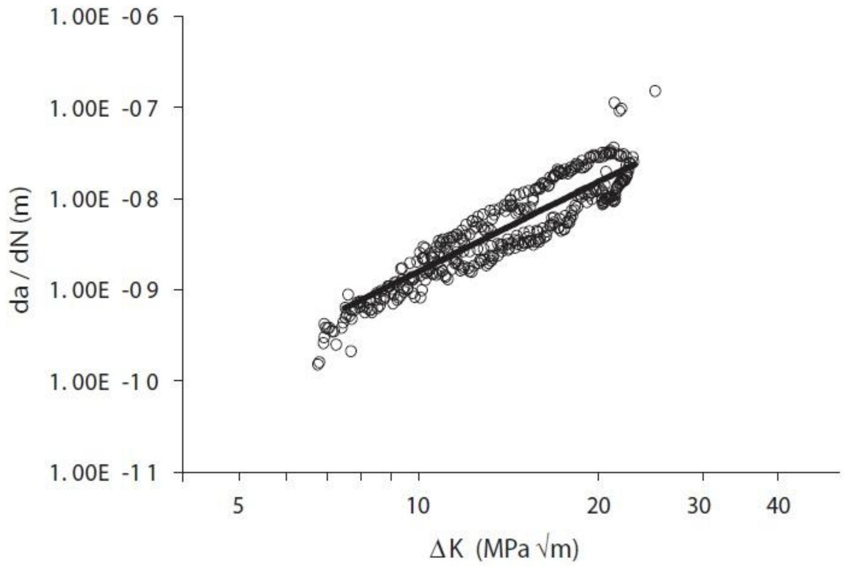

Figure 9.3 : Fitting Paris law to measurements of crack growth in SENB test specimens.

fitting, it is found that C = $9\text{x}10^{-13}$ and n = 3.25 in Eq. (9.5) when the unit of ΔK is MPa√m and the crack growth distance is calculated in meters. These values are in agreement with values of standard construction steel with E=200GPa and $\nu = 0.3$. In the literature, ΔK_{eff} is illustrated by two different ways for the 2D plane problem as

$$\Delta K_{eff} = f(\Delta K_{I}, \Delta K_{II}) \qquad (\mathbf{9.6})$$

$$\Delta K_{eff} = K_{eff}^{max} - K_{eff}^{min} \qquad (\mathbf{9.7})$$

where Equation (9.6) does not takes into account the relative variation of the K_I and K_{II} while Equation (9.6) does. Thus, ΔK_{eff} is selected to calculate the fatigue crack growth rate where the relative variation of the K_I and K_{II} is important. There are four effective stress intensity factor formulas, commonly used to illustrate the fatigue crack growth in the literature. These can be listed as

$$K_{eff} = \sqrt{K_I^2 + K_{II}^2} \qquad (\mathbf{9.8})$$

$$K_{eff} = \sqrt{K_I^2 + 2K_{II}^2} \qquad (\mathbf{9.9})$$

$$K_{eff} = \sqrt[4]{K_I^4 + 8K_{II}^4} \qquad (\mathbf{9.10})$$

$$K_{eff} = \frac{1}{2}\cos\frac{\theta}{2}\,[K_I(1 + \cos\theta) - 3K_{II}\,\sin\theta] \qquad (\mathbf{9.11})$$

where K_I and K_{II} are the calculated stress intensity factors and θ is the crack growth angle at current load step. Equations from (9.8) to (9.11) are given by Rhee [32], Gerstle [33], Tanaka [34] and Yan eta. [35], respectively. By using different K_{eff} formulas and the modified Paris law by means of K_{eff}, the four cases can be simulated for fatigue crack growth under non-proportional loading. But during a load cycle, it is necessary to illustrate the fatigue crack growth direction beside the crack growth rate. To illustrate the crack growth angle the maximum tangential stress will be used where it gives more accurate results and is easier to implement in to the Matlab codes than minimum strain energy density. To calculate the crack growth angle during a load cycle, tree models are considered as

$$\theta = \theta\left(K_{eff}^{max}\right) \qquad (\mathbf{9.12})$$

$$\theta = \frac{\theta\left(K_{eff}^{max}\right)K_{eff}^{max} + \theta(K_{eff}^{min})K_{eff}^{min}}{K_{eff}^{max} + K_{eff}^{min}} \qquad (\mathbf{9.13})$$

$$\theta = \frac{\sum \theta(K_{eff}^{i})\,K_{eff}^{i}}{\sum K_{eff}^{i}} \quad for\; K_{eff}^{i} > \; K_{eff}^{i-1} \qquad (\mathbf{9.14})$$

The first example assumes the crack deviation occurs at the maximum value of the K_{eff} where it is a function of current KI, KII and the crack growth angle θ, also function of current stress intensity factors. The superscript max over K_{eff} does not mean that it occurs at the maximum load. The second formula assumes that the crack growth angle varies linearly and the K_{eff}^{max} and K_{eff}^{min} are used as a weight. And both formulas are lack of taking into account each load step and fluctuation of K_{eff}. Thus, to consider the fluctuation of K_{eff}, the third formula is assumed to use during the simulation and K_{eff}^{i} is used as a weight for $K_{eff}^{i} > K_{eff}^{i-1}$ says just ignore the decreasing values of K_{eff}^{i} during the one cycle loading.

9.3 Numerical Simulation of a Fatigue Crack Growth Under Non-proportional Loading Given by Case I

To illustrate the fatigue crack growth under non-proportional loading, the first case will be presented here and for other three cases will be presented by three separate examples in Appendix E. The crack growth for the case I is illustrated in Figure 9.4 by different K_{eff} formulas for a 0.16*0.12 m rectangular plate with a center crack lies from (0.055, 0.08) to (0.065, 0.08). The non-proportional loading illustrated in Figure 9.2 is given for the case I by

$$\left.\begin{aligned} \sigma &= 12 \times 10^7 (1 + 0.6 \sin(wt))\ Pa \\ \tau &= -8.5 \times 10^7 (1 + 0.8 \sin(2wt))\ Pa \end{aligned}\right\} \qquad (\mathbf{9.15})$$

The crack path estimated nearly the same by each of K_{eff} formulas. As expected, the crack growth rate fluctuates on the order of 10^{-9} to 10^{-6} m/cycle where the modified Paris law with K_{eff} for mix mode fatigue crack growth describes the region II in Figure 8.1. To visualize the crack incensement in each crack propagation, it is assumed that the crack grows in the same direction, given by (9.14) and the same crack growth rate given by (9.5) during 10^4 cycle. If the calculated crack rates are directly used, it is necessary to increase the mess density as much as possible that the program could be able to catch the kicking (~10^{-8} m in length). That is why it is used as a scale factor. The crack angles, estimated by Equations from (9.8) to (9.11) in the first propagation, are 50.36°- 230.37º, 49.27º- 229.28°, 49,28°- 229,30º and 49.16°- 229.18º for both crack tips, respectively. The estimations perfectly correlate with

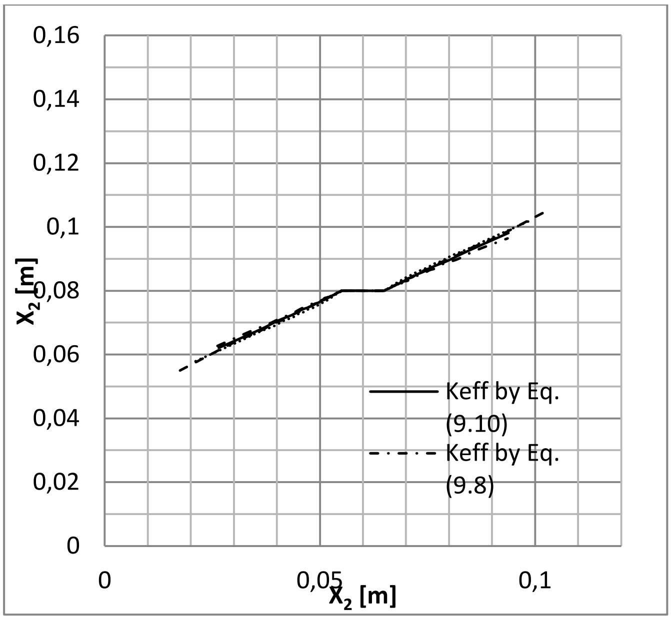

Figure 9.4 : Estimated crack paths for Case I by each K_{eff} formula.

each other where the calculated set of K_I and K_{II} are the same. For next iterations also correlates with each other too as illustrated in Figure 9.4 for the current loads.

The loads are applied in 36 steps to catch the change of K_{eff} correctly. The change of K_{eff} according to the different K_{eff} formulas is illustrated in Figure 9.5 for the first iteration. As seen from Figure 9.5, K_{eff} makes the maximum at the 5th load step and the minimum at the 30th load step. To calculate the crack growth direction related to each of K_{eff} definitions, the increasing parts of each K_{eff} are take into account to evaluate θ given by Equation (9.14).

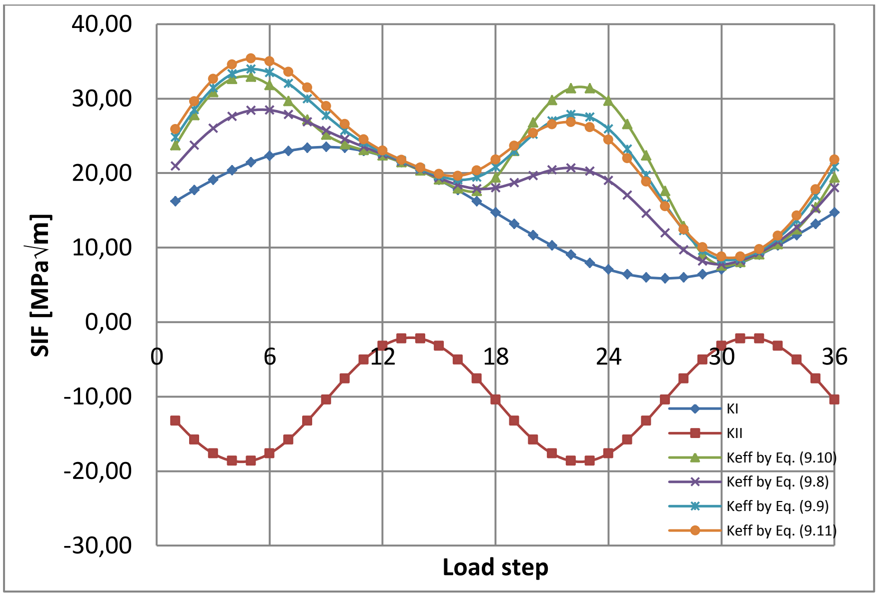

Figure 9.5 : Stress intensity factors calculated at the first iteration for Case I.

Figure 9.6 shows that chances of K_I, K_{II} and K_{eff} for each formula at the fifth iteration. The calculated stiffness's vary differently due to the fact that the crack grow rate determined by ΔK_{eff} are different for previous four iteration. Eighter the crack tips not take place inside the same element for each K_{eff} formula or the crack tips not in the same position inside of an element, even if they end in the same element for each K_{eff} formula is the cause of the different K_I and K_{II} values.

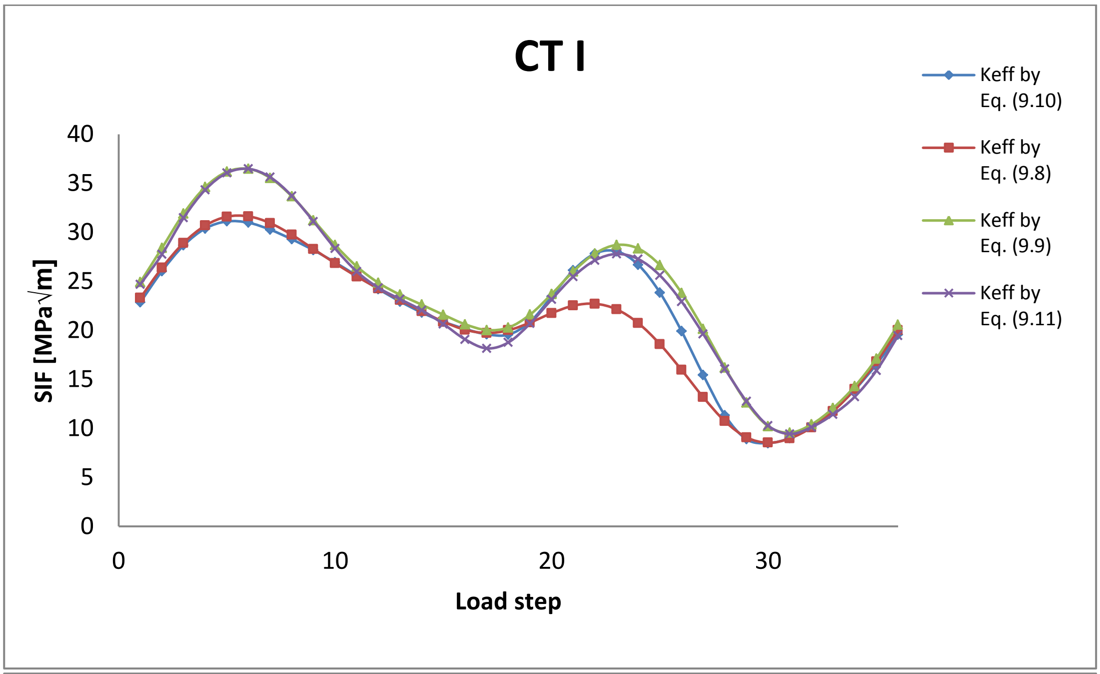

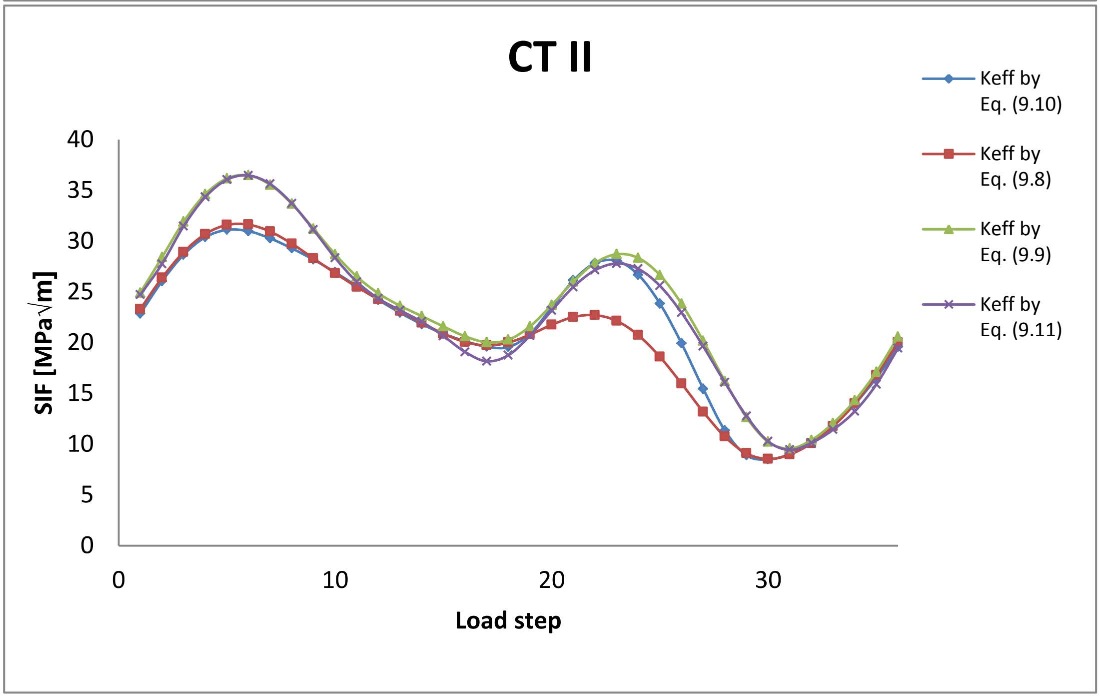

Figure 9.6 : Variation of the effective stiffness on the crack tips for each of K_{eff} formulas at the fifth iteration.

Figure 9.7 shows the change of crack growth rate respect to the employed K_{eff} formula at each crack tip with Case I loadings. The both crack tip grow symmetrically as seen in Figures 9.4 and 9.7. The crack grow rates are in the range of 10^{-9} to 10^{-6} m/cycle. The last grow rates are slightly different from each other due to fact that the deviations in each propagation stage are added for next stage. The deviations originate from the difference of the locations of the crack tip for the same propagation stage and the difference in ΔK_{eff}. That is why crack growths vary differently for each formula due to the crack growth rates are scaled with $dN=10^4$

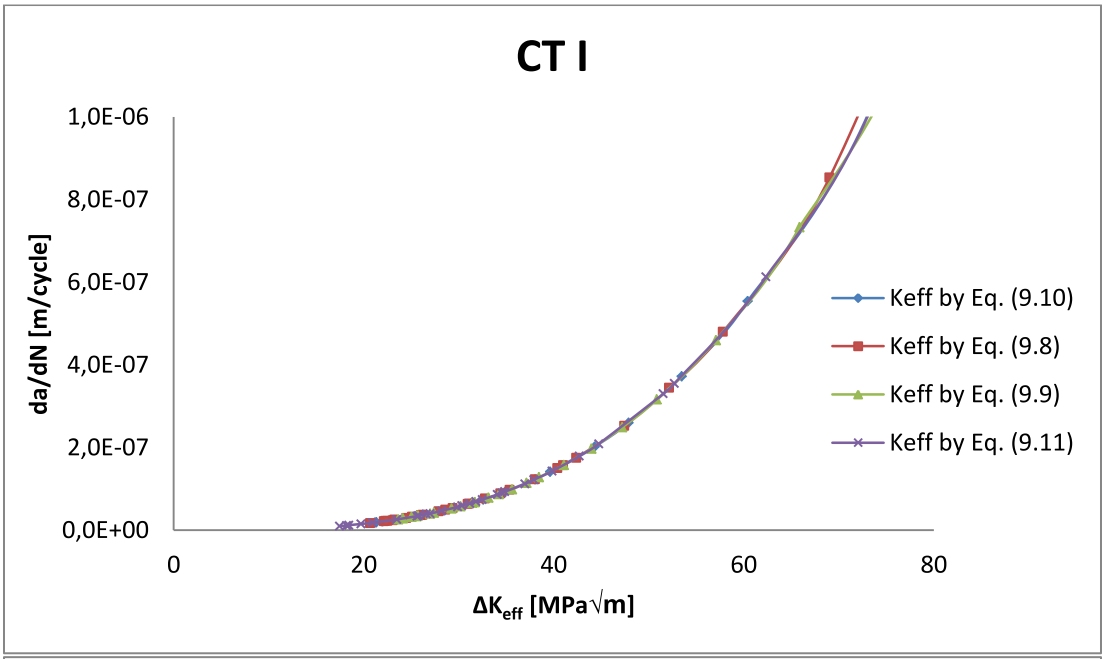

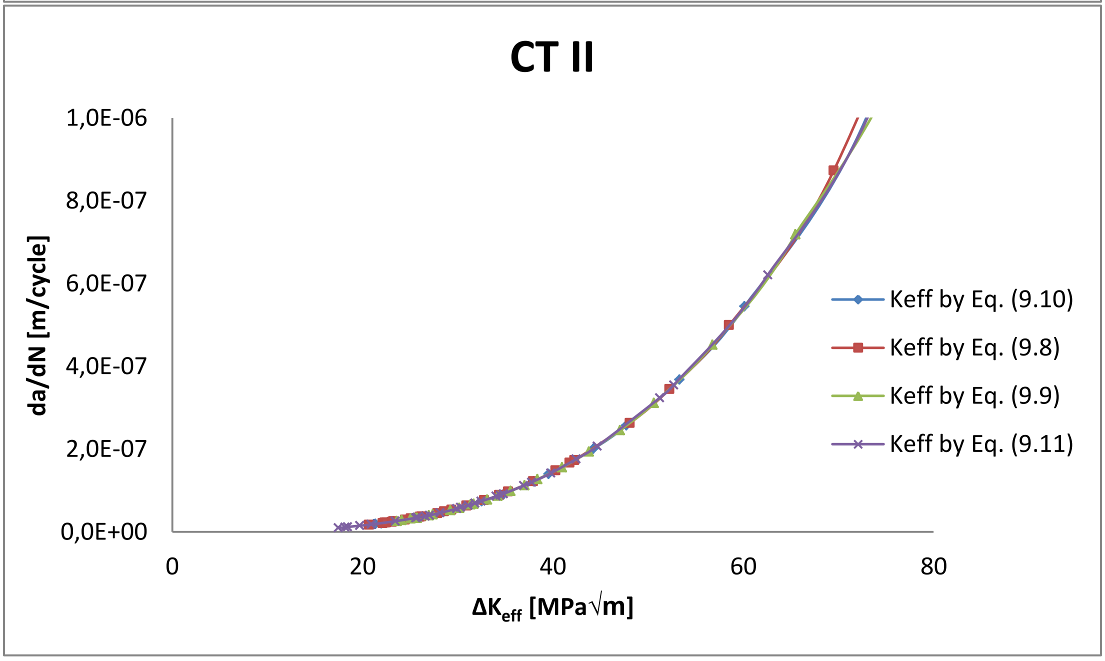

Figure 9.7 : The change of crack growth rate respect to the employed K_{eff} formula at each crack tip for Case I.

cycle (increase the rate of the deviations). Although, the crack propagation varies for each K_{eff} formula, the crack path is approximated nearly the same by each of them.

On the other hand, the other objective of this paper is to find a loading case that the crack grows differently for each K_{eff} formula. To obtain an experimental case, the same plate is subject to different loading cases. After many try the case is found as

$$\left.\begin{aligned} \sigma &= 4.4 \times 10^7(1 + 0.8\sin(wt))\ Pa \\ \tau &= -5.9 \times 10^7(0.5 + \sin(2wt))\ Pa \end{aligned}\right\} \qquad (\mathbf{9.16})$$

The same cracked plate in the Case I is used to illustrate the crack propagation. During the simulation the crack propagates with a constant incensement of 0.0025 m. The constant deviation is assumed to eliminate the effects of crack growth rate where already varies due to ΔK_{eff}. The deviation of crack angle respect to each K_{eff} formula is given in Table 9.1 for initial five crack propagation. The crack growth angle deviates slightly different from each other. That is why the succeeded test case can be used to illustrate which of the K_{eff} formula is the best to estimate the crack path by means of the crack growth rate and the crack growth angle for non-proportional loading.

Table 9.1 : Deviation of the crack growth angle determined by each K_{eff} formula separately.

Number of iteration	K_{eff} by (9.10)		K_{eff} by (9.8)		K_{eff} by (9.9)		K_{eff} by (9.11)	
	CTI [Degree]	CTII [Degree]	CTI [Degree]	CTII [Degree]	CTI [Degree]	CTII [Degree]	CTI [Degree]	CTII [Degree]
1	45,38	225,39	38,21	218,22	35,18	216,16	34,53	214,54
2	15,67	-164,32	29,11	-150,88	36,00	-145,41	37,10	-142,88
3	39,79	-140,20	42,74	-137,24	41,63	-137,78	39,36	-140,62
4	24,74	-155,23	29,97	-150,02	30,15	-150,41	35,83	-144,15
5	31,30	-148,67	39,44	-140,54	40,45	-139,29	35,67	-144,31

10. PROGRAM FLOW CHART

A code for the xFEM has been built in the present work based on the theory, previously discussed. The program has been used to produce the presented examples and to simulate the fatigue crack growth under non-proportional loading. The written *MATLAB* source code will be explained in the following in relation to the flow diagram in Figure 10.1 and with reference to the listed source code in Appendix E, where the sours code given in a CD is briefly described. Referring to Figure 10.1 an overview of the X-FEM code is given. After starting the calculations the program firstly reads the impute file, which defines the problem to be solved.

Then it creates the mesh and connectivity matrices, which includes nod numbering, coordinates of nodes etc. After the Heaviside nodes and crack tip nodes, the initial crack, are defined in the file Discontinuity.m, the total DOF is calculate to initialize the force and displacement vectors, and the global stiffness matrix. By finding the elements to be enriched by Heaviside function or/and branch functions, the global stiffness matrix is assembled in GlobalStifnessMatrixK.m.

For each load step during the current load cycle, the global force vector is defined and by mans of the boundary condition the global equation system is set up and solved. Regarding to the calculated displacement the stress intensity factors are evaluated in the file JIntegral.m. After a load cycle is finished, in the file CrackGrowth.m the crack growth rate da/dN and the crack growth angle θ are evaluated for each crack tip. Furthermore, by using da/dN and θ the crack is redefined as a step wise linear function as illustrated in Figure 7.10. The new crack increments have been defined, and the next step can begin.

The iterations consist of two different iterations. The sub iteration is 36 steps which each step represents the current loading step during a load cycle. The each step of main iteration represents the each crack incensement. After a load cycle is finished, according to the calculated K_I, K_{II} and θ values the crack growth rate and the crack growth angle are calculated by the way of Equations (9.5) and (9.14), respectively.

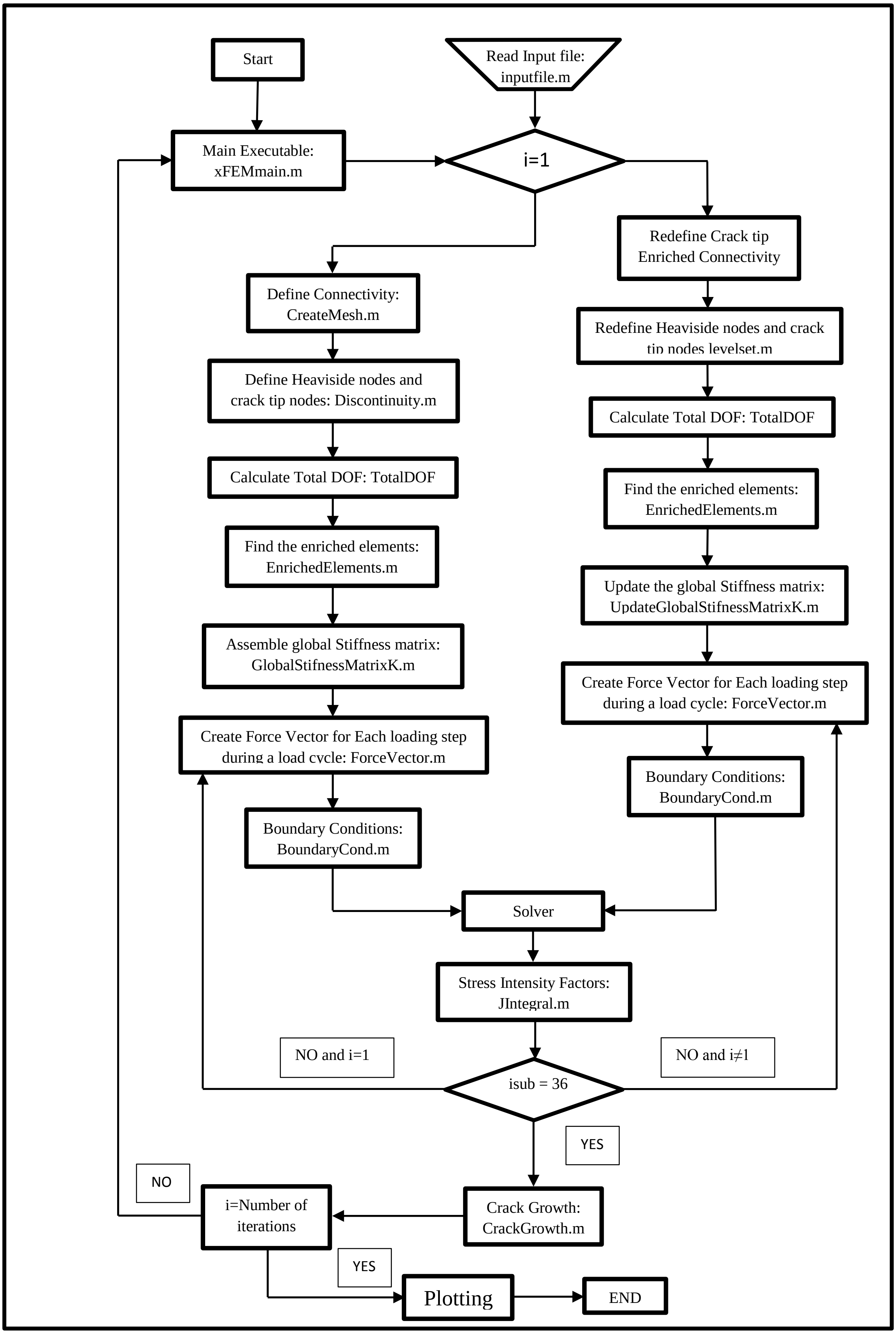

Figure 10.1 : Program flow chart.

11. CONCLUSION

The extended finite element method has been implemented into a MATLAB code to solve mixed mode crack problem. The classical FEM formulation extended to the xFEM by introducing the enriched functions, Heaviside function and Branch functions. The crack body (where the crack passing through elements) is defined by means of Heaviside function and the crack tips (where the crack tips end inside of an element) are illustrated by four branch functions to increase the accuracy of the calculations. The major benefit of using the X-FEM is that the crack path, defined by a step wise linear function, does not have to be known in advance, and there is no need for remeshing. The remashing can only be necessary to catch the crack tips correctly. That is why the mesh is kept in minimal.

Furthermore, the crack analyses carried out in this paper are based on linear elastic fracture mechanic by neglecting the plastic zone that is sufficiently small near the crack tips. That is why the problems cowered are considered linear elastic all the way to brittle fracture. The crack is subject to the mixed mode loadings that force the evaluation of the both of KI and KII stress intensity factors. The stress intensity factors for each mode are evaluated by means of the interaction integral based on the path-independent J-integral. The interaction integral has been converted into a domain integral, which simplifies implementation of the interaction integral into numerical integration, by applying the divergence theorem and making tensor calculus. As the J-integral is path-independent, the domain form of the interaction integral is domain independent as long as it surrounds the crack tip.

On the other hand, to verify results obtained by the developed xFEM program, many problems are solved to ensure that the program is works properly. The results have good agreement with reference ones. Thus, it can be said that the xFEM program can be used to simulate the mixed mode fatigue crack growth with a sufficient accuracy.

The main problem of this paper is the fatigue crack growth under mixed mode non-proportional loading illustrated in Figure 9.2. Both maximum tangential stress criterion and minimum strain energy density criterion are employed to illustrate the crack growth angle for a load cycle. It is found that the crack growth angle can be evaluated either with MTS criterion or with S criterion. MTS criterion is preferred to determine the crack growth angle for each step of load cycle because it minimizes the solution time respect S criterion. The strain energy density citation is in need of much time than maximum tangential stress criterion due to fact that it is necessary to employ an iterative solution to obtain the crack growth angle with the minimum strain energy density citation. Furthermore, to determine the crack growth rate the Paris law is modified with ΔK_{eff} to cover mixed mode cracks.

By the way, the four case is covered to demonstrate the fatigue crack grow angle and the fatigue crack growth rate. The results obtained for the all cases are identical in the Region II where the linear elastic fracture mechanic is valid. The crack growth rates for each case under the variation of the K_{eff} formulas is in the range of 10^{-9} to 10^{-6} m/cycle as expected. The crack growth angle is approximated with Equation (9.14) during a load cycle. It takes into account increasing part of the K_{eff} for a load cycle where K_{eff} values are used as a weight. This means that the larger K_{eff} results in larger effect on the crack growth direction. Under the variation of crack growth rates (evaluated for each K_{eff} formula) the crack growth angle is evaluated nearly the same by each of K_{eff} formulas for all cases. The crack path is determined by different K_{eff} are follows the same direction with a negligible deviation as seen from Figure 9.4, i.e.

The test case is derived to show which of the crack propagation evaluated by any of the K_{eff} formulas is the best suitable to determine the crack path correctly. After examining the many of load combinations for four cases, a test condition is found where the loads are given by (9.15) for a 0.16x0.12 m plate. The material properties of the plate, used during the simulation, are E=200GPa and $\nu = 0.3$ and, Paris law constants are C = $9\text{x}10^{-13}$ and n = 3.25. For the succeeded test case, the crack growth angle deviates slightly deferent from each other where the crack growth rate also deviates respect to ΔK_{eff}. The succeeded test case is one that the larges deviation occurs within covered loadings to find a test condition and can be used to demonstrate the best estimated crack path according to K_{eff}.

In conclusion, an xFEM program developed to demonstrate the fatigue crack growth under non-proportional loading and to derive a test condition that demonstrates which of the K_{eff} formula is the best suitable for determining the crack path correctly. Although good results are obtained for fatigue crack growth under non-proportional loading and a good test condition is derived, the experimental observation is needed for both with given material properties and Paris coefficients.

REFERENCES

[1] **Qian, J. and Fatemi, A.**, Mixed mode fatigue crack growth: A literature survey. *Engineering Fracture Mechanics,* Vol. 55, No.6, pp. 969–990, 1996.

[2] **Rice, J.R.**, Stress in an Infinite Strip Containing a Semi-Infinite Crack, Trans. ASME, Ser. E, J. Appl. Mech., Vol. 34, pp. 248-249, 1967.

[3] **Paris, P. and Erdogan, F.**, A Critical analysis of fatigue crack growth laws, *Journal of Basic Engineering,* Vol.85, No.4, pp. 528-534, 1963.

[4] **Erdogan, F. and Ratwani, M.**, Fatigue and fracture of cylindrical shells containing a circumferential crack, *International Journal of Fracture Mechanics,* Vol. **6, No.**4, pp.379-392, 1970.

[5] **Inglis, C.E.**, Stresses in a Plate Due to the Presence of Cracks and Sharp Corners, *Transactions of the Institute of Naval Architects,* Vol. 55, pp. 219-241, 1913.

[6] **Griffith, A. A.**, The Phenomena of Rupture and Flow in Solids, *Philosophical Transactions,* Series A. Vol. 221. 1920. pp. 163-198.

[7] **Irwin, G.R.**, Fracture Dynamics, Fracturing of Metals, *American Society for Metals*, Cleveland, pp. 147-166, 1948.

[8] **Orowan, E.**, Fracture and Strength of Solids, Reports on Progress in Physics, Vol. 12, 1948.

[9] **Irwin, G.R.**, Analysis of Stresses and Strains near the End of a Crack Traversing a Plate, *Journal of Applied Mechanics,* Vol. 24, pp. 361-364, 1957.

[10] **Westergaard, H.M.**, Bearing Pressures and Cracks, *Journal of Applied Mechanics,* Vol. 6, pp. 49-53, 1939.

[11] **Williams, M.**, On the stress distribution at the base of a stationary crack, *Journal of Applied Mechanics*, Vol. 24, pp. 109-114, 1957.

[12] **Jensen, H. M.**, Notes in Fracture Mechanics, Technical University of Denmark, 2005.61, pp. A49-A53, 1939.

[13] **Eshelby , J.**, The Continuum Theory of Lattice Defects, *Solid state physics advances in research and applications* Vol. 3, pp. 79-144, 1956.

[14] **Rice, J. R.**, A Path Independent Integral and the Approximate Analysis of Strain Concentration by Notches and Cracks, *Journal of Applied Mechanics*, Vol. 35, pp. 379-386, 1968.

[15] **Cook, R. D., Malkus, D. S., Plesha, M. E. and Witt, R. J.**, Concepts and Applicationsof Finite Element Analysis, Wiley, 4th edition, 2002.

[16] **Moës , N., Dolbow , J. and Belytschko, T.**, A finite element method for crack growth without remeshing, *International Journal for Numerical Methods in Engineering*, vol. 46, pp. 131–150, 1999.

[17] **Belytschko, T. and Black, T.**, Elastic Crack Growth in Finite Elements with Minimal Remeshing, *International Journal for Numerical Methods in Engineering*, Vol. 45, pp. 601-620, 1999.

[18] **Yau, J. F., Wang, S. S. and Corten, H. T.**, "A Mixed-Mode Crack Analysis of Isotropic Solids Using Conservation Laws of Elasticity", *Journal of Applied Mechanics*, Vol. 47, pp. 335-341, 1980.

[19] **Moran, B. and Shih, C.**, Crack Tip and Associated Domain Integrals from Momentum and Energy Balance, *Engineering Fracture Mechanics*, Vol. 27, No. 6, pp. 615-642, 1987.

[20] **Shih C., Asaro R.**, Elastic-plastic analysis of cracks on bimaterial interfaces: part I—small scale yielding, *Journal of Applied Mechanics*, Vol. 55, pp. 299 – 316, 1988.

[21] **Isida, M.**, Effect of Width and Length on Stress Intensity Factors of Internally Cracked plates Under Various Baundary Condiyions, *International Journal of Fracture*, Vol.7, No. 3, pp. 301-316, 1971.

[22] **Kitagavwa, H. and Yuuki, R.**, Analysis of Arbitrarily shaped Crack in a Finite Plate Using Conformal Mapping, 1st Report – Construction of Analysis Procedure and its Applicability, Trans. Japan Soc. Mech. Engrs., Vol. 43, No. 376, pp. 4354-4362, 1977.

[23] **Wilson, W. K.**, Numerical Method for Determining Stress Intensity Factors of an Interior Crack in a Finite Plate, Trans. ASME, Ser. D, J. Basic Eng., Vol. 93, pp. 685-690, 1971.

[24] **Freese, C. E.**, Solution of Plane Crack Problems by Mapping Technique, *Mechanics of Fracture* (Ed. G. C. Sih), Vol. 1, pp.1-55, 1973.

[25] **Wilson, W. K.**, Research Report 69-1E7-FMECH-R1, *Westinghouse Research Laboratories*, Pittsburgh 1969.

[26] **Kitagavwa, H. and Yuuki, R.**, Analysis of Branched Cracks Under Biaxial Stresses, *in Fracture* 1977, Vol. 3, University of Waterloo Press 1977, p. 201

[27] **Sih, G. C. and Barthelemy, B. M.**, Mixed mode fatigue crack growth predictions, *Engineerin Fracture Mechanics*, Vol. 13, pp. 439-451, 1980.

[28] **Badaliance, R.**, Application of strain energy factor to fatigue crack growth analysis, *Engineering Fracture Mechanics*, 13, 657-666, 1980.

[29] **Erdogan, F. and Sih, G. C.**, On the Crack extension in plates under plane loading and transverse shear. *Journal of Basic Engineering*, Vol.85, No. 4, pp. 519-527, 1963.

[30] **Sih, G. C.**, Strain energy density factor applied to mixed mode crack problems, *International Journal of Fracture*, 1974, Vol. 10, No.3, pp. 305-321

[31] **Lucht T.**, Adaptive FE analysis of non-planar 3D crack growth by the use of a BE submodel, 2007.

[32] **Rhee, H. C.**, The behavior of stress intensity factors of weld toe surface flaw of tubular X-Joints, OTC Paper 5136,18th Annual Offshore Technology Conference, Texas, May 1896

[33] **Gerstle,W.**, Finite and boundary element modeling of crack propagation in two and three dimensions using interactive computer graphics, *PhD Thesis, Cornell University, New York*,1985.

[34] **Tanaka, K.**, Fatigue crack propagation from a crack inclined to the cyclic tensile axis. *Engineering Fracture Mechanics* Vol. 6, No.2, pp. 493–507, 1974.

[35] **Yan, X., Du, S. and Zhang, Z**., Mixed-Mode Fatigue Crack Growth Prediction in Biaxially Stretched Sheets, *Engineering Fracture Mechanics*, Vol. 43, pp. 471-475, 1992.

[36] **Murakami, Y.**, Stress Intensity Factors Handbook volume 1, Pergamon Press, 1987.

[37] **Murakami, Y.**, A Method of Stress Intensity Factor Calculation for the Crack Emanating from an Arbitrarily Shaped Hole or the Crack in the Vicinity of Arbitrarily Shaped Hole, Trans. Japan Soc. Mech. Engrs.,Vol. 44,No. 378, pp. 423-432, 1978.

[38] **Bainbridge, C. M.**, Aliabadi, M. H. and Rooke, D. P., A path-independent integral for stress intensity factors in three dimensions, *Journal of Strain Analysis*, Vol. 32, No. 6, pp. 411-423, 1997.

[39] **Führing, H.**, Approximation Functions for K-Factors of Cracks in Notches, *International Journal of Fracture*, Vol.9, pp. 328-331, 1973.

[40] **Hellen, T. K. and Blackburn, W. S.**, The calculation of stress intensity factors for combined tensile and loading, *International Journal of Fracture*, Vol. 11, No. 4, pp. 605-617, 1975

[41] **Liu, Y. and Mahadevan, S.**, Threshold stress intensity factor and crack growth rate prediction under mixed-mode loading, *Engineering Fracture Mechanics*, Vol. 74, pp. 332-345, 2007.

[42] **Ma, Y. L., Shimizu, K. and Torii, T.**, Fatigue crack propagation behavior bent from precrack under Mixed mode conditions, *Memoirs of the Faculty of Engineering*, Okayama University, Vol. 40, pp.1-8, 2006

[43] **Magıll, M. A. and Zwerneman, F. J.**, Sustained mode I and mode II fatigue crack growth in flat plates, *Engineering Fracture Mechanics*, Vol. 55, No. 6, pp. 883-899, 1996.

[44] **Nakamura, H., Takanashi, M., Itoh, T., Wu, M. and Shimizu, Y.**, Fatigue crack initiation and growth behavior of Ti-6Al-4V under non-proportional multiaxial loading, *International Journal of Fatigue*, Vol. 33, pp. 842-848, 2011.

[45] **Plank, R. and Kuhn, G.**, Fatigue crack propagation under non-proportional mixed mode loading, *Engineering Fracture Mechanics*, Vol. 62, pp. 203-229, 1999.

[46] **Rhee, H. C., Han, S. and Gipson, G. S.**, Reliability of solution Method and empirical formulas of stress intensity factors for weld toe cracks of tubular joints materials engineering, Proc. Conf. Offshore Mechanics and Arctic Engineering, III(B), pp. 441-452, 1991,

[47] **Roberts, R. and Kibler, J. J.**, Mode II fatigue crack propagation, *Journal of Basic Engineering (Trans. ASME, D)*, Vol. 93, No. 4, pp. 671-680, 1971

[48] **Sneddon, I.N.**, The Distribution of Stress in the Neighbourhood of a Crack in an Elastic, Solid, Proceedings, *Royal Society of London*, Vol. A-187, pp. 229-260, 1946.

[49] **Williams, T. N., Newman, Jr, J. C., Gullett, P. M.**, Crack–surface displacements for cracks emanating from a circular hole under various loading conditions, *Fatigue & Fracture of Engineering Materials & Structures*, Vol.34, No.4, pp. 250–259, April 2011

APPENDICES

APPENDIX A: The Stress and the Displacement Fields for Pure Mode I and Mode II , Auxiliary Stages

APPENDIX B: Matrices and expressions Used in the report

APPENDIX B.1: Selected Matrices from Standard FEM Formulations

APPENDIX B.2: Displacement Approximated with the Heaviside Function and the Evaluation of Strain-displacement Matrix for Heaviside Enriched Elements

APPENDIX B.3: Displacement Approximated with the Four Branch Functions and the Evaluation of Strain-displacement Matrix for Crack Tip Enriched Elements

APPENDIX B.4: Evaluation of the Derivatives of the Four Branch Functions

APPENDIX C: Gauss Quadrature Coefficients for Rectangle and Triangle Elements

APPENDIX D: Extra Examples

APPENDIX D.1: Crack Emanating from a Circular Hole in a Rectangular Plate under Tension

APPENDIX D.2: Crack Emanating from a Rectangular Hole in a Rectangular Plate Under Tension

APPENDIX D.3: The crack Propagation Near a Hole

APPENDIX E: The illustration of the tree remain non-proportional loading cases with an additional Case I

APPENDIX E.1: Additional Case I: A Cyclic Proportional Mixed Mode Loading + A Static Mode I

APPENDIX E.2: Case II: A Cyclic Mode I or II + A Static Proportional Mixed Mode Loading

APPENDIX E.3: Case III: A Cyclic Mode II + A Static Mode I Loading

APPENDIX E.4: Case IV: A Cyclic Mode I + A Static Mode II Loading

APPENDIX F: Brief Description of the MATLAB Source Code

APPENDIX A

The stress fields and the displacement fields near the crack tip for the Auxiliary stages derived by Westergaard [10], Williams [11] and Jensen [12] are listed below for Cartesian Coordinates x_i for 2D problems.

For Pure Mode I: KII=0 and KIII =0

Stress field:

$$\sigma_{11} = \frac{1}{\sqrt{2\pi r}}\left\{K_I \cos\frac{\theta}{2}\left[1 - \sin\frac{\theta}{2}\sin\frac{3\theta}{2}\right]\right\} + \sigma_{11}^0 + \Phi(\sqrt{r}) \qquad (\mathbf{A.1})$$

$$\sigma_{22} = \frac{1}{\sqrt{2\pi r}}\left\{K_I \cos\frac{\theta}{2}\left[1 + \sin\frac{\theta}{2}\sin\frac{3\theta}{2}\right]\right\} + \Phi(\sqrt{r}) \qquad (\mathbf{A.2})$$

$$\sigma_{12} = \sigma_{21} = \frac{1}{\sqrt{2\pi r}}\left\{K_I \sin\frac{\theta}{2}\cos\frac{\theta}{2}\cos\frac{3\theta}{2}\right\} + \Phi(\sqrt{r}) \qquad (\mathbf{A.3})$$

$$\sigma_{33} = \begin{Bmatrix} 0 & for\ plane\ stress \\ \upsilon(\sigma_{11} + \sigma_{22}) & for\ plane\ strain \end{Bmatrix} \qquad (\mathbf{A.4})$$

$$all\ other\ \sigma_{ij} = 0 \qquad (\mathbf{A.5})$$

Displacement field:

$$u_1 = \frac{(1+\upsilon)K_I}{4\pi E}\sqrt{2\pi r}\left\{[2\kappa - 1]\cos\frac{\theta}{2} - \cos\frac{3\theta}{2}\right\} + \Phi(r) \qquad (\mathbf{A.6})$$

$$u_2 = \frac{(1+\upsilon)K_I}{4\pi E}\sqrt{2\pi r}\left\{[2\kappa + 1]\sin\frac{\theta}{2} - \sin\frac{3\theta}{2}\right\} + \Phi(r) \qquad (\mathbf{A.7})$$

$$u_3 = \begin{Bmatrix} -\frac{\upsilon}{E}\int(\sigma_{11} + \sigma_{22})dx_3 & for\ plane\ stress \\ 0 & for\ plane\ strain \end{Bmatrix} \qquad (\mathbf{A.8})$$

For Pure Mode II: KI=0 and KIII =0

Stress field:

$$\sigma_{11} = -\frac{1}{\sqrt{2\pi r}}\left\{K_{II} \sin\frac{\theta}{2}\left[2 + \cos\frac{\theta}{2}\cos\frac{3\theta}{2}\right]\right\}\Phi(\sqrt{r}) \qquad (\mathbf{A.9})$$

$$\sigma_{22} = \frac{1}{\sqrt{2\pi r}}\left\{K_{II} \sin\frac{\theta}{2}\cos\frac{\theta}{2}\cos\frac{3\theta}{2}\right\}\Phi(\sqrt{r}) \qquad (\mathbf{A.10})$$

$$\sigma_{12} = \sigma_{21} = \frac{1}{\sqrt{2\pi r}}\left\{K_{II} \cos\frac{\theta}{2}\left[1 - \sin\frac{\theta}{2}\sin\frac{3\theta}{2}\right]\right\} + \Phi(\sqrt{r}) \qquad (\mathbf{A.11})$$

$$\sigma_{33} = \begin{Bmatrix} 0 & for\ plane\ stress \\ \upsilon(\sigma_{11} + \sigma_{22}) & for\ plane\ strain \end{Bmatrix} \quad (\mathbf{A.12})$$

$$all\ other\ \sigma_{ij} = 0 \quad (\mathbf{A.13})$$

Displacement field:

$$u_1 = \frac{(1+\upsilon)K_{II}}{4\pi E}\sqrt{2\pi r}\left\{[2\kappa + 3]\sin\frac{\theta}{2} + \sin\frac{3\theta}{2}\right\} + \Phi(r) \quad (\mathbf{A.14})$$

$$u_2 = \frac{(1+\upsilon)K_{I}}{4\pi E}\sqrt{2\pi r}\left\{[2\kappa - 3]\cos\frac{\theta}{2} + \cos\frac{3\theta}{2}\right\} + \Phi(r) \quad (\mathbf{A.15})$$

$$u_3 = \begin{Bmatrix} -\frac{\upsilon}{E}\int(\sigma_{11} + \sigma_{22})dx_3 & for\ plane\ stress \\ 0 & for\ plane\ strain \end{Bmatrix} \quad (\mathbf{A.16})$$

where υ is passion's ratio, E is Young's modulus , $\theta\ and\ r$ are respectively the polar coordinates at the crack tip, the term Φ is includes just the higher order terms that nor considered in this paper and κ is the Kolosov constant. The Kolosov constant is defined as

$$\kappa = \begin{Bmatrix} \frac{3-\upsilon}{1+\upsilon} & for\ plane\ stress \\ 3-4\upsilon & for\ plane\ strain \end{Bmatrix} \quad (\mathbf{A.17})$$

APPENDIX B

It is preferred to present some of matrices and expressions in this section for avoiding confusion of the report.

APPENDIX B.1

The constitutive law for linear elastic materials under plane stress ($\sigma_{33} = \sigma_{13} = \sigma_{23} = 0$) is

$$\begin{Bmatrix} \sigma_{11} \\ \sigma_{22} \\ \sigma_{12} \end{Bmatrix} = \frac{E}{1-\nu^2} \begin{bmatrix} 1 & \nu & 0 \\ \nu & 1 & 0 \\ 0 & 0 & 1-\nu \end{bmatrix} \begin{Bmatrix} \varepsilon_{11} \\ \varepsilon_{22} \\ \varepsilon_{12} \end{Bmatrix} \qquad (\boldsymbol{B.1})$$

and the constitutive law under plane strain condition ($\varepsilon_{33} = \varepsilon_{13} = \varepsilon_{23} = 0$) is

$$\begin{Bmatrix} \sigma_{11} \\ \sigma_{22} \\ \sigma_{33} \\ \sigma_{12} \end{Bmatrix} = \frac{E}{1-\nu^2} \begin{bmatrix} 1-\nu & \nu & \nu & 0 \\ \nu & 1-\nu & \nu & 0 \\ \nu & \nu & 1-\nu & 0 \\ 0 & 0 & 0 & 1-2\nu \end{bmatrix} \begin{Bmatrix} \varepsilon_{11} \\ \varepsilon_{22} \\ \varepsilon_{33}(=0) \\ \varepsilon_{12} \end{Bmatrix} \qquad (\mathbf{B.2})$$

The strain – displacement matrix in Equation (3.10) defined by the three matrix can be defined as:

$$[B] = [L][\Gamma][N,] \qquad (\mathbf{B.3})$$

The $[L]$ matrix in (C.1) is the link matrix between strains and displacement derivatives according to global coordinates. The matrix $[L]$ for plane stress is

$$\begin{Bmatrix} \varepsilon_{11} \\ \varepsilon_{22} \\ \varepsilon_{12} \end{Bmatrix} = \begin{bmatrix} 1 & 0 & 0 & 0 \\ 0 & 0 & 0 & 1 \\ 0 & \frac{1}{2} & \frac{1}{2} & 0 \end{bmatrix} \begin{Bmatrix} u_{1,1} \\ u_{1,2} \\ u_{2,1} \\ u_{2,2} \end{Bmatrix} = [L] \begin{Bmatrix} u_{1,1} \\ u_{1,2} \\ u_{2,1} \\ u_{2,2} \end{Bmatrix} \qquad (\mathbf{B.4})$$

and for plane strain;

$$\begin{Bmatrix} \varepsilon_{11} \\ \varepsilon_{22} \\ \varepsilon_{33}(=0) \\ \varepsilon_{12} \end{Bmatrix} = \begin{bmatrix} 1 & 0 & 0 & 0 \\ 0 & 0 & 0 & 1 \\ 0 & 0 & 0 & 0 \\ 0 & \frac{1}{2} & \frac{1}{2} & 0 \end{bmatrix} \begin{Bmatrix} u_{1,1} \\ u_{1,2} \\ u_{2,1} \\ u_{2,2} \end{Bmatrix} = [L] \begin{Bmatrix} u_{1,1} \\ u_{1,2} \\ u_{2,1} \\ u_{2,2} \end{Bmatrix} \qquad (\mathbf{B.5})$$

It can be simplify as

$$\begin{Bmatrix} \varepsilon_{11} \\ \varepsilon_{22} \\ \varepsilon_{12} \end{Bmatrix} = \begin{bmatrix} 1 & 0 & 0 & 0 \\ 0 & 0 & 0 & 1 \\ 0 & \frac{1}{2} & \frac{1}{2} & 0 \end{bmatrix} \begin{Bmatrix} u_{1,1} \\ u_{1,2} \\ u_{2,1} \\ u_{2,2} \end{Bmatrix} = [L] \begin{Bmatrix} u_{1,1} \\ u_{1,2} \\ u_{2,1} \\ u_{2,2} \end{Bmatrix} \qquad (\mathbf{B.6})$$

where it enables the [L] matrix to be the same for both plane stress and plane strain.

The [Γ] matrix is used in (C.1) connects the displacement derivatives in the global coordinates with the displacements differentiated according to the mapped coordinates, $\eta - \xi$. The [Γ] matrix can be written as an expansion of the invers of Jacobian matrix to take the two dimensions of the displacements, u_1 *and* u_2, into account. It takes the following form

$$\begin{Bmatrix} u_{1,1} \\ u_{1,2} \\ u_{2,1} \\ u_{2,2} \end{Bmatrix} = \begin{bmatrix} \Gamma_{11} & \Gamma_{12} & 0 & 0 \\ \Gamma_{21} & \Gamma_{22} & 0 & 0 \\ 0 & 0 & \Gamma_{11} & \Gamma_{12} \\ 0 & 0 & \Gamma_{21} & \Gamma_{22} \end{bmatrix} \begin{Bmatrix} u_{1,\xi} \\ u_{1,\eta} \\ u_{2,\xi} \\ u_{2,\eta} \end{Bmatrix} = [\Gamma] \begin{Bmatrix} u_{1,\xi} \\ u_{1,\eta} \\ u_{2,\xi} \\ u_{2,\eta} \end{Bmatrix} \qquad (\mathbf{B.7})$$

The $[\mathrm{N},]$ matrix is the matrix of derivatives of shape functions respect to the mapped coordinate system. Is enables to write the displacement derivatives respect to the mapped coordinates, $\eta - \xi$. In matrix notation $[\mathrm{N},]$ can be expressed as

$$\begin{Bmatrix} u_{1,\xi} \\ u_{1,\eta} \\ u_{2,\xi} \\ u_{2,\eta} \end{Bmatrix} = \begin{bmatrix} \mathrm{N}_{1,\xi} & 0 & \mathrm{N}_{2,\xi} & 0 & \mathrm{N}_{3,\xi} & 0 & \mathrm{N}_{4,\xi} & 0 \\ \mathrm{N}_{1,\eta} & 0 & \mathrm{N}_{2,\eta} & 0 & \mathrm{N}_{3,\eta} & 0 & \mathrm{N}_{4,\eta} & 0 \\ 0 & \mathrm{N}_{1,\xi} & 0 & \mathrm{N}_{2,\xi} & 0 & \mathrm{N}_{3,\xi} & 0 & \mathrm{N}_{4,\xi} \\ 0 & \mathrm{N}_{1,\eta} & 0 & \mathrm{N}_{2,\eta} & 0 & \mathrm{N}_{3,\eta} & 0 & \mathrm{N}_{4,\eta} \end{bmatrix} \begin{Bmatrix} u_1 \\ u_2 \\ u_3 \\ u_4 \\ u_5 \\ u_6 \\ u_7 \\ u_8 \end{Bmatrix} = [N,] \begin{Bmatrix} u_1 \\ u_2 \\ u_3 \\ u_4 \\ u_5 \\ u_6 \\ u_7 \\ u_8 \end{Bmatrix} \qquad (\boldsymbol{B.8})$$

And the strain displacement matrix transforms for both case to

$$[B] = \begin{bmatrix} N_{1,1} & 0 & N_{2,1} & 0 & N_{3,1} & 0 & N_{4,1} & 0 \\ 0 & N_{1,2} & 0 & N_{2,2} & 0 & N_{3,2} & 0 & N_{4,2} \\ N_{1,2} & N_{1,1} & N_{2,2} & N_{2,1} & N_{3,2} & N_{3,1} & N_{4,2} & N_{4,1} \end{bmatrix} \qquad (\mathbf{B.9})$$

where numbers 1,2,3 and 4 shows the set of nodes initial with the current node.

APPENDIX B.2

$[B^b]$ can be easily evaluated as the previous strain-displacement matrix found for the classical elements. Displacement formulation of an element, initial with Heaviside function, is given in matrix notation by

$$(u^h)_b = H\,[N^b]\{b\} \qquad (\boldsymbol{B.10})$$

The differentiation of the b-enriched displacement respect to global coordinates is given by

$$(u^h)'_b = (H\,[N^b])'\{b\} = H([N^b])'\{b\} \qquad (\boldsymbol{B.11})$$

The strain-displacement matrix can be evaluated as

$[B^b] = H([N^b])'$ where the comma means the derivatives respect to global coordinates, x_1 and x_2. The derivation of the Heaviside function will not appear on the strain-displacement formulation due to fact that it takes the values of +1 and -1 by passing the discontinuity.

The strain-displacement matrix can be evaluated as

$$[B^b] = H[L][\Gamma]\left[N^b_{,}\right] \qquad (\boldsymbol{B.12})$$

where the all matrices are already available from Appendix B.1. It has a similar form with Equation (B.9) as

$$B_i^b = \begin{bmatrix} H\,N_{i,1} & 0 \\ 0 & H\,N_{i,2} \\ H\,N_{i,2} & H\,N_{i,1} \end{bmatrix} \qquad (\boldsymbol{B.13})$$

where $i = \{1,2,3,4\}$ is the linear combinations of nodes that are enriched by Heaviside function. For example, for any element that has b-enriched nodes of 1,3 and 4, the strain displacement matrix initial with b-DOFs becomes as

$$[B^b] = \begin{bmatrix} H\,N_{1,1} & 0 & H\,N_{3,1} & 0 & H\,N_{4,1} & 0 \\ 0 & H\,N_{1,2} & 0 & H\,N_{3,2} & 0 & H\,N_{4,2} \\ H\,N_{1,2} & H\,N_{1,1} & H\,N_{3,2} & H\,N_{3,1} & H\,N_{4,2} & H\,N_{4,1} \end{bmatrix} \qquad (\boldsymbol{B.14})$$

APPENDIX B.3

The contributions of the displacements connected with the four branch functions – cDOFs, see Equation (4.9), are for each element has crack tip enrichment

$$u^h = \sum_{k=1}^{4} N_k(x)\left(\sum_{l=1}^{4} F_l(x)\; c_k^l\right) \qquad (\boldsymbol{B.15})$$

The summation of shape functions over four nodes can be written in matrix notation as

$$[N] = \begin{bmatrix} N_1 & 0 & N_2 & 0 & N_3 & 0 & N_4 & 0 \\ 0 & N_1 & 0 & N_2 & 0 & N_3 & 0 & N_4 \end{bmatrix} \qquad (\boldsymbol{B.16})$$

and similarly the four branch function in matrix form can be expressed as

$$[F] = \begin{bmatrix} [F^*] & & & \\ & [F^*] & & \\ & & [F^*] & \\ & & & [F^*] \end{bmatrix} \qquad (\boldsymbol{B.17})$$

where the blanks are zero and

$$[F^*] = \begin{bmatrix} F_1 & 0 & F_2 & 0 & F_3 & 0 & F_4 & 0 \\ 0 & F_1 & 0 & F_2 & 0 & F_3 & 0 & F_4 \end{bmatrix} \qquad (\boldsymbol{B.18})$$

Displacement formulation of an element, initial with the four branch function, is given in matrix notation by

$$(u^h)_c = [N^c][F]\{c\} \qquad (\boldsymbol{B.19})$$

a fully crack tip enriched element is shown ın Figure B.1 with u-DOFs and cDOFs.

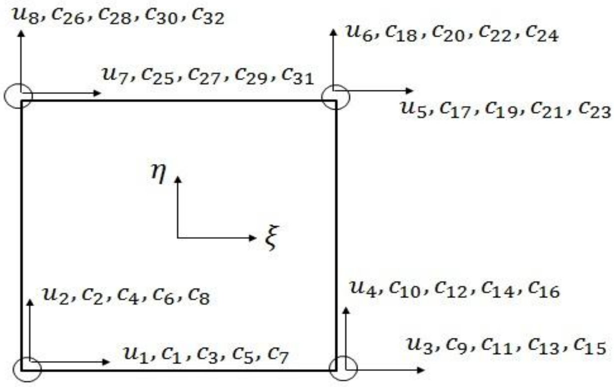

Figure B.1 : An element with four crack tip enriched nodes.

The differentiation of the c-enriched displacement respect to global coordinates is given by

$$(u^h)'_c = ([N^c][F])'\{c\} = [N^c]'[F]\,\{c\} + [N^c]\,[F]'\,\{c\} \qquad (\boldsymbol{B.20})$$

The strain-displacement matrix for the c-enrichment can be evaluated as

$$[B^c] = [N^c]'[F] + [N^c]\,[F]' \qquad (\boldsymbol{B.21})$$

where the comma means the derivatives respect to global coordinates, x_1 and x_2. By applying the chain rule the shape function derivatives matrix $[N^c]'$ can be evaluated easily as

$$[N^c]' = [L][\Gamma][N^c_{,}] \qquad (\boldsymbol{B.22})$$

The strain-displacement matrix can be rewritten as

$$[B^c] = [L][\Gamma][N^c_{,}][F] + [N^c]\,[F]' \qquad (\boldsymbol{B.23})$$

It has a similar form with Equation (B.13) as

$$B_i^c = [B_i^{c1}\; B_i^{c2}\; B_i^{c3}\; B_i^{c4}] \qquad (\boldsymbol{B.24})$$

where B_i^{cl} are given as

$$\left.\begin{aligned}
B_i^{c1} &= \begin{bmatrix} N_{i,1}F_1 + N_iF_{1,1} & 0 \\ 0 & N_{i,2}F_1 + N_iF_{1,2} \\ N_{i,2}F_1 + N_iF_{1,2} & N_{i,1}F_1 + N_iF_{1,1} \end{bmatrix} \\
B_i^{c2} &= \begin{bmatrix} N_{i,1}F_2 + N_iF_{2,1} & 0 \\ 0 & N_{i,2}F_2 + N_iF_{2,2} \\ N_{i,2}F_2 + N_iF_{2,2} & N_{i,1}F_2 + N_iF_{2,1} \end{bmatrix} \\
B_i^{c3} &= \begin{bmatrix} N_{i,1}F_3 + N_iF_{3,1} & 0 \\ 0 & N_{i,2}F_3 + N_iF_{3,2} \\ N_{i,2}F_3 + N_iF_{3,2} & N_{i,1}F_3 + N_iF_{3,1} \end{bmatrix} \\
B_i^{c4} &= \begin{bmatrix} N_{i,1}F_4 + N_iF_{4,1} & 0 \\ 0 & N_{i,2}F_4 + N_iF_{4,2} \\ N_{i,2}F_4 + N_iF_{4,2} & N_{i,1}F_2 + N_iF_{4,1} \end{bmatrix}
\end{aligned}\right\} \qquad (\boldsymbol{B.25})$$

For example, for any element that has b-enriched nodes of 1 and 2, the strain displacement matrix initial with b-DOFs becomes as

$$[B^c] = [B_1^{c1}\ B_1^{c2}\ B_1^{c3}\ B_1^{c4}\ B_2^{c1}\ B_2^{c2}\ B_2^{c3}\ B_2^{c4}] \qquad (\boldsymbol{B.26})$$

APPENDIX B.4

The four branch functions have already been defined in terms of the local crack tip polar coordinates system (r, θ) as

$$F_l = \left\{\sqrt{r}\sin\frac{\theta}{2},\ \ \sqrt{r}\cos\frac{\theta}{2},\ \ \sqrt{r}\sin\theta\sin\frac{\theta}{2},\ \ \sqrt{r}\sin\theta\cos\frac{\theta}{2}\right\} \qquad (\boldsymbol{B.27})$$

Derivatives of $F_l(r.\theta)$ with respect to the crack tip polar coordinates $(r.\theta)$ become

$$\left.\begin{aligned}
F_{1,r} &= \frac{1}{2\sqrt{r}}\sin\frac{\theta}{2}, & F_{1,\theta} &= \frac{\sqrt{r}}{2}\cos\frac{\theta}{2} \\
F_{2,r} &= \frac{1}{2\sqrt{r}}\cos\frac{\theta}{2}, & F_{2,\theta} &= -\frac{\sqrt{r}}{2}\sin\frac{\theta}{2} \\
F_{3,r} &= \frac{1}{2\sqrt{r}}\sin\theta\sin\frac{\theta}{2}, & F_{3,\theta} &= \sqrt{r}\left(\cos\theta\sin\frac{\theta}{2} + \frac{1}{2}\sin\theta\cos\frac{\theta}{2}\right) \\
F_{4,r} &= \frac{1}{2\sqrt{r}}\sin\theta\cos\frac{\theta}{2}, & F_{3,\theta} &= \sqrt{r}\left(\cos\theta\cos\frac{\theta}{2} - \frac{1}{2}\sin\theta\sin\frac{\theta}{2}\right)
\end{aligned}\right\} \qquad (\boldsymbol{B.28})$$

and the derivatives of $F_l(r.\theta)$ with respect to the local crack coordinate system $(\tilde{x}_1, \tilde{x}_2)$,by means of coordinate transformation, can then be defined as:

$$\left.\begin{aligned}
F_{1,\tilde{x}_1} &= -\frac{1}{2\sqrt{r}}\sin\frac{\theta}{2}, & F_{1,\tilde{x}_2} &= \frac{1}{2\sqrt{r}}\cos\frac{\theta}{2} \\
F_{2,\tilde{x}_1} &= \frac{1}{2\sqrt{r}}\cos\frac{\theta}{2}, & F_{2,\tilde{x}_2} &= \frac{1}{2\sqrt{r}}\sin\frac{\theta}{2} \\
F_{3,\tilde{x}_1} &= -\frac{1}{2\sqrt{r}}\sin\theta\sin\frac{3\theta}{2}, & F_{3,\tilde{x}_2} &= \frac{1}{2\sqrt{r}}\left(\sin\frac{\theta}{2}+\cos\theta\sin\frac{3\theta}{2}\right) \\
F_{4,\tilde{x}_1} &= \frac{1}{2\sqrt{r}}\sin\theta\cos\frac{3\theta}{2}, & F_{3,\tilde{x}_2} &= \frac{1}{2\sqrt{r}}\left(\cos\frac{\theta}{2}+\cos\theta\cos\frac{3\theta}{2}\right)
\end{aligned}\right\} \qquad (\boldsymbol{B.29})$$

Finally, the derivatives in the global coordinate system,(x_1, x_2), are obtained as

$$\left.\begin{aligned}
F_{l,1} &= F_{1,\tilde{x}_1}\ \cos(\alpha) - F_{1,\tilde{x}_2}\ \sin(\alpha) \\
F_{l,2} &= F_{1,\tilde{x}_1}\ \sin(\alpha) + F_{1,\tilde{x}_2}\ \cos(\alpha)
\end{aligned}\right\} \qquad (\boldsymbol{B.30})$$

where α is the angle of crack path with respect to the x_1 axis.

APPENDIX C

Table C.1 : Gauss points and weights for rectangular elements.

Order n	Location of Gauss Points (ξ_i, η_j)	Weight factors W_i, W_j
6	∓ 0.932469514203152	0.171324492379170
	∓ 0.661209386466265	0.360761573048139
	∓ 0.238619186083197	0.467913934572691

Table C.2 : Gauss points and weights for triangular elements.

Number of Gauss Points	Location of Gauss Points ξ_i	η_j	Weight factors W_i
3	0.166666666666667	0.166666666666667	0.333333333333333
	0.666666666666667	0.166666666666667	0.333333333333333
	0.166666666666667	0.666666666666667	0.333333333333333
7	0.101286507323456	0.101286507323456	0.125939180544827
	0.470142064105115	0.059715871789770	0.132394152788506
	0.797426985353087	0.101286507323456	0.125939180544827
	0.333333333333333	0.333333333333333	0.225030000300000
	0.059715871789770	0.470142064105115	0.132394152788506
	0.470142064105115	0.470142064105115	0.132394152788506
	0.101286507323456	0.797426985353087	0.125939180544827

APPENDIX D

APPENDIX D.1

The next problem is simulation of a crack emanating from a circular hole in a rectangular plate under tension (ACECHRPUT) in Figure D.1. To calculate the stress

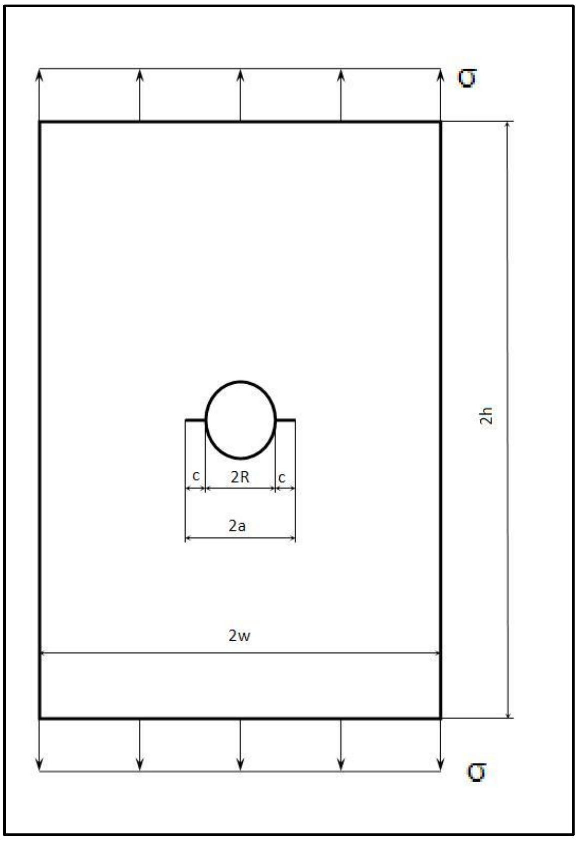

Figure D.1 : A crack emanating from a circular hole in a rectangular plate under tension.

intensity factor for current example, it is necessary to define the hole and additional boundary conditions. The circular hole is defined by a piecewise function f_h in Figure D.2 (a). the piecewise function fh is given by

$$f_h = \begin{cases} -1 & if\ d - r > 0 \\ 0 & if\ d - r = 0 \\ +1 & if\ d - r < 0 \end{cases} \qquad (\boldsymbol{D.1})$$

where d is the distance of any node from the center of the circular hole and r is the radius of the circular hole. Figure D.2 (b) illustrates an element has a discontinuity due to the circular hole. The nodes on the hole boundary is kept stress free and the nodes inside of the hole are skipped during the calculation of the global stiffness

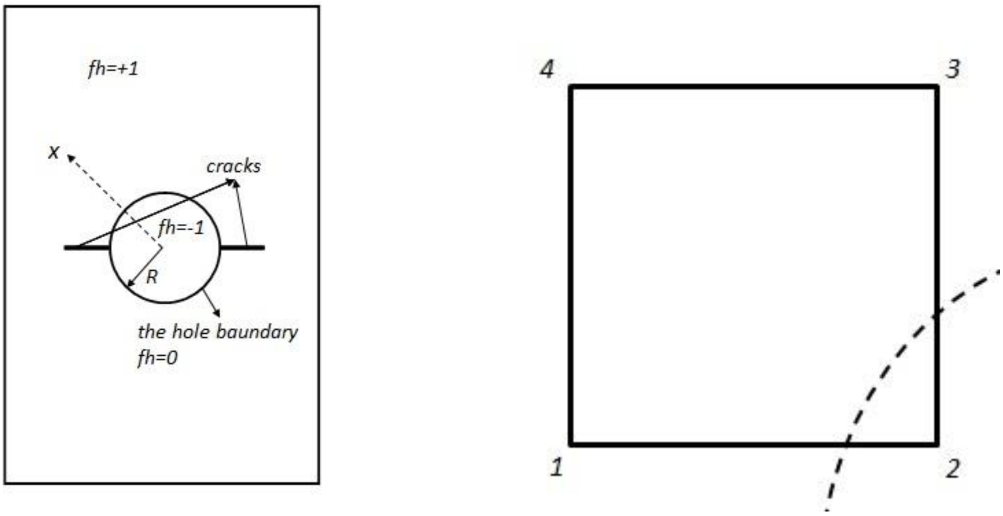

(a) The piecewise function fh for a circular hole

(b) An element has a discontinuity due to circular hole

Figure D.2 : Illustration of the piecewise function f_h for a circular hole.

matrix. The factor F_I is given in Stress Intensity Factors Handbook [36] by:

$$F_I = \frac{K_I}{\sigma\sqrt{\pi\, L}} \qquad (\boldsymbol{D.2})$$

where K_I is the calculated mode I stress intensity factor, σ is tensional stress and a is half of the crack length where the crack has a circular hole (R is the radius of circular hole) at the center; a=R+c. The parameters, α and β, given by

$$\alpha = \frac{a}{m} \qquad (\boldsymbol{D.3})$$

$$\beta = \frac{c}{R} \qquad (\boldsymbol{D.4})$$

The results for the Crack Emanating From A Circular Hole in A Rectangular plate Under Tension is represented in Table D.1 for various values of α and β for h/w=2 and R/w=0.25, which are kept constant during the analysis. The results have a good agreement with the reference ones even if they are not exact. The maximum of error is less than 4%.

The error decreases while α and β are increased and it starts to increase for higher values of α and β than α=0.5 and β=1.0. It is because of the dimensions of plate kept constant while both a and R were increasing.

Table D.1 : The factor F_I for ACECHRPUT with variation of α and β by Stress Intensity Factors Handbook [36] and the MATLAB code.

		Stress Intensity Factors Handbook [36]		With My MATLAB Code	
		FI	FI (Newman)	FI	
α	β	CT1 and CT2	CT1 and CT2	CT1	CT2
0,30	0,20	1,0750	1,0776	1,0385	1,0385
0,35	0,40	1,1780	1,1783	1,1584	1,1584
0,40	0,60	1,2216	1,2156	1,1996	1,1996
0,50	1,00	1,2850	1,2853	1,2692	1,2692
0,60	1,40	1,3960	1,3965	1,3765	1,3765
0,70	1,80	1,5760	1,5797	1,5511	1,5511
0,80	2,20	1,8900	1,9044	1,8553	1,8553

APPENDIX D.2

The new example is similar with pervious one except the hole is a square turned 45° in clockwise direction and the crack lies at the corner of the square in Figure D.3.

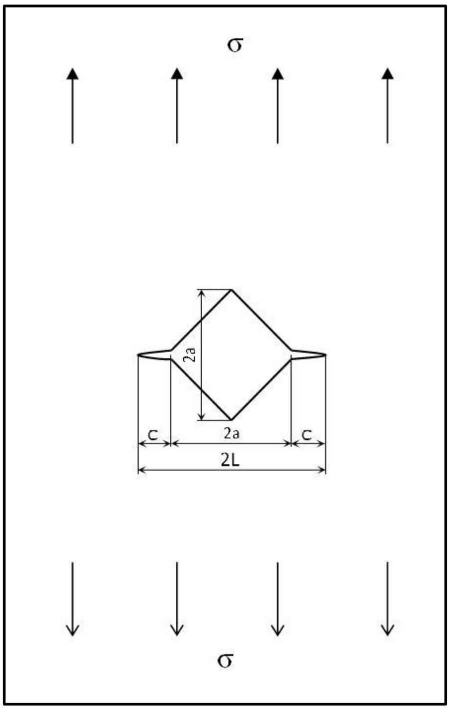

Figure D.3 : A crack emanating from a rectangular hole in a rectangular plate under tension.

The square hole described similarly in Figure D.4 (a) with

$$f_h = \begin{cases} -1 & if\ the\ nodes\ is\ inside\ of\ the\ hole \\ 0 & if\ the\ nodes\ is\ on\ the\ baundary\ of\ the\ hole \\ +1 & if\ the\ nodes\ is\ outside\ of\ the\ hole \end{cases} \qquad (\boldsymbol{D.5})$$

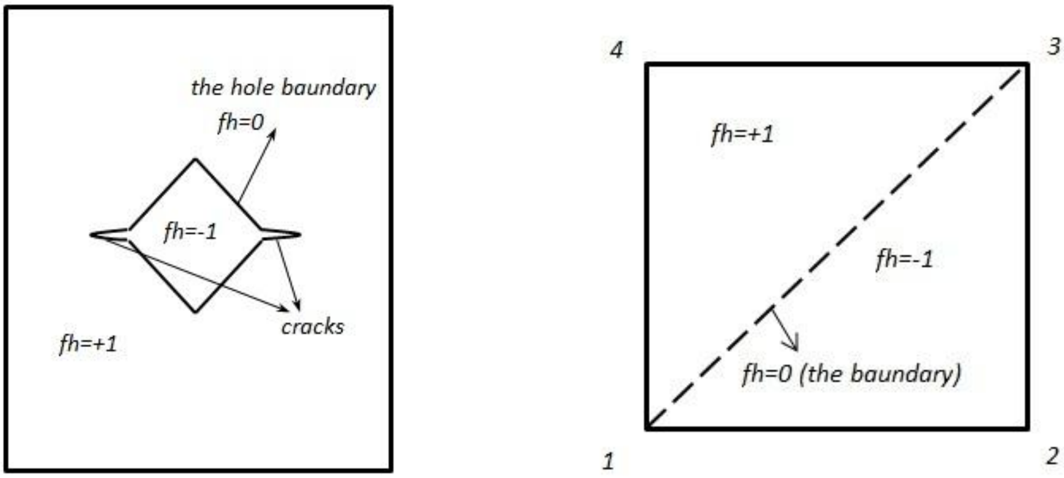

(a) The piecewise function fh for a rectangular hole

(b) An element has a discontinuity due to rectangular hole

Figure D.4 : Illustration of the piecewise function f_h for a rectangular hole.

The factor F_I is given in Murakami [37] by:

$$F_I = \frac{K_I}{\sigma\sqrt{\pi L}} \qquad (\boldsymbol{D.6})$$

where K_I is the calculated mode I stress intensity factor, σ is tensional stress and L is half of the crack length where the crack has a rectangular hole at the center; L=a+c.

The analysis of the crack emanating from a rectangular hole in a rectangular plate under tension (ACERHRPUT) is represented in Table D.2 and D.3 for various values of c/a ratio. First situation has a maximum error of 2% for h/w=1 and R/w=0.05 while the second has the maximum error of 4% for h/w=1 and a/w=0.1. The results have a good agreement with the reference ones and have the maximum error of 4%. As discussed for the circular hole, the plate includes largest hole is the plate where the largest error occurs.

APPENDIX D.3

the hole is described as discussed in the Crack Emanating from a Circular Hole in A Rectangular plate Under Tension problem and it is also described as a hard inclusion such that the nodes lies on the boundary of the hole and inside of the hole are fixed in both direction.

The crack growth angle is given by

$$\theta = 2\tan^{-1}\left(\frac{K_I}{4K_{II}} \pm \frac{1}{4}\sqrt{\left(\frac{K_I}{4K_{II}}\right)^2 + 8}\right) \qquad (\boldsymbol{D.7})$$

where K_I and K_{II} are the calculated mode I and mode II stress intensity factors, respectively. The crack growth direction given by Equation (D.7) is known as Maximum tangential stress criterion and was covered in the previous sections in more detail.

Table D.2 : The factor F_I for ACERHRPUT with h/w=1 and a/w=0.05 and variation of c/a by Murakami [37] and the MATLAB code.

For h/w=1 and a/w=0.05			
	by Murakami [37]	With My MATLAB Code	
	FI	FI	
c/a	CT1 and CT2	CT1	CT2
0,30	1,0635	1,0499	1,0499
0,40	1,0580	1,0485	1,0485
0,50	1,0520	1,0470	1,0470
0,60	1,0460	1,0442	1,0442
0,80	1,0370	1,0396	1,0396
1,00	1,0300	1,0366	1,0366

Table D.3 : The factor F_I for ACERHRPUT with h/w=1 and a/w=0.10 and variation of c/a by Murakami [37] and the MATLAB code.

For h/w=1 and a/w=0.1			
	by Murakami [37]	With My MATLAB Code	
	FI	FI	
c/a	CT1 and CT2	CT1	CT2
0,30	1,0635	1,0869	1,0869
0,40	1,0580	1,0866	1,0866
0,50	1,0520	1,0862	1,0862
0,60	1,0460	1,0862	1,0862
0,80	1,0370	1,0781	1,0781
1,00	1,0300	1,0629	1,0629

Figure D.5 shows a series of crack part for different positions of the rectangular hole that described as

$$f_h = \begin{cases} -1 & if\ the\ nodes\ is\ inside\ of\ the\ hole \\ 0 & if\ the\ nodes\ is\ on\ the\ baundary\ of\ the\ hole \\ +1 & if\ the\ nodes\ is\ outside\ of\ the\ hole \end{cases} \qquad (\boldsymbol{D.8})$$

The hole boundary is stress free which means nodes are stress free if they are on the boundary of the hole. This means the hole boundary also deforms during the load is applied. And the nodes, inside of the hole, have no participation for the calculation of global stiffness matrix and they are decrease the number of the total degree of freedom.

The each line shows how the crack propagates near the hole. The hole starts to extend from the dark red line to the magenta. The crack path has directed to the

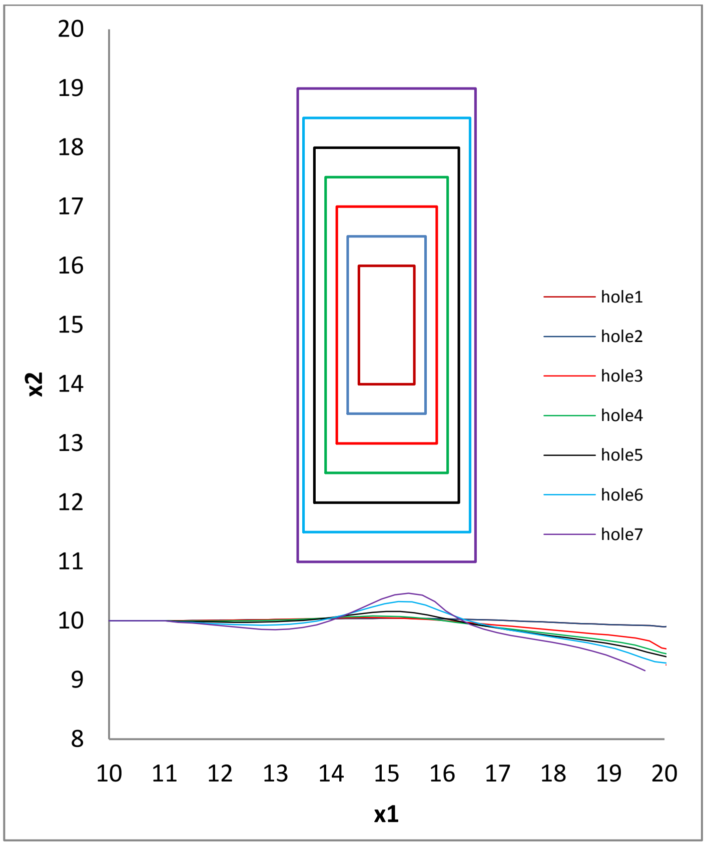

Figure D.5 : A series of crack part for different positions of the rectangular hole defined by (D.8).

downward of the plate and after the crack tip start to get closer to the hole it starts to change the direction to the upward of the plate. After the crack path reaches a pick, it starts to go downward again. During the simulation at each step of crack path, the crack grows with a constant crack growth of 0.25. The crack tip where there is no hole near by the crack paths are nearly the same. The hole centers are placed to (15, 15) and the dimensions of rectangular hole increase. While the hole becomes larger, it starts to get closer to the crack. That is why the deviation of the crack path near the hole becomes larger as expected.

Figure D.6 shows a series of crack part for different positions of the rectangular hole that described as

$$f_h = \begin{cases} -1 & \text{if the nodes is inside of the hole} \\ 0 & \text{if the nodes is on the baundary of the hole} \\ +1 & \text{if the nodes is outside of the hole} \end{cases} \qquad (\boldsymbol{D.9})$$

The hole in Figure D.6 is simulated as a hard rectangular inclusion. It means that both nodes inside of hole and nodes lies on the hole boundary are fixed in both direction. Those nodes, inside of the hole and on boundary of hole, have no participation for the number of the total degree of freedom due to their fixed displacements.

The each line shows how the crack propagates near the hole, defined as a hard inclusion and placed to the center at (15, 15). The hole starts to extend from the light blue line to the black one. The crack path has directed to the downward of the plate

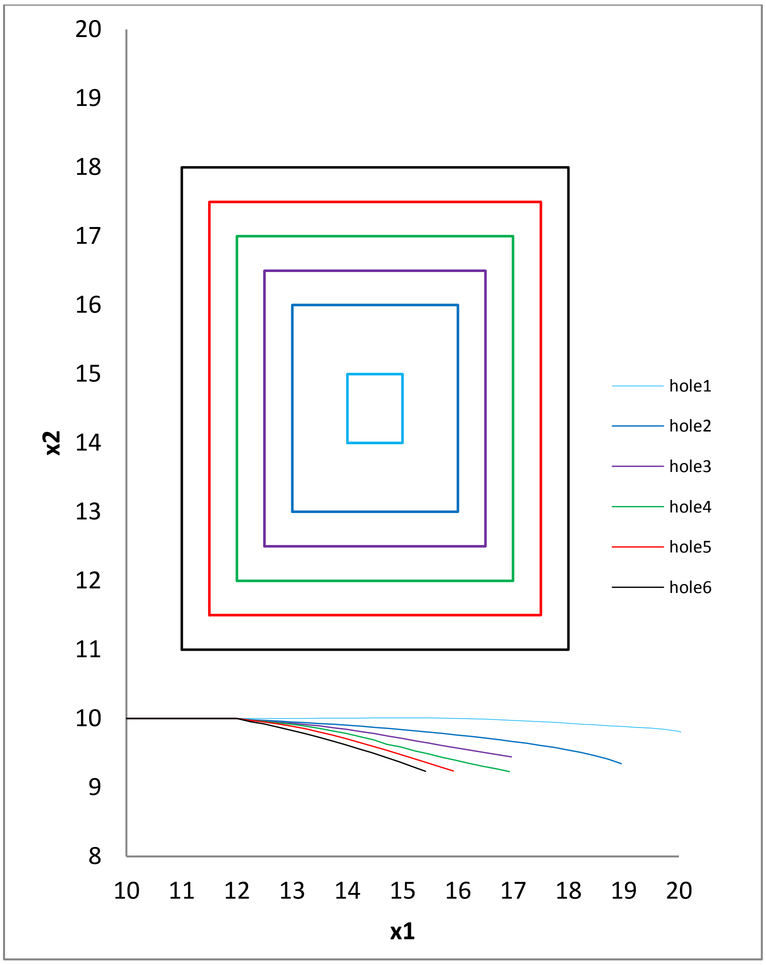

Figure D.6 : A series of crack part for different positions of the rectangular hole defined as a hard inclusion .

away from the inclusion as expected. The deviation of the hole to downward of the plate increases while the rectangular hole is getting closer to the crack.

In this section different types of examples are covered to illustrate the program is working properly and the evaluated results have good agreement with each other.

APPENDIX E

APPENDIX E.1

The crack growth for additional Case I is illustrated in Figure E.1 by different K_{eff} formulas for a 0.16*0.12 m rectangular plate with a center crack lies from (0.055, 0.08) to (0.065, 0.08). The non-proportional loading illustrated in Figure E.1 is given for additional Case I by

$$\left.\begin{aligned} \sigma &= 12 \times 10^7 (1 + 0.6\sin(wt))\ Pa \\ \tau &= -8.5 \times 10^7 0.8 Abs(\sin(2wt))\ Pa \end{aligned}\right\} \qquad (\boldsymbol{E.1})$$

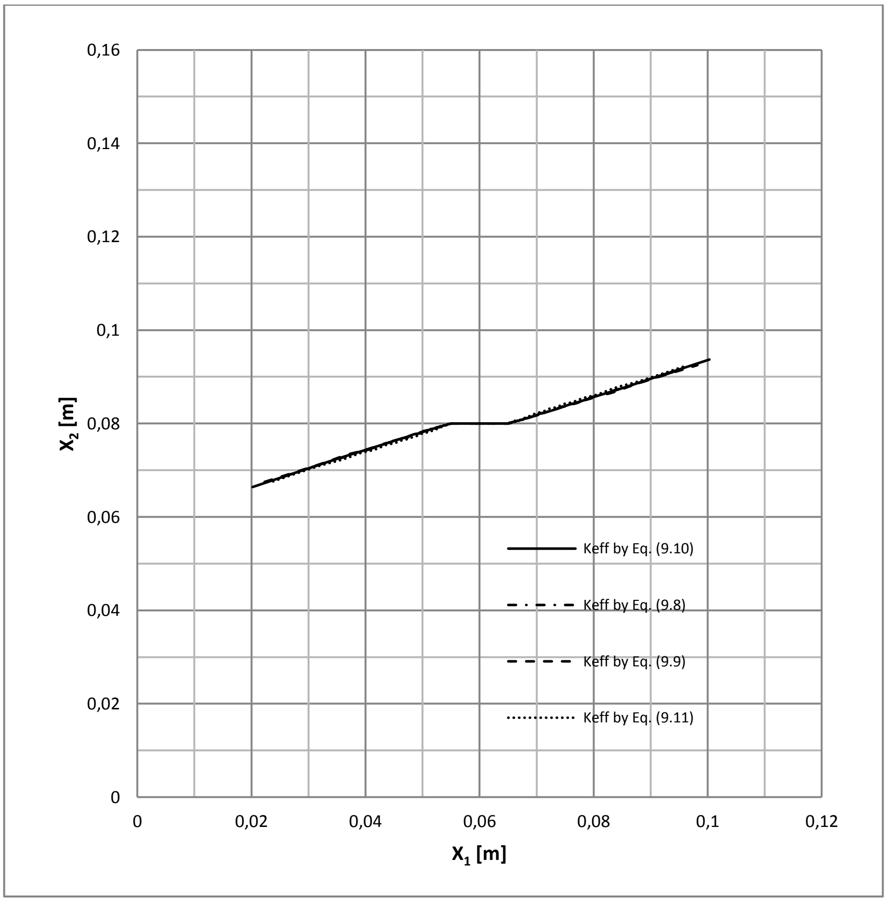

Figure E.1 : Estimated crack paths for additional Case I by each K_{eff} formula.

The loads are applied in 36 steps to catch the change of K_{eff} correctly. The change of K_{eff} according to the different K_{eff} formulas is illustrated in Figure E.2 for the first iteration. As seen from Figure E.2, K_{eff} makes the maximums at the 5th, 13th, 22th and 32th load steps and, the minimums at the 9th, 19th, 27th and 35th load steps.

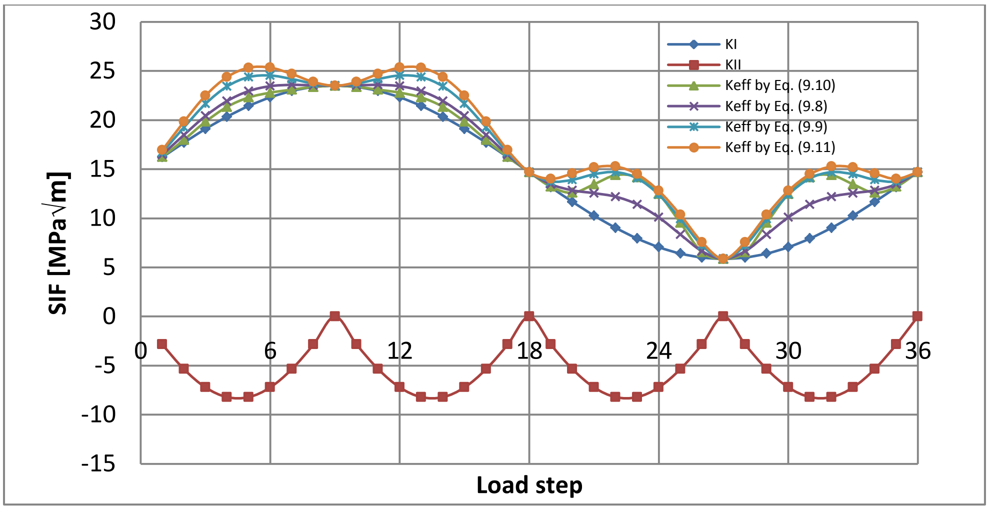

Figure E.2 : Stress intensity factors calculated at the first iteration for additional Case I.

Figure E.3 shows the change of crack growth rate respect to the employed K_{eff} formula at each crack tip with Case I loadings. The both crack tip grow symmetrically as seen in Figures E.1 and E.3. The crack grow rates are in the range of 10^{-9} to 10^{-6} m/cycle.

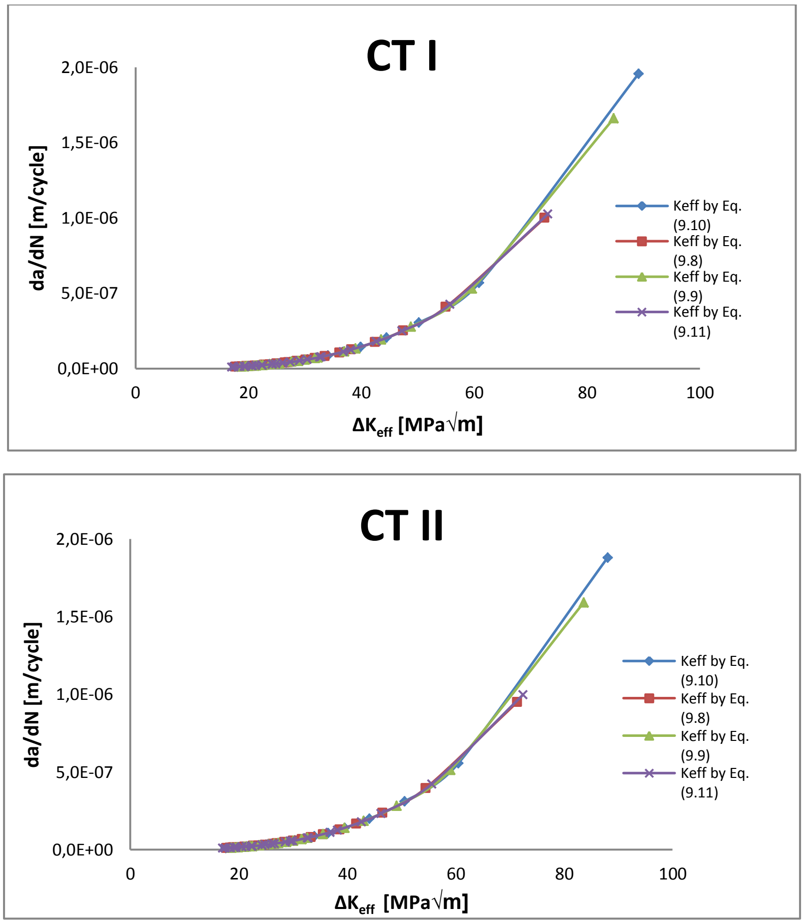

Figure E.3 : The change of crack growth rate respect to the employed K_{eff} formula at each crack tip for additional Case I.

APPENDIX E.2

The crack growth for Case II is illustrated in Figure E.4 by different K_{eff} formulas for a 0.16*0.12 m rectangular plate with a center crack lies from (0.055, 0.08) to (0.065, 0.08). The non-proportional loading illustrated in Figure E.4 is given for Case II by

$$\left.\begin{aligned} \sigma = 20 \times 10^7 Pa \\ \tau = -\frac{13}{0.8} \times 10^7 (1 + 0.8\sin(2wt))\; Pa \end{aligned}\right\} \qquad (\boldsymbol{E.2})$$

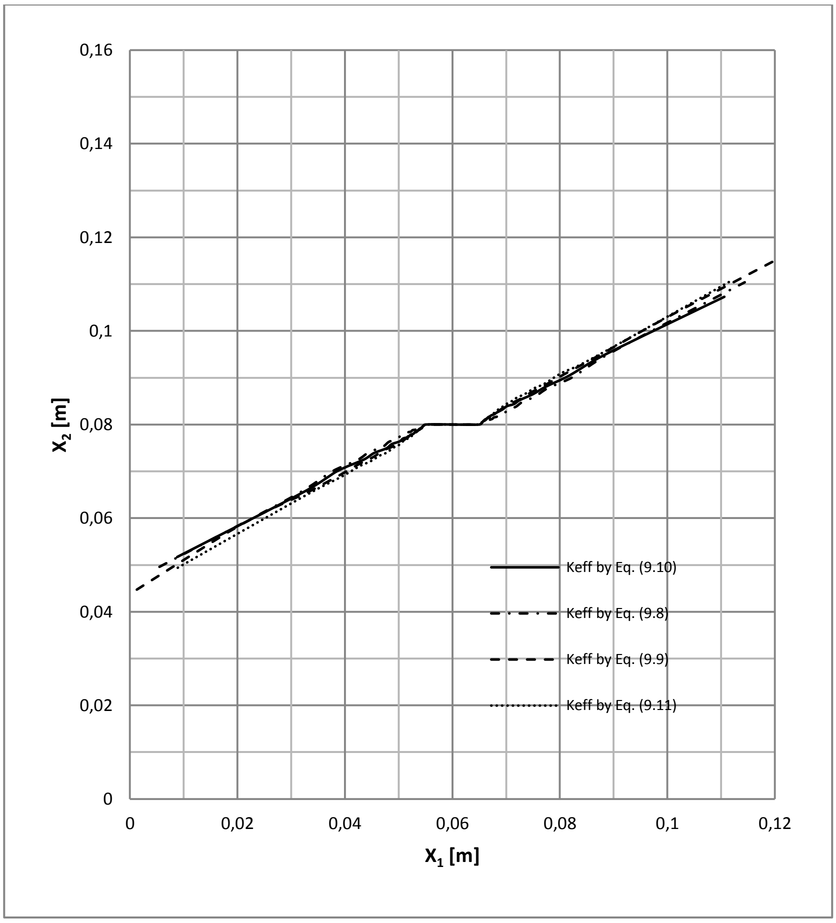

Figure E.4 : Estimated crack paths for Case II by each K_{eff} formula.

The loads are applied in 36 steps to catch the change of K_{eff} correctly. The change of K_{eff} according to the different K_{eff} formulas is illustrated in Figure E.5 for the first iteration. As seen from Figure E.5, K_{eff} makes the maximums at the 4th or 5th and 22th or 23th load steps and, the minimums at the 13th or 14th and 31th or 32th load steps.

Figure E.6 shows the change of crack growth rate respect to the employed K_{eff} formula at each crack tip with Case II loadings. The both crack tip grow symmetrically as seen in Figures E.4 and E.6. The crack grow rates are in the range of 10^{-9} to 10^{-6} m/cycle.

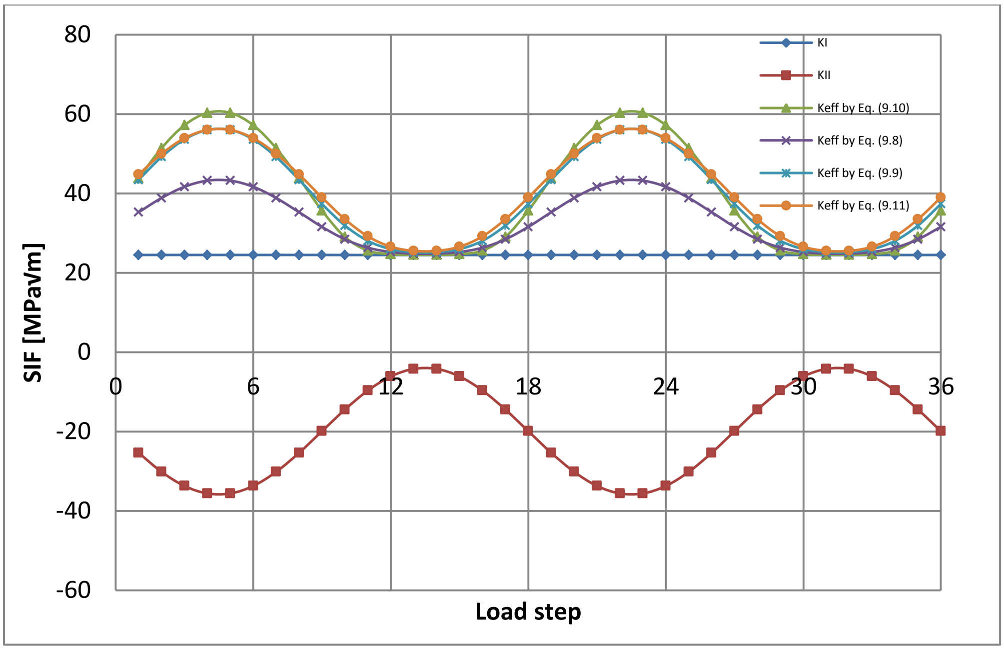

Figure E.5 : Stress intensity factors calculated at the first iteration for Case II.

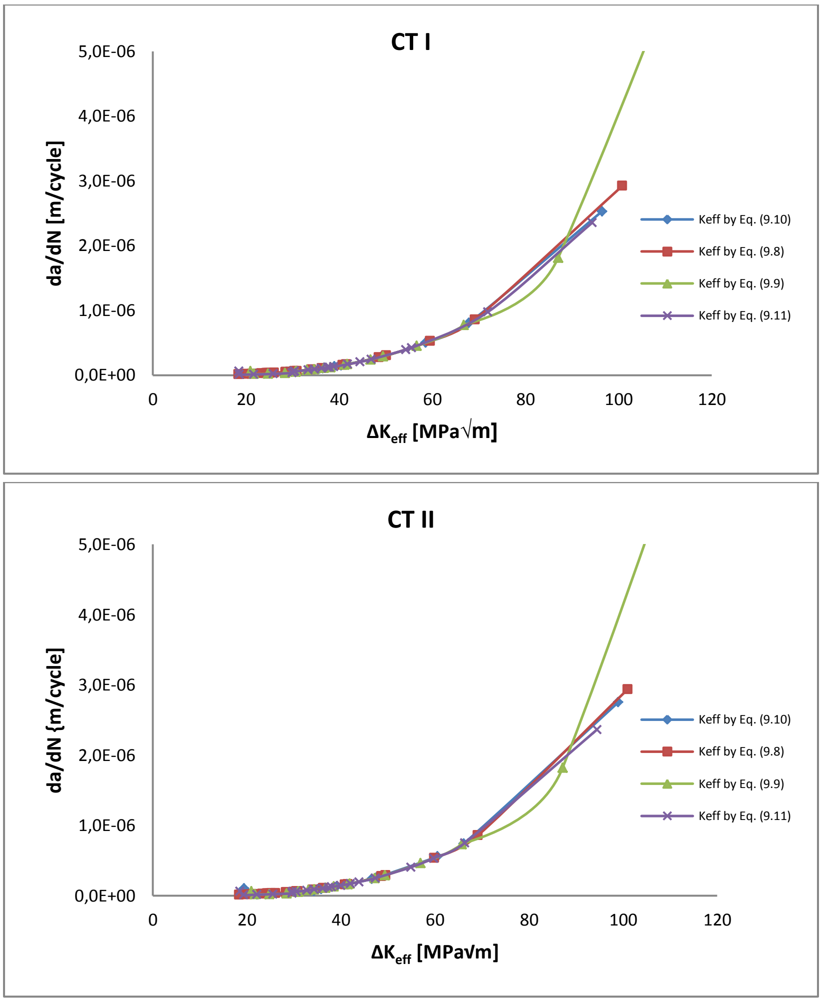

Figure E.6 : The change of crack growth rate respect to the employed K_{eff} formula at each crack tip for Case II.

APPENDIX E.3

The crack growth for Case III is illustrated in Figure E.7 by different K_{eff} formulas for a 0.16*0.12 m rectangular plate with a center crack lies from (0.055, 0.08) to (0.065, 0.08). The non-proportional loading illustrated in Figure E.7 is given for Case III by

$$\left.\begin{aligned} \sigma &= \frac{25}{0.6} \times 10^7 \ Pa \\ \tau &= -40 \times 10^7 \sin(2wt) \ \ Pa \end{aligned}\right\} \qquad (\boldsymbol{E.3})$$

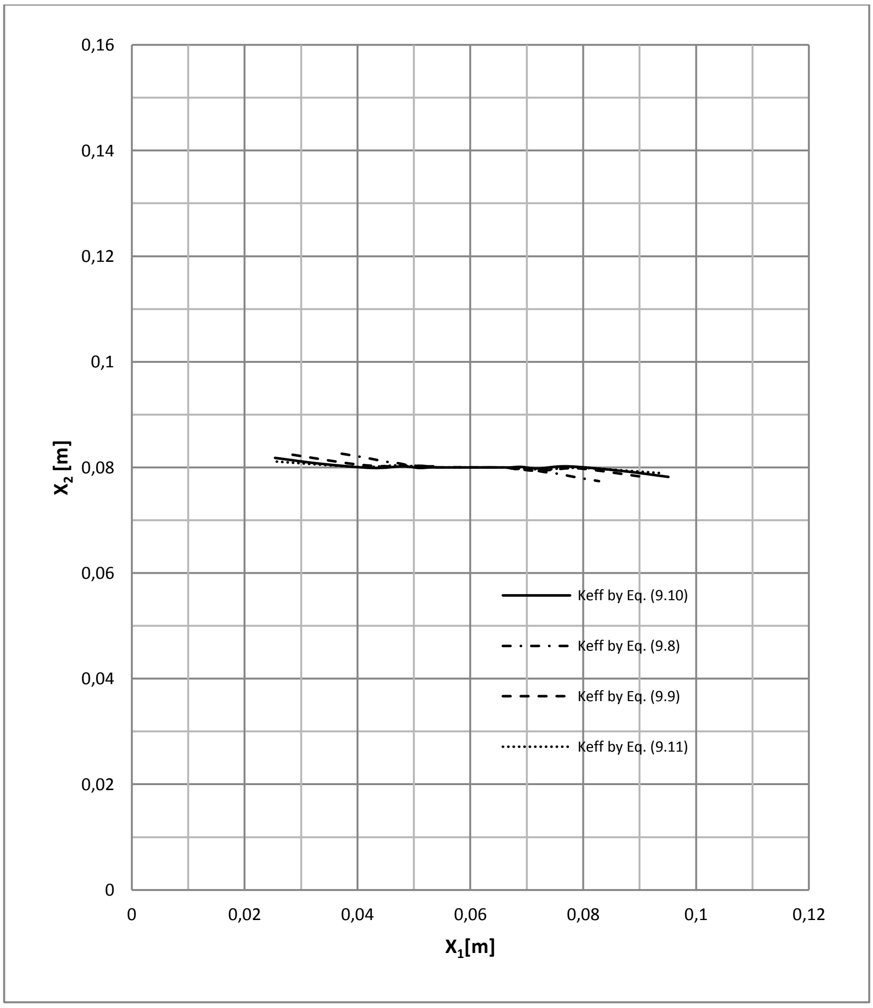

Figure E.7 : Estimated crack paths for Case III by each K_{eff} formula.

The loads are applied in 36 steps to catch the change of K_{eff} correctly. The change of K_{eff} according to the different K_{eff} formulas is illustrated in Figure E.8 for the first iteration. As seen from Figure E.8, K_{eff} makes the maximums at the 4th or 5th, 13th or 14th, 22th or 23th and 31th or 32th load steps and, the minimums at the 9th, 18th, 27th and 36th load steps.

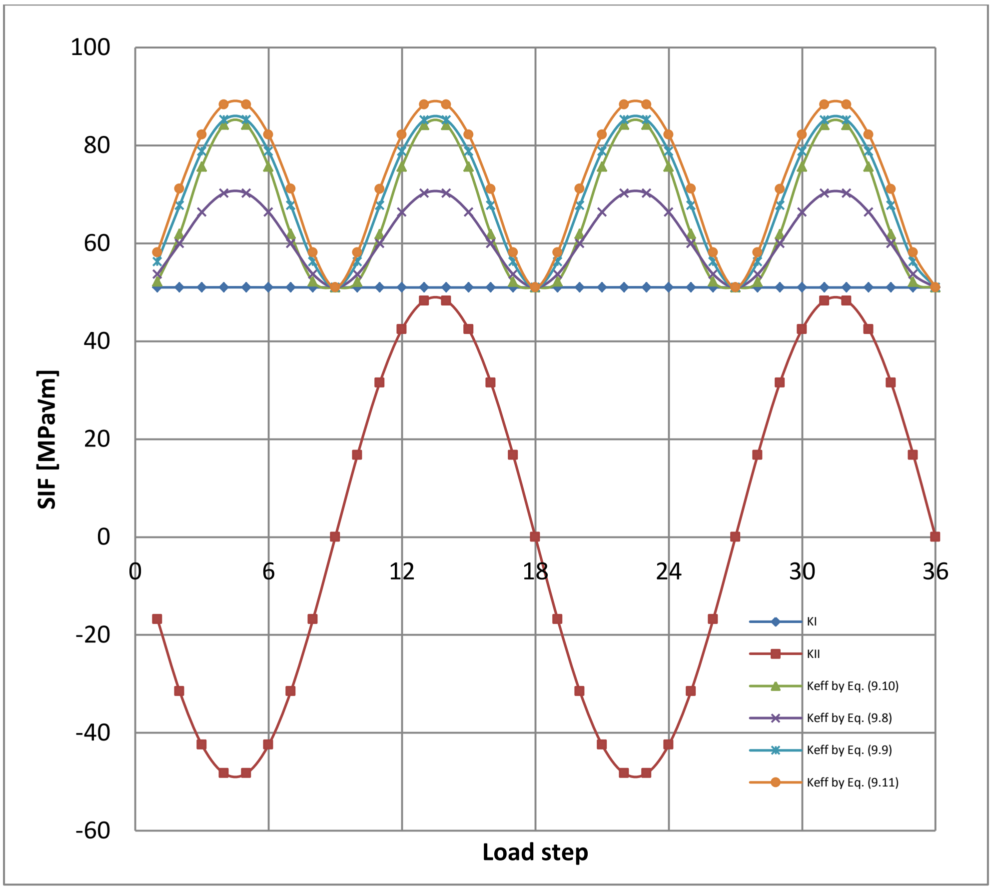

Figure E.8 : Stress intensity factors calculated at the first iteration for Case III.

Figure E.9 shows the change of crack growth rate respect to the employed K_{eff} formula at each crack tip with Case III loadings. The both crack tip grow symmetrically as seen in Figures E.7 and E.9. The crack grow rates are in the range of 10^{-9} to 10^{-6} m/cycle. The K_{eff} given by Equation (9.8) has the slowest crack grow rate due to fact that the cycle mode II loading is larger than the static mode I loading and K_{II} is weighted with 1. The mode II loading is selected such largely to sustain the crack growth that is identical the Region II.

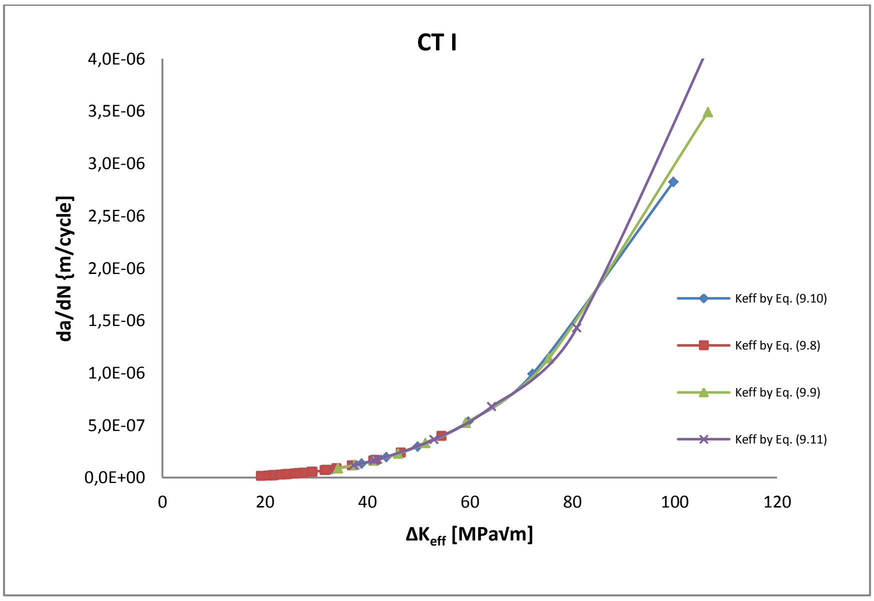

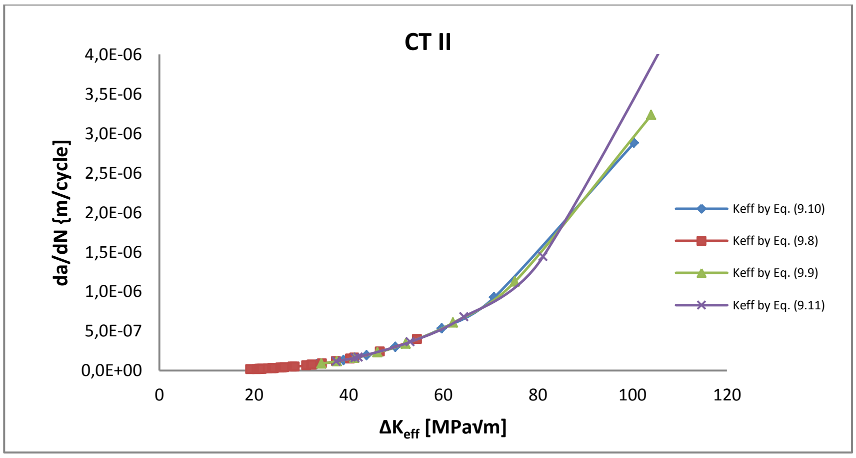

Figure E.9 : The change of crack growth rate respect to the employed K_{eff} formula at each crack tip for Case III.

APPENDIX E.4

The crack growth for Case IV is illustrated in Figure E.10 by different K_{eff} formulas for a 0.16*0.12 m rectangular plate with a center crack lies from (0.055, 0.08) to (0.065, 0.08). The non-proportional loading illustrated in Figure E.10 is given for Case IV by

$$\left.\begin{aligned} \sigma &= 30 \times 10^7 \sin(wt)\ Pa \\ \tau &= -\frac{5}{0.8} \times 10^7\ Pa \end{aligned}\right\} \qquad (\boldsymbol{E.4})$$

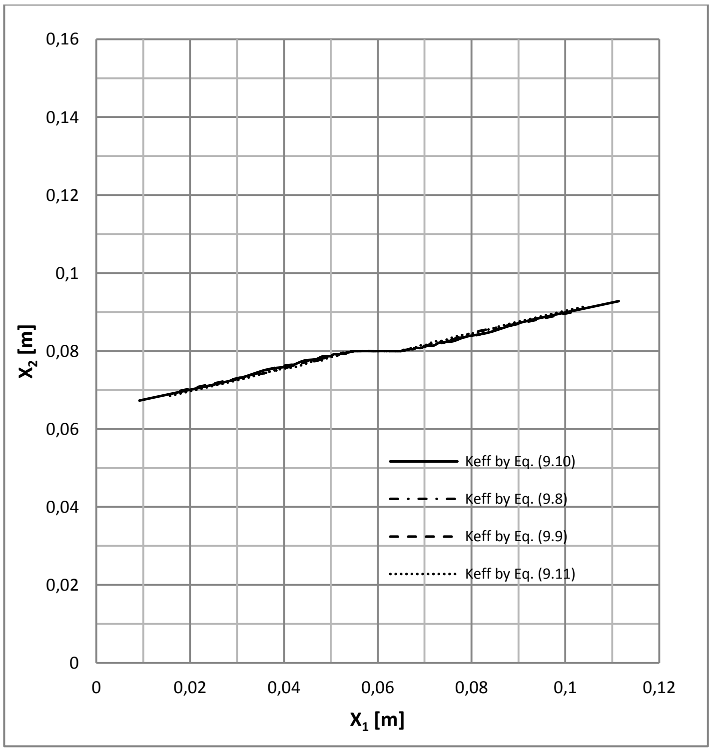

Figure E.10 : Estimated crack paths for Case VI by each K_{eff} formula.

The loads are applied in 36 steps to catch the change of K_{eff} correctly. The change of K_{eff} according to the different K_{eff} formulas is illustrated in Figure E.11 for the first iteration. As seen from Figure E.11, K_{eff} makes the maximums at the 9th and 27th load steps and, the minimums at the 18th and 36th load steps.

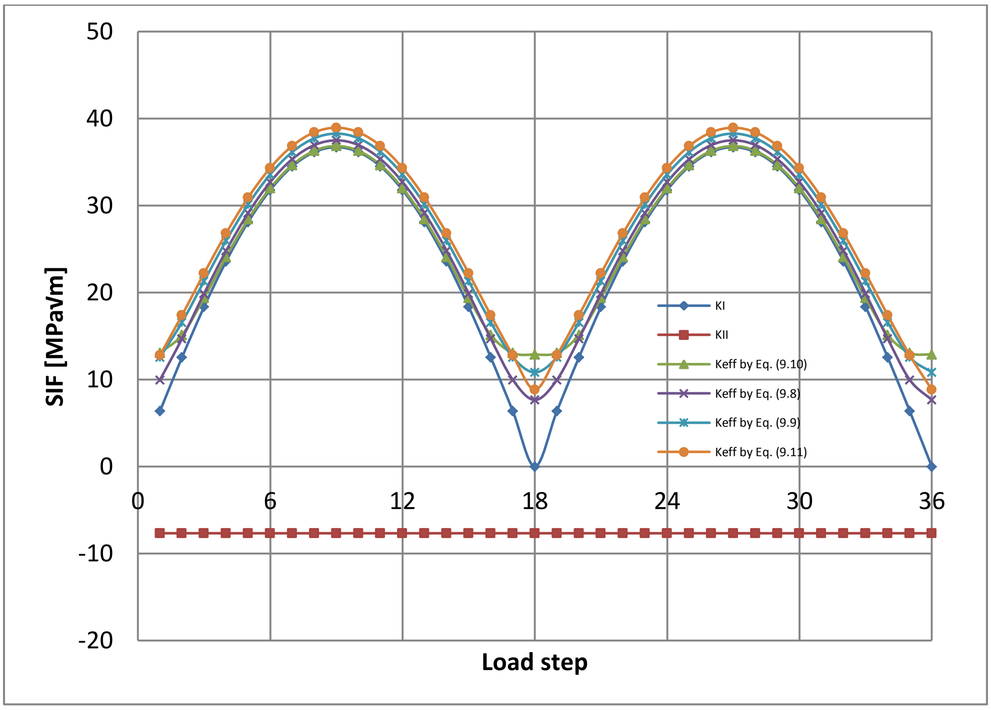

Figure E.11 : Stress intensity factors calculated at the first iteration for Case IV.

Figure E.12 shows the change of crack growth rate respect to the employed K_{eff} formula at each crack tip with Case III loadings. The both crack tip grow symmetrically as seen in Figures E.10 and E.12. The crack grow rates are in the range of 10^{-9} to 10^{-6} m/cycle.

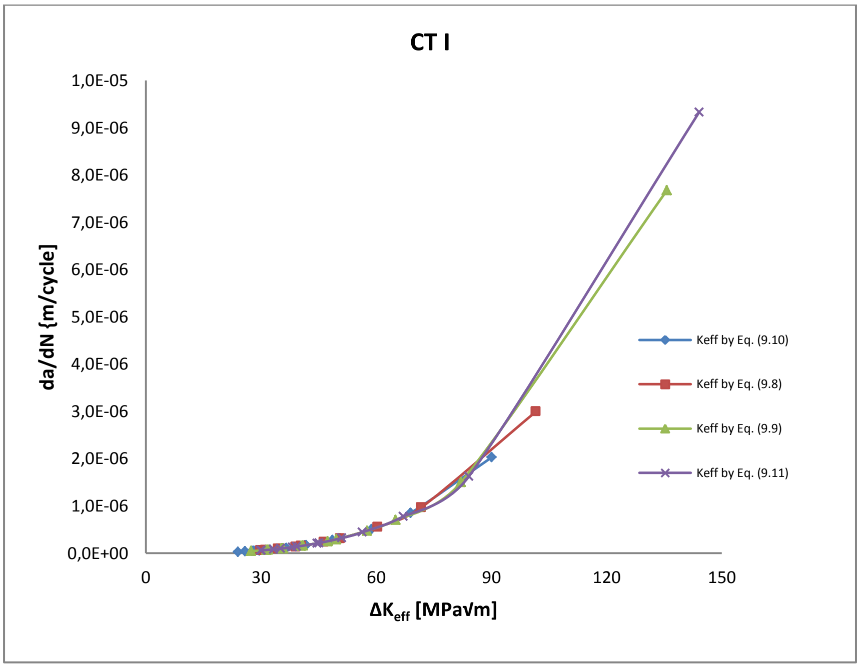

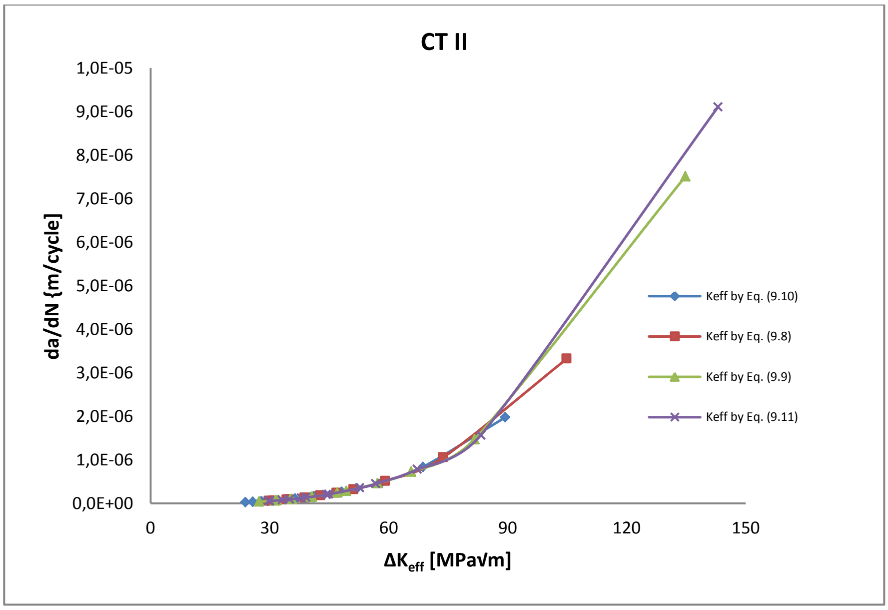

Figure E.12 : The change of crack growth rate respect to the employed K_{eff} formula at each crack tip for Case IV.

APPENDIX F

The implemented MATLAB source code is listed on the following pages for the Flow chart is illustrated in Section 10. The MATLAB code has been prepared such that the user modifies the InputFile.m file, then runs xfemMain.m from the MATLAB Command Window to solve a fatigue crack problem under mixed mode non-proportional loading. A detailed description of the input variables follows as well as a brief summary of the functions which make up the complete code follows.

- BoundaryCond.m

This function applies the specified boundary conditions to the domain. For the hole, the additional fixed degrees of freedom are also calculated and added to the global system of equations.

- TotalDOF.m

This function calculates the total number of degrees of freedom in the system considering traditional, Heaviside, and crack tip degrees of freedoms.

- CreateMesh.m

This function calculates the global coordinates of all the nodes, generates the mesh, defines element connectivity and also begins to build the Nodes matrix which keeps track of the numbering for the enriched degrees of freedom.

- ElementStresses.m

This function calculates the stresses at each node for the given geometry to plot the nodal stress values.

- EnrichedElements.m

This function identifies the enriched elements and redefines the enriched elements which will cause from the crack propagation.

- ForceVector.m

This function creates the global force vector and redefines the global force vector for each load step during a load cycle.

- GaussPoints.m

This function contains the values of integration points and weights that will be used for Gauss quadrature in quadrilaterals and triangles.

- CrackGrowth.m

This function evaluates the angle and magnitude of the next crack growth increment for both crack tips. The direction of future crack growth is determined based on the Maximum tangential stress criterion. If the Paris Law constants are assigned in InputFile.m then the Paris Law with different Keff formulas are used to determine the increment of crack growth. If the Paris Law constants are not defined, the crack will propagate with the specified amount of crack growth.

- InputFile.m

The following input variables are used to define the problem of interest: Domain, MAT, CRACK, HOLE, GROW, FORCE, BC, PLOT. In order for an analysis to successfully run, the minimum required variables to be defined are DOMAIN, MAT, GROW, FORCE and BC.

- JIntegral.m

This function calculates the mixed-mode stress intensity factors for the crack tip enrichment functions. The default J-domain search radius is 4 elements around the crack tip. The stress intensity factors are retuned such that the last tip in CRACK is first and the first tip in CRACK is second.

- Discontinuty.m

This function creates the functions used to track the crack tips, crack body, and holes. In addition this file defines the locations of the enriched degrees of freedom and assigns these enriched nodes tracking values in the Nodes matrix.

- plotDeformation.m

This function plots the deformed mesh. If it is needed, node and element numbers, the enriched nodes can be plotted

- plotStress.m

This function plots the stress distribution within each element and discontinuities. As an option, the average nodal stress values are also available.

- GlobalStifnessMatrixK.m

This function calculates the global stiffness matrix for the global equation system.

- Triangularization.m

This function subdivides elements containing discontinuities into triangles so that accurate integration can be performed in these elements.

- UpdateGlobalStifnessMatrixK.m

This function redefines the global stiffness matrix according to redefined crack tip elements and Heaviside elements.

- xfemMain.m

This function controls the calling of the various functions to perform the desired analysis. The analysis or the simulation consists of main and sub iterations. The sub iterations calculate the KI and KII for a load cycle with the crack described by the step wise linear function. The main iterations calculate the crack growth rate and the crack angle for each crack tip according to the calculated KI and KII. And then the crack incensements are added to each crack tip to define the crack as a step wise linear function.

The source codes are given in a CD at the end of the thesis to avoid the unnecessary paper consumption and to simplify the usage of the program.

CURRICULUM VITAE

NAİT MUTLU

Kartal tepe Mah. Yeniyol Sok.

No:8/1 Bayrampaşa/İSTANBUL

TEL: +90 212 616 61 25 - +90 535 427 05 73

e-mail:naitmtl@gmail.com

PERSONEL DETAILS:

Date of Birth	: 29.11.1984 - Bulgaria
Marital Status	: Single
Military Service	: Not completed
Nationality	: Turkish & Bulgaria

EDUCATİON :

Master Thesis Project	**:** Technical University of Denmark	Solid Mechanics	(2010-2011)	degree: 10/12
Master degree	**:** Istanbul Technical University	Solid Mechanics	(2009- 2010)	degree: 3.88/4
Bachelor's degree	: Istanbul Technical Universit	Mechanical Engineering	(2004-2009)	degree: 3.20/4
High school	: Otakçılar High School	-	(1999-2003)	degree: 4.50/5

WORK EXPERIENCES

BOZ PROJE - DANIŞMANLIK Mechanical Engineer August 2009 - June 2010

(HVAC system design of high buildings)

Duty and Responsibilities:

In BOZ PROJE, we design the HVAC systems of high buildings and provide consultancy service to operate the systems efficiently as they designed. I am taking part in all stage of the system design and installation of the components correctly as they designed. Furthermore, a research that comparing two different capacity heat exchangers is carried on for Danfoss- Turkey. In this research project, I am responsible to make the necessary measurements (for example: temperatures and flow rates of the water inlets and outlets of) and preparing necessary reports of this measurements.

EÜ A.Ş. 18 MART ÇAN Therm. Power Plant Mechanical Engineer (intern) 2008 (August - 20 work days)

(Electricity production)

Duty and Responsibilities:

I worked in control and Manufacturing departments of 18 MART ÇAN thermoelectric power plants. I took part in all Manufacturing processes of electricity. I examined each process of electric production (for example preparing the water for water cycle, the boiler, the turbines (each 160 MW) etc.) and I worked in the controlling department (for instance starting processes of sector A (the turbine the boiler and water cycling systems; pumps, evaporators and super heaters etc.). On the other hand, I took part in transport systems of both ash and coal.

SPINNER A.Ş. Mechanical Engineer (intern) 2007 (August - 20 work days)

(CNC manufacturer)

Duty and Responsibilities:

I worked in Design and Manufacturing departments of SPINNER Company. I took part in all Manufacturing processes. We produce many of products (for example spindles and electrical circuits of CNC and calibration of CNC positions etc.) and we all examine the product’s properties in the control laboratory of the department. On the other hand, I draw most of parts of CNC (like sheet metal, spindles etc.) by using Inventor 10 in Design department

FOREIGN LANGUAGE:

- English : Advanced (Technical University of Denmark)

COMPUTER & APPARATUS SKILLS:

Windows 98-2000-XP, Vista, windows7 , Microsoft Office Programs 2007 (Excel, Word, PowerPoint), Carrier HAP 4.3 , Matlab 7.0.1, Abaqus 6.9-1, AutoCAD Mechanical 2008, Inventor 10, Catia, Solidworks 2008+ Cosmosworks, Ansys Workbench 11

PREPARING PROJECT

- Master thesis project " Fatigue Crack Growth under Non-proportional Loading " is done for MAN Diesel at Technical University of Denmark during August 2010 - August 2011.
- Comparing two different types of heat exchangers that in use at two high building, their effects on the system performance of eacth building and preparing a handbook for designer (the research is carried out for Danfoss- Turkey 2009-2010)
- Dynamic analysis of the thoracic vertebras (T5-T6) with the tissues between them by means of Abaqus 6.9-1 (FEM Design Project 2009)
- Comparing personal and central systems for a site respect their sustainability (Graduation Project 2009)
- VAV and CAV systems design with controllers and preparing the automation scenario for each one and compare to which one is more efficient (Building Automation Term Project 2009)
- Destructive and non-destructive tests applied to a weldment (Welding Technology Design Project 2009)
- Initializations and dimensioning of electricity/plumbing/gas/central heating/fire extinguisher systems of an apartment with 12 stories according TSE and ISO standards (Mechanical Installation for Buildings Term Project 2009)
- Design of an experimental setup for measuring flow velocity and direction by means of a constant temperature hotwire anemometer in 3D (Experimental Methods in Mechanical Eng. Term Project 2009)
- Design of a storage with a refrigeration system and its components for apple, honey, meat, pouty, fish and potato storage (Refrigeration Term Project 2009)
- Design of air conditioning system with components for a luxury residence of 2 stories for winter and summer condition by means of Carrier HAP 4.15 (HVAC Fundamentals Term Project 2009)
- Design of air conditioning system with components for a company building of 3 stories (Uygulamalı Termodinamik Term Project 2008)
- Design of a fan blower with components for an oven of Bosch and both strain-stress and temperature gradient analyzing with Abaqus 6.7-1 (FEM Design Project 2008)
- Transmission mechanism of a vehicle control (1) and Cardan Gear Mechanism (2) (Makina Elemanları-II Projects 2008)
- Motion and force analysis of a caterpillar mechanism (Makina Teorisi Project 2008)
- Design of a speed controller for a high speed train (Sys. Dynamics & Control Project 2007)

INTEREST:

Reading historical and political novels, Chess, Cinema, Theater, Sport and Travel.

<u>REFERENCES</u>:

Prof. Dr. Ata MUGAN	ITU	Mechanical Engineering Faculty	+90 539 277 67 60
Prof. Dr. Ahmet ARISOY	ITU	Mechanical Engineering Faculty	+90 212 293 13 00 (dahili 22480)
B. Erdinç Boz	Boz Proje - Danışmanlık	The owner of the company	+90 532 265 43 44
Prof. Dr. Viggo Tvergaard	Technical University of Denmark	Mechanical Eng. Faculty	+45 4525 4273